



Dominik Leutnant M.Sc.

Monitoring, Analysis and Modelling of Urban Stormwater Quality

DISSERTATION

zur Erlangung des akademischen Grades
Doktor der technischen Wissenschaften (Dr. techn.)
der Studienrichtung Bauingenieurwissenschaften

eingereicht an der

Technischen Universität Graz

Betreuer:

Prof. Dr.-Ing. Dirk Muschalla

Prof. Dr.-Ing. Mathias Uhl

Korreferent:

Prof. Dr.-Ing. Theo G. Schmitt

Institut für Siedlungswasserwirtschaft und Landschaftswasserbau

Graz, im Mai 2018

EIDESSTATTLICHE ERKLÄRUNG

AFFIDAVIT

Ich erkläre an Eides statt, dass ich die vorliegende Arbeit selbstständig verfasst, andere als die angegebenen Quellen/Hilfsmittel nicht benutzt, und die den benutzten Quellen wörtlich und inhaltlich entnommenen Stellen als solche kenntlich gemacht habe. Das in TUGRAZonline hochgeladene Textdokument ist mit der vorliegenden Doktorarbeit identisch.

I declare that I have authored this thesis independently, that I have not used anything other than the declared sources/resources, and that I have explicitly indicated all material which has been quoted either literally or contextually from the sources used. The text document uploaded to TUGRAZ-online is identical to the present doctoral thesis.

Ort / Place, Datum / Date

Unterschrift / Signature

Preface

Acknowledgements

Kurzfassung

Um einen wirksamen Gewässerschutz zu erreichen, sind Niederschlagsabflüsse urbaner Siedlungsgebiete hinsichtlich ihrer Stoffbelastung zu bewerten und abhängig des Verschmutzungspotenzials einer zentralen oder dezentralen Behandlungsanlage zuzuführen. Zur Abschätzung der einzugsgebietsspezifischen Stoffemissionen und zur Bemessung von Niederschlagswasserbehandlungsanlagen werden Stofffrachtmodelle eingesetzt, die jedoch die maßgebenden Stoffprozesse Entstehung, Akkumulation und Abtrag lediglich stark vereinfacht abbilden. Aufgrund der mangelnden Prozessnähe ist die Modellierung von Stoffprozessen von großen Unsicherheiten geprägt. Hierdurch kann die Kosteneffizienz von Behandlungsanlagen sinken oder sogar eine inakzeptable Gewässerbelastung entstehen. Die notwendige Verbesserung bestehender Modellkonzepte bedingt ein verbessertes Prozessverständnis. Hierzu sind zeitlich hochaufgelöste Messdaten erforderlich, die sowohl die räumliche und zeitliche Prozessvariabilität berücksichtigen als auch meteorologische und anthropologische Einflüsse einbeziehen.

In der vorliegenden Arbeit wurde daher die Niederschlagsabflussqualität von vier repräsentativen, urbanen Einzugsgebietstypen i) Flachdach, ii) Parkplatz, iii) Wohngebiet mit Trennsystem und iv) stark befahrene Hauptverkehrsstraße mittels kontinuierlicher Gütemesstechnik und begleitender Beprobung erfasst. Im Vordergrund der Untersuchung stand der Summenparameter abfiltrierbare Stoffe (AFS), dessen orts- und ereignisspezifische Dynamik durch den Surrogatparameter Trübung ermittelt wurde.

Die erhobenen Messdaten wurden ereignisbasiert mit statistischen Methoden untersucht und Abhängigkeiten zu meteorologischen Randbedingungen ausgewertet. Es zeigte sich eine signifikante Korrelation zwischen Niederschlagsintensität und AFS-Ereignisfracht für kleine Einzugsgebiete mit einem hohen Versiegelungsanteil. Weiterhin wurde die Stoffabtragsdynamik innerhalb eines Ereignisses mit Masse-Volumen-Kurven (MV-Kurven) analysiert. Erstmals wurden diese je Abfluss Quantil gruppiert und statistisch mit Boxplots beschrieben, um eine generelle Einzugsgebietscharakteristik des Stoffabtrags zu identifizieren. Während das Flachdach eine frachtlimitierende Abtragscharakteristik aufwies, konnte am Parkplatz und für die stark befahrene Straße eine transportlimitierte Dynamik beobachtet werden. Eine jahreszeitliche Auswertung verdeutlichte jedoch die hohe Prozessvariabilität.

Die beobachtete Prozessvariabilität und die damit verbundenen stochastischen Einflüsse auf Stoffgenese und -transport führte zur probabilistischen Prozessbeschreibung. Hierzu wurden empirische Verteilungsfunktionen der AFS-Ereignisfrachten für alle Standorte ermittelt und zur Anpassung von theoretischen Verteilungsfunktionen verwendet. Funktionsparameter wurden mittels *maximum likelihood estimation* (MLE) ermittelt. Es konnte gezeigt werden, dass die Lognormal-

Verteilung zur Beschreibung des Datenmaterials gut geeignet ist. Allerdings fiel auch auf, dass der Stichprobenumfang signifikant die Anpassungsgüte beeinflusst. Ergebnisse einer Monte-Carlo-Simulation empfehlen einen Stichprobenumfang von mindestens 40 Ereignissen.

Die parametrisierten Lognormal-Verteilungen wurden weiterhin verwendet um einen innovativen Kalibrierungsansatz des Niederschlags-Abfluss Modells SWMM zu entwickeln. Im Gegensatz zur konventionellen Kalibrierung, der eine ereignisbasierte Bewertung zugrunde liegt, wird hierbei die empirisch ermittelte Verteilungsfunktion der simulierten AFS-Ereignisfrachten durch die vorgegebene, theoretische Verteilungsfunktion approximiert. Die numerische Differenz der Verteilungsfunktionen wird durch die Kolmogorov-Smirnov Statistik ausgedrückt, die als Zielfunktion der Kalibrierung dient. Modellparameter der Stoffprozesse wurden mit Hilfe eines evolutionären Algorithmus optimiert. Obwohl die Stoffprozesse vereinfacht abgebildet werden, verdeutlichen die Kalibrierergebnisse und Parameterunsicherheiten die erfolgreiche Anwendbarkeit des Kalibrieransatzes zur Ermittlung von Jahresfrachten. Im Vergleich zur Simulation mit mittleren Ereigniskonzentrationen bleibt zudem noch die Ereignisdynamik erhalten, dass eine weitergehende Analyse durch MV-Kurven ermöglicht. Der entwickelte Kalibrieransatz verbessert stadthydrologische Planungen durch realitätsnähere Simulationsergebnisse von Stofffrachtmodellen und trägt somit zu einer höheren Kosteneffizienz im Gewässerschutz bei.

Abstract

The pollution of urban stormwater runoff requires measures to reduce negative impacts on the receiving water. Depending on land usage or level of pollution, common stormwater management strategies employ both centralized and decentralized measures. To design stormwater treatment facilities and to evaluate the emission of pollutants from an urbanized environment, stormwater quality models are usually applied. However, available models only provide simplified model concepts to simulate the origin, accumulation and transport of pollutants on urban surfaces which subsequently leads to uncertain model results. As a consequence, stormwater management measures are less cost-effective designed or even do not appropriately protect the receiving water. Hence, more realistic model outputs relating to stormwater quality are required. In this respect, the analysis and an in-depth understanding of natural stormwater pollutant processes is crucial to improve model concepts. Spatial and temporal variations need to be considered as well as meteorologic and anthropologic conditions. For this, high-resolution monitoring data of stormwater quality is essential.

In this thesis, a long-term monitoring and sampling program has therefore been conducted at four common types of urban subcatchments to obtain the required measurement data. Stormwater quality data from i) a flat roof, ii) a parking lot, iii) a residential catchment with a separated sewer system and iv) a high traffic street was collected. With primary focus on the quality parameter Total Suspended Solids (TSS), turbidity signals were used as a surrogate to derive continuous TSS time series.

Measurement data were subjected to extensive statistical analyses and correlated with meteorological characteristics. The analysis revealed a strong relationship between rainfall intensity and event loads for small catchments with a high proportion of impervious surface. Moreover, intra-event TSS load distributions were studied with dimensionless Mass-Volume-Curves (MV-Curves). For the first time, MV-curves were grouped at runoff quantiles and statistically described with box-plots. From this analysis the wash-off process could be site-specifically assessed. While the wash-off process of subcatchment flat roof tends to be source-limited, a transport-limited behavior could be observed at sites parking lot and high traffic street. A seasonal analysis of MV-curve distributions demonstrated a large variability.

Empirical TSS event load distributions were derived for all experimental sites and used to fit a set of theoretical distribution functions. Parameters of the targeted distribution functions were optimized with respect to a likelihood function. The lognormal distribution function was found to be most expressive to approximate empirical TSS event load distributions at all experimental sites. However, the goodness-of-fit of the statistical model strongly depends on the number of events

taken into account. Results of a Monte-Carlo resampling strategy suggest to provide about 40 events.

Fitted lognormal distribution functions were finally used to develop an innovative calibration approach of the stormwater quality model SWMM. The method incorporates practical needs, respects stochasticity of pollutant processes and prioritizes to probabilistically simulate TSS event load characteristics instead of replicating its occurrence and extent with chronologic precision. For this purpose, SWMM's model parameters of the exponential equations for pollutant accumulation and washoff have been numerically optimized by means of a differential evolution algorithm. The objective function to be minimized describes the numerical difference between the cumulated distribution function of simulated TSS event loads and the catchment-specific lognormal distribution function. Although a simplified stormwater quality model concept is applied, both model results and parameter uncertainties demonstrate the suitability of the approach to estimate annual TSS event loads. Additionally, compared to the conventional Event-Mean-Concentration (EMC) concept, intra-event dynamics are still preserved. This in turn facilitates purposive stormwater management strategies which consequently yield to both environmental and economic benefits.

Table of Contents

| | |
|---|------|
| List of Figures | III |
| List of Tables | V |
| List of Acronyms | VII |
| List of Publications..... | VIII |
| Author's contributions | X |
| Part A | |
| 1 Introduction | 1 |
| 1.1 Background | 1 |
| 1.1.1 Stormwater runoff quality and urbanization..... | 1 |
| 1.1.2 Process overview and phenomenology..... | 2 |
| 1.1.3 Modelling stormwater quality..... | 4 |
| 1.2 Research gap | 6 |
| 1.3 Objectives..... | 8 |
| 2 Experimental sites and monitoring setup | 11 |
| 2.1 Experimental sites | 11 |
| 2.2 Monitoring and sampling setup..... | 13 |
| 2.3 Data management | 15 |
| 3 Methodology | 17 |
| 3.1 Analysis of monitoring data..... | 17 |
| 3.1.1 Continuous TSS time series from turbidity data | 17 |
| 3.1.2 Rainfall event definition | 18 |
| 3.1.3 Calculation of runoff and TSS event characteristics..... | 18 |
| 3.1.4 Correlation analysis..... | 18 |
| 3.1.5 Analysis of TSS intra-event dynamics..... | 19 |
| 3.2 Probabilistic modelling of TSS event loads..... | 19 |
| 3.2.1 Theoretical distribution functions..... | 19 |
| 3.2.2 Monte-Carlo resampling to determine minimum sample size..... | 21 |
| 3.3 Software environment for model calibration..... | 22 |
| 3.4 Continuous modelling of stormwater quality | 25 |
| 3.4.1 Stormwater management model SWMM | 25 |
| 3.4.2 Concept of model calibration..... | 25 |
| 3.4.3 Parameter estimation and goodness-of-fit assessment ... | 26 |

II

| | | | |
|---|---|----|-----|
| 3.4.4 | Concept of model validation | 27 | |
| 3.4.5 | Model parameter uncertainty analysis | 27 | |
| 3.4.6 | Estimation of annual TSS loads..... | 28 | |
| 3.5 | Summary of methods applied..... | 28 | |
| 4 | Results and discussion..... | 29 | |
| 4.1 | Stormwater quality analysis..... | 29 | |
| 4.1.1 | TSS sample statistics | 29 | |
| 4.1.2 | Relationship between TSS and turbidity | 30 | |
| 4.1.3 | Event database..... | 31 | |
| 4.1.4 | Correlation analysis | 33 | |
| 4.1.5 | Intra-event TSS load distributions..... | 34 | |
| 4.1.6 | Seasonal intra-event TSS load distributions..... | 36 | |
| 4.2 | Probabilistic modelling of TSS event loads | 38 | |
| 4.2.1 | Derived theoretical distribution functions | 38 | |
| 4.2.2 | Minimum sample size | 41 | |
| 4.3 | Distribution-based calibration of SWMM | 43 | |
| 4.3.1 | Calibration results..... | 43 | |
| 4.3.2 | Annual TSS loads..... | 48 | |
| 5 | Conclusions and outlook | 49 | |
| 5.1 | Stormwater quality processes at small sites | 49 | |
| 5.2 | Stormwater quality modelling | 50 | |
| 5.3 | Outlook..... | 51 | |
| 6 | References..... | 53 | |
| Part B | | | |
| Paper I - Stormwater Pollutant Process Analysis with Long-Term Online Monitoring Data at Micro-Scale Sites | | | 67 |
| Paper II - Statistical Distribution of TSS Event Loads From Small Urban Environments | | | 81 |
| Paper III - swmmr - An R package to interface SWMM..... | | | 95 |
| Paper IV - Distribution-based Calibration of a Stormwater Quality Model | | | 111 |

List of Figures

| | | |
|-------------|---|----|
| Figure 2-1. | Location of experimental sites Flat Roof (FR), Parking Lot (PL), Residential Catchment (RC) and High Traffic Street (HT) in the City of Muenster, North Rhine-Westphalia, Germany. | 12 |
| Figure 2-2. | Installation of monitoring devices at site FR..... | 13 |
| Figure 2-3. | Schematic overview of the monitoring station developed (Leutnant et al. 2016). | 14 |
| Figure 2-4. | Installation of suction hose and flow meter in separated sewers (left) and compact monitoring station for urban stormwater runoff (right). Runoff is pumped by a peristaltic pump from the sewer into a measurement pipe equipped with quality sensors. | 14 |
| Figure 3-1. | Overview of methods used in this thesis..... | 28 |
| Figure 4-1. | Empirical cumulative distribution functions and boxplots of site-specific monitored TSS event loads (FR: Flat Roof, HT: High Traffic Street, PL: Parking Lot, RC: Residential Catchment) (Leutnant et al. 2018c). | 33 |
| Figure 4-2. | Site-specific MV-curves (FR: flat roof, RC: residential catchment, PL: parking lot, HT: high-traffic street) (modified from Leutnant et al. (2016)). | 34 |
| Figure 4-3. | Site-specific boxplots of MV-curve distributions at runoff volume quantiles (FR: flat roof, RC: residential catchment, PL: parking lot, HT: high-traffic street). Box ranges correspond to the first and third quartiles. Median is indicated by a solid black horizontal line. Whiskers comprise lowest/highest value within $1.5 \times$ inter-quartile range. Outliers exceed whiskers' ends and are indicated by solid black dots (modified from Leutnant et al. (2016)). | 35 |
| Figure 4-4. | Seasonal- (horizontal) and site- (vertical) specific boxplots of MV-curve distributions at runoff volume quantiles (FR: flat roof, RC: residential catchment, PL: parking lot, HT: high-traffic street). Box ranges correspond to the first and third quartiles. Median is indicated by a solid black horizontal line. Whiskers comprise lowest/highest value within $1.5 \times$ inter-quartile range (IQR). Outliers exceed whiskers' ends and are indicated by solid black dots (modified from Leutnant et al. (2016)). | 37 |
| Figure 4-5. | Site-specific approximation of empirical TSS event load distribution functions with lognormal distribution function at all sites (Leutnant et al. 2018c). | 39 |
| Figure 4-6. | Approximation of empirical TSS event load distribution function grouped by year with lognormal distribution function at site FR and PL (Leutnant et al. 2018c). | 40 |
| Figure 4-7. | Mean and regions of one and two standard deviations of Kolmogorov-Smirnov's statistic as function of sample size from Monte-Carlo-based sampling for sites FR and PL. Critical values for 90% confidence are indicated as black solid line (Leutnant et al. 2018c). | 42 |

IV

Figure 4-8. Cumulative distribution functions of lognormal, observed and simulated TSS event loads (left) and distribution of residuals between observed and simulated event loads (right) at site Flat roof (Leutnant et al. 2018b). 44

Figure 4-9. Cumulative distribution functions of lognormal, observed and simulated TSS event loads (left) and distribution of residuals between observed and simulated event loads (right) at site Flat roof (Leutnant et al. 2018b). 45

Figure 4-10. Comparison of observed and simulated Mass-Volume-Curves for sites Flat Roof (left) and Parking Lot (right) (Leutnant et al. 2018b). 46

Figure 4-11. Cumulative distribution functions of lognormal and simulated TSS event loads for the observation period (calibration) and the 5 years period (validation) for sites Flat Roof (left) and Parking Lot (right) (Leutnant et al. 2018b). 47

List of Tables

| | | |
|------------|--|----|
| Table 2-1. | Site-specific time range of stormwater quality measurement data acquired | 15 |
| Table 3-1. | Theoretical distribution functions (Leutnant et al. 2018c)..... | 20 |
| Table 3-2. | Goodness-of-fit statistics used to evaluate the fitting (F_n denotes the empirical distribution function, F represents the fitted theoretical distribution function, sup abbreviates supremum which indicates the least element of x that is greater than or equal to all elements of x (“least upper bound”)) (Leutnant et al. 2018c)..... | 20 |
| Table 3-3. | Functions for the R environment provided by swmmr (modified from Leutnant et al. 2018a). | 24 |
| Table 3-4. | Quality model parameter and corresponding ranges used for calibration (Leutnant et al. 2018b) | 25 |
| Table 3-5. | Summary of simulation period and rainfall-runoff event selection criteria | 27 |
| Table 4-1. | Site-specific TSS sample statistics (FR: flat roof, RC: residential catchment, PL: parking lot, HT: high-traffic street) (Leutnant et al. 2016)..... | 30 |
| Table 4-2. | Site-specific TSS sample statistics of samples used for turbidity correlation (FR: flat roof, RC: residential catchment, PL: parking lot, HT: high-traffic street) (Leutnant et al. 2016)..... | 30 |
| Table 4-3. | Linear regression coefficients for correlation of TSS and turbidity ($TSS = f(turbidity) = a + b * turbidity$, FR: flat roof, RC: residential catchment, PL: parking lot, HT: high-traffic street) (Leutnant et al. 2016)..... | 31 |
| Table 4-4. | Description of event database with continuous monitoring data (FR: flat roof, RC: residential catchment, PL: parking lot, HT: high-traffic street) (Leutnant et al. 2016)..... | 31 |
| Table 4-5. | Descriptive statistic data (min, 0.1-, 0.25-, 0.5-, 0.75-, 0.9-percentiles, max, mean, standard deviation) of site-specific event characteristics; rainfall depth: H , max. rainfall intensity in 60 minutes (I_{max60}), max runoff (Q_{max}), runoff volume (Vol), TSS loads (Loads), and TSS event mean concentrations (EMC) (FR: flat roof, RC: residential catchment, PL: parking lot, HT: high-traffic street) (Leutnant et al. 2016)..... | 32 |
| Table 4-6. | Site-specific Pearson correlation coefficients (FR: flat roof, RC: residential catchment, PL: parking lot, HT: high-traffic street) for TSS loads and selected variables: rainfall depth, duration, and intensities (H , D_p , $I_{mean}:I_{max60}$), runoff characteristics (Q_{mean} , Q_{max} , volume), and antecedent dry weather period (ADWP). Bold values indicate correlation coefficients > 0.5 (Leutnant et al. 2016)..... | 33 |
| Table 4-7. | Results of fitting empirical TSS load distribution functions to theoretical distribution functions (FR: Flat Roof, HT: High Traffic Street, PL: Parking Lot, RC: Residential Catchment, LL: LogLikelihood, AD: Anderson-Darling | |

| | | |
|-------------|---|----|
| | statistic A^2 , KS: Kolmogorov-Smirnov statistic D_n) (Leutnant et al. 2018c)..... | 38 |
| Table 4-8. | Results of fitting empirical TSS load distribution functions grouped by year to lognormal distribution function (FR: Flat Roof, HT: High Traffic Street, PL: Parking Lot, LL: LogLikelihood, AD: Anderson-Darling statistic A^2 , KS: Kolmogorov-Smirnov statistic D_n) (Leutnant et al. 2018c). | 39 |
| Table 4-9. | Calibrated model parameters and corresponding uncertainty statistics (FR: Flat Roof, PL: Parking lot, sd: standard deviation, CoV: Coefficient of Variation, KS D_n : Kolmogorov-Smirnov distance) (Leutnant et al. 2018b)..... | 43 |
| Table 4-10. | Observed and simulated total TSS event loads (Leutnant et al. 2018b). | 45 |
| Table 4-11. | Observed (obs) and simulated (sim) TSS event mean concentrations (Leutnant et al. 2018b). | 46 |
| Table 4-12. | Goodness-of-fit matrix for observation period (calibration) and 5 years period (validation) (FR: Flat Roof, PL: Parking lot, KS D_n : Kolmogorov-Smirnov distance) (Leutnant et al. 2018b). | 48 |
| Table 4-13. | Simulated annual TSS loads (FR: Flat Roof, PL: Parking lot) (Leutnant et al. 2018b). | 48 |

List of Acronyms

| | | |
|--------------|--|--------------|
| α | rate constant of buildup per day (model parameter) | d^{-1} |
| AD | Anderson-Darling test statistic | - |
| B_0 | masses available at the beginning of simulation (t = 0) (model parameter) | $g\ m^{-2}$ |
| C_1 | washoff coefficient (model parameter) | - |
| CDF | Cumulative distribution function | - |
| CF | capacity factor (with regard to rainfall event) | - |
| COD | Chemical oxygen demand | $mg\ L^{-1}$ |
| ECDF | Empirical cumulative distribution function | - |
| EMC | TSS event mean concentration | - |
| Exp | Exponential distribution function | - |
| FNU | Formazin nephelometric units (unit of turbidity) | - |
| FR | Flat roof (monitoring site) | - |
| Gamma | Gamma distribution function | - |
| GIS | Geographical information system | - |
| H | Rainfall depth | mm |
| HT | High traffic street (monitoring site) | - |
| I_{max60} | Maximum rainfall intensity within 60 minutes | $mm\ h^{-1}$ |
| IQR | Inter quartile range | - |
| K | maximum possible buildup (model parameter) | $g\ m^{-2}$ |
| KS (D_N) | Kolmogorov-Smirnov test statistic | - |
| LL | Logarithm of likelihood | - |
| Lnorm | Lognormal distribution function | - |
| Loads | TSS loads | kg |
| MCMC | Markov chain Monte-Carlo | - |
| MV-Curve | Mass-Volume-Curve | - |
| NSE | Nash-Sutcliffe-Efficiency | - |
| OSCAR | Online Supervisory Control and Urban Drainage Data Acquisition system with R | - |
| PAH | polycyclic aromatic hydrocarbons | - |
| PL | Parking lot (monitoring site) | - |
| RC | Residential catchment (monitoring site) | - |
| SCADA | Supervisory Control and Data Acquisition | - |
| sf | Simple features (with regard to spatial objects) | - |
| SS | Suspended solids | $mg\ L^{-1}$ |
| SWMM | Stormwater management model | - |
| TN | Total nitrogen | $mg\ L^{-1}$ |
| TSS | Total suspended solids | $mg\ L^{-1}$ |
| UV-Vis | ultraviolet and visible spectroscopy | - |
| Vol | Runoff volume | L |
| Weibull | Weibull distribution function | - |
| μ EMC | mean of TSS event mean concentration | $mg\ L^{-1}$ |

List of Publications

This doctoral dissertation consists of a summary and of the following publications which are referred to in the text by their numerals:

- Paper I** *Stormwater Pollutant Process Analysis with Long-Term Online Monitoring Data at Micro-Scale Sites*
- Leutnant D.**, Muschalla D. and Uhl M.
Water, 8(7), S. 299. 2016.
- Paper II** *Statistical Distribution of TSS Event Loads From Small Urban Environments*
- Leutnant D.**, Muschalla D. and Uhl M.
Water (revised version submitted May 15th 2018).
- Paper III** *swmmr - An R package to interface SWMM*
- Leutnant D.**, Döring A. and Uhl M.
Environmental Modelling & Software (submitted March 7th 2018).
- Paper IV** *Distribution-based Calibration of a Stormwater Quality Model*
- Leutnant D.**, Muschalla D. and Uhl M.
Water (submitted April 26th 2018).

List of additional Publications

Peer reviewed conference publications:

- **Model-based time drift correction of asynchronous measurement data in urban drainage**
Leutnant D., Hofer T. Henrichs M., Muschalla D., and Uhl M.
 10th International Conference on Urban Drainage Modelling UDM 2015, Quebec, Canada, 20-23 September 2015.
- **OSCAR - An online supervisory control and urban drainage data acquisition system with R**
Leutnant D., Henrichs M., Muschalla D., and Uhl M.
 10th International Conference on Urban Drainage Modelling UDM 2015, Quebec, Canada, 20-23 September 2015.
- **Performance Benchmark for Urban Drainage Model Calibration**
Schleifenbaum R., Henrichs M., Leutnant D., Fuchs L., and Uhl M.
 10th International Conference on Urban Drainage Modelling UDM 2015, Quebec, Canada, 20-23 September 2015.
- **Stormwater pollutant process analysis with long-term on-line monitoring data at micro scale sites**
Leutnant D., Muschalla D., and Uhl M.
 8th International Conference on Sewer Processes and Networks SPN, Rotterdam, The Netherlands, 31 August - 2 September 2016.
- **Machine Learning und Messdaten – Parameterfreie Detektion von Trockenwettertagen und Fremdwasseranalyse**
Leutnant D., Henrichs M., and Uhl M.
 AQUA URBANICA 2017 - Urbanes Niederschlagswassermanagement zwischen zentralen und dezentralen Maßnahmen, Graz, Austria, 3–4 July 2017.
- **Pollutant modelling based on empirical TSS load distributions**
Leutnant D., Muschalla D., and Uhl M.
 14th International Conference on Urban Drainage ICUD 2017, Prague, Czech Republic 10-15 September 2017.
- **Using Mass-Volume-Curves to Assess the Empirical Pollutant Modelling Concept**
Leutnant D., Muschalla D., and Uhl M.
 11th International Conference on Urban Drainage Modelling UDM 2018, Palermo, Italy, 23-26 September 2018.

Author's contributions

- Paper I** Dominik Leutnant and Mathias Uhl conceived, designed, performed and evaluated the experiments. Dominik Leutnant analyzed the data. Dirk Muschalla contributed to Sections 3 and 4. Dominik Leutnant wrote the paper.
- Paper II** Dominik Leutnant, Dirk Muschalla and Mathias Uhl conceived and designed the numerical experiments; Dominik Leutnant performed the numerical computations and evaluated the results; Dominik Leutnant wrote the paper and thanks Dirk Muschalla and Mathias Uhl for professional discussions.
- Paper III** Dominik Leutnant designed and developed the R package. Dominik Leutnant wrote the paper. Anneke Döring contributed to the code basis and the paper (GIS to SWMM conversion). Mathias Uhl participated in the writing of the paper.
- Paper IV** Dominik Leutnant, Dirk Muschalla and Mathias Uhl conceived and designed the numerical experiments; Dominik Leutnant performed the numerical computations and evaluated the results; Dominik Leutnant wrote the paper and thanks Dirk Muschalla and Mathias Uhl for professional discussions.

Part A

1 Introduction¹

A general introduction is given in the following chapter. First, an overview of urban stormwater quality, contaminants and influences is outlined. Relevant processes and phenomena are presented. Stormwater quality modelling approaches and current limitations are introduced. Based on this, research gaps are identified. Finally, the objectives of this thesis are specified.

1.1 Background

1.1.1 Stormwater runoff quality and urbanization

Stormwater runoff from urban areas is considered as a major nonpoint source of pollutants affecting the quality of the receiving water (Allen Burton and Pitt 2001). Makepeace et al. (1995) presented a literature review of stormwater pollution research and differentiated the hazardous effects of various contaminants with regard to humans and aquatic life. Their summary showed that especially i) solids, ii) heavy metals, iii) hydrocarbons and iv) nutrients are the most critical contaminants. However, the effect on the receiving environment depends on the contaminant and may result in acute or chronic toxicity (Aryal et al. 2010, Welker 2004). Certain polycyclic aromatic hydrocarbons (PAH) are classified as carcinogenic. Besides aesthetical issues, suspended solids (SS) fill interstitial spaces and adsorb PAHs and organic matter (Bilotta and Brazier 2008). Consequently, urban stormwater related emissions significantly degrade the aquatic environment and compromise the receiving ecosystem. To mitigate negative impacts stormwater treatment measures are required. However, naturally stormwater quality processes are complex and highly dynamic (Hvitved-Jacobsen et al. 2010) which impedes to implement cost-effective stormwater management strategies. Knowing relevant processes is therefore of high relevance (Barbosa et al. 2012, Beck and Birch 2013).

Numerous studies were conducted in the last three decades to investigate pollution processes and to quantify stormwater pollution with respect to i) solids (Charters et al. 2015, Chebbo and Bachoc 1992, Deletic and Maksimovic 1998, Rossi et al. 2013, Sansalone and Buchberger 1997), ii) heavy metals (Beck and Birch 2012, Davis and Birch 2010, Wijesiri et al. 2016, Zafra et al. 2017), iii) hydrocarbons (Aryal et al. 2005, Hengren 2005, Krein and Schorer 2000, Mummullage et al. 2016) and iv) nutrients (Bratieres et al. 2008, Miguntanna et al. 2013, Yang and Toor 2017).

The studies generally revealed that distribution and concentration of pollutants spatially and temporarily varies and stormwater quality is further affected by climatic and anthropologic conditions. However, land use (Goonetilleke et al. 2005), surface characteristic and human induced traffic (Fallah Shorshani et al. 2014, Li et al. 2017, Liu et al. 2015, Markiewicz et al. 2017) are identified as key influential

¹ This chapter is partly composed of paragraphs from Leutnant et al. (2018a, 2016, 2018c, 2018b)

factors which are coherently related to urban infrastructure and processes of urbanization.

According to United Nations (2015), urbanization is expected to increase notably on a global level in the next decades: In 1950 one third of the world's populations was urban which is projected to be the case for two thirds of the population by the year 2050. With respect to stormwater quality, this highlights the needs for purposive urban stormwater strategies as land use and traffic will significantly change (Gunawardena et al. 2018).

1.1.2 Process overview and phenomenology

Stormwater quality is affected by processes occurring both in the atmosphere and close to urbanized surfaces.

Pollutants accumulating in the atmosphere are assigned to atmospheric buildup. In contrast, atmospheric deposition describes the process of pollutants being transferred to the ground. It is further distinguished, whether particles are deposited due to humid (wet deposition, "rain washout") or due to windy conditions (dry deposition). Surface buildup describes the process of pollutant accumulation on urbanized surfaces which is assumed to take place during dry weather periods. In case of rainfall-induced washoff, pollutants on surface are first separated from the surface, subsequently mobilized or dissolved and finally transported by surface runoff (Gunawardena et al. 2018).

Atmospheric dry deposition of pollutants to terrestrial environments is mainly influenced by meteorological factors (wind velocity, humidity), particle size and shape and surface characteristics (roughness, temperature, friction velocity) (Amodio et al. 2014). Wet deposition additionally is dependent on rainfall intensity and duration (Gunawardena et al. 2018). Frequent rainfall with longer duration may cause dilution effects resulting in low pollutant concentrations.

Pollutant buildup on surfaces is influenced by both internal and external factors (Gunawardena et al. 2018). Particle size distribution is considered as major internal factor as different fractions tend to have different buildup characteristics (Wijesiri et al. 2015). In their study, in which particles were fractioned into the two groups $> 150 \mu\text{m}$ and $< 150 \mu\text{m}$, the buildup rate of the finer particle fraction decreased as function of time. The fraction with coarser particles was observed to behave conversely. External factors may either promote or suppress the accumulation of particles. Emissions from both anthropogenic (e.g. traffic, land use) and natural activities (e.g. soil erosion) promote buildup on surface and in the atmosphere as they increase the general availability of pollutants. In fact, traffic-related emissions are known to substantially contribute to heavy metal, PAH and particulate matter loadings (Egodawatta et al. 2013, Fallah Shorshani et al. 2014, Grottker 1987, Gunawardena et al. 2012, 2013, 2014, Helmreich et al. 2010, Petrucci et al. 2014, Sansalone and Buchberger 1997).

It is also reported, that accumulation of pollutants is subjected to seasonal influences. For example, Deletic and Orr (2005) showed that during road salting periods sediment loading significantly increased. A study by Brezonik and Stadelmann (2002) also indicated significant seasonal differences in loadings and concentrations of contaminants with highest pollutant contributions during snow-melt and spring runoff period (late January to early March). Seasonal affects were also studied by Lee et al. (2004). Their research revealed that initial storms of the wet season are higher polluted than storms near the end of the wet season. Helmreich et al. (2010) highlighted the use of gravel during winter periods which causes an increased wear and tear of surfaces and tires. Additionally, surface characteristics such as texture, roughness and relief affect buildup because refugial areas for pollutants are potentially created. International studies investigated pollutant contributions from different urban environments. Wang et al. (2013) determined stormwater contaminant concentration and loadings from common land uses (roofs, roads, residential and commercial catchments) in China. They found that urban roads contribute significantly higher total suspended solids (TSS) and chemical oxygen demand (COD) loads than other catchments. Egodawatta et al. (2012) quantified pollutant contributions from roof surfaces in Australia (Gold Coast) by means of simulated rainfall. They concluded, that roof surfaces play an import role concerning stormwater quality especially when roofs are dominating the land usage. Liu et al. (2015) point out that pollutant buildup on roads differs with different surface roughness or traffic characteristics. Especially, heavy metal buildup was observed to be more related to traffic congestion instead of traffic volume. The impact of antecedent dry weather period is however controversially presented in the literature. While several studies reported a significant impact (Miguntanna et al. 2010, Murphy et al. 2015, Shen et al. 2016), others found only a weak influence (Deletic and Orr 2005, Helmreich et al. 2010, Leutnant et al. 2016). Relevant processes suppressing pollutant buildup on urbanized surfaces are street sweeping, wind and air turbulences. However, effectiveness of street sweeping depends on frequency and method applied (Bender and Terstriep 1984).

Pollutant washoff is mostly influenced by rainfall characteristics such as intensity (Shen et al. 2016) and duration (Liu et al. 2012). In recent years, researchers used rainfall simulation to get a more in-depth understanding of the washoff process. Rainfall simulators were originally developed to analyse soil erosion and infiltration (Iserloh et al. 2012). For example, an Australian study used simulated rainfall to evaluate the effect of rainfall intensity, surface slope and texture (Egodawatta et al. 2007). Their study highlights that rainfall has only a specific capacity to mobilise a fraction of pollutants available on surface. Based on their findings they introduce the capacity factor (CF), reflecting the kinetic energy of rainfall and the turbulence in overland flow induced. It is further noted that high intensity rainfall events are able to mobilise coarser particles due to the injection of high turbulence. Default values for CF as function of rainfall intensity are given for three intensity classes.

A portable rainfall simulator configuration equipped with continuous flow and turbidity measurements was used on three sidewalks in the Paris region (Al Ali et al. 2017). Their application used a constant intensity of 120mm h^{-1} and demonstrated that especially fine ($<16\mu\text{m}$) to medium-sized ($<100\mu\text{m}$) particles are conveyed by surface runoff. It is also shown that smooth surfaces support particle transportation and that residual particles still remain after an event although the intensity was of high intense.

Muthusamy et al. (2018) conducted an experiment in which the influences of parameters i) rainfall intensity, ii) surface slope and iii) initial load were systematically investigated. They observed an increased washoff with increasing slope and rainfall intensity. It has been seen that only a fraction of available masses was completely washed-off, confirming previous studies. However, the maximum fraction that can be washed off from the surface increases with both rainfall intensity and the surface slope.

1.1.3 Modelling stormwater quality

Stormwater quality models are essential tools to support planning of urban water infrastructure. They are mainly used to evaluate emissions of pollutants from an urbanized environment which in turn affects stormwater management strategies and consequently the design of treatment devices. Having reliable model outputs is therefore of high relevance since infrastructural stormwater measures are cost-intensive and have a long service life. However, available stormwater quality models still replicate natural pollutant processes in a simplified manner, which in turn lead to uncertain model results (Dotto et al. 2011, 2009).

Stormwater quality models commonly differentiate the two conceptual phases i) buildup and ii) washoff (cf. 1.1.2) which both are deterministically described by empirical formula developed in the early 1970s (Sartor and Boyd 1972). In principle, this model concept assumes that the amount of pollutant masses at surface generally increases to a maximum as a function of antecedent dry weather periods and decreases in consequence of rainfall/runoff.

Previous studies however demonstrated the inadequacy of this simplified concept to continuously model pollutant concentrations. Muschalla et al. (2008) calibrated a buildup/washoff approach of a stormwater quality model to simulate chemical oxygen demand (COD) concentrations in stormwater discharges by means of a multi-objective auto-calibration scheme. Results obtained did not outperform a model employing a constant stormwater concentration approach. Sage et al. (2015) applied a bayesian calibration scheme based on Markov chain Monte-Carlo (MCMC) method to assess the build/washoff model performance to replicate continuous total suspended solid (TSS) concentrations and event loads. The authors confirmed the poor predictive power of the model applied and generally questioned the buildup/washoff approach.

Bonhomme and Petrucci (2017) indicate that pollutant models and its parameters lack of a physical meaning and thus represent rather black-box models. In fact, numerous authors propose a modified washoff equation to appropriately account

for rainfall characteristics. Egodawatta et al. (2007) and Muthusamy et al. (2018) for example suggest a capacity factor to reflect the impact of rainfall intensity and that only a fraction of pollutants are mobilized during storm events (cf. 1.1.2). Both rainfall intensity and a ratio of sediment mass per unit catchment area to rainfall intensity are also considered in a modification suggested by Zhao et al. (2015). Besides the sensitivity of rainfall intensity on the washoff process, Alias et al. (2014) highlights the intra-event variability of rainfall as another influential factor. Obviously, washoff is also influenced by particle characteristics and environmental variables such as surface type and land use as pointed out by Egodawatta et al. (2007) and Zhao et al. (2018).

Recent model developments have shown that physically-based washoff models are outperforming long-existing conceptual models. For example, Shaw et al. (2006) developed a saltation-type washoff model from laboratory experiments. Being mainly adapted from soil erosion research, the model detaches particles proportional to rainfall intensity and masses available at surface. Hong et al. (2016b) modelled the washoff process of a small road near Paris using a model system coupling the shallow water equations for overland flow and the Hairsine-Rose model for sediment detachment and transport (Delestre et al. 2017, Le et al. 2015). Results for water quantity and quality indicated a well agreement with in-situ observations. However, as a significant amount of input data is required and the simulation is computational expensive, the authors point out that the method proposed is currently not suitable for large urban catchments.

While a more physically-based description of rainfall induced washoff which also appropriately respects environmental and surface conditions would clearly improve representativity of model outputs, both pollutant buildup and washoff are significantly affected by stochastic inputs (Shaw et al. 2010) which in turn can hardly be predicted. As a consequence, Sage et al. (2015) stress the need for an alternative modelling approach, which also incorporates effects of stochasticity on pollutant buildup and washoff. This aligns with Harremoës (1988) who already claimed to respect stochasticity when using stormwater quality data.

Calibration of stormwater quality models conventionally aims to minimize the difference between observed and simulated pollutographs (Niazi et al. 2017). While this allows to incorporate intra-event variability, pollutant stochasticity is rarely taken into account as goodness-of-fit is generally calculated event-specific.

Several studies in the past decades respected probabilistic pollutant characteristics. Scholz (1995) applied an autoregressive moving-average modelling approach for both continuously buildup and washoff of pollutant concentrations to account for unpredictable environmental impacts. However, the approach could not be appropriately calibrated because of lack of data. Motivated by unavailable urban storm runoff quality data, Osman Akan (1988) analytically derived a frequency distribution to predict annual solids washoff from impervious urban areas.

His concept takes rainfall characteristics and catchment parameters for buildup and washoff into account and is exemplified for an artificial industrial catchment. Due to lack of data, the approach could also not be validated. A probabilistic approach to model TSS loads and dynamics of urban areas has also been proposed by Rossi et al. (2005). Their concept uses i) a parameterized power function to approximate intra-event TSS dynamics with normal distributed exponent ii) log-normal distributed event mean concentrations (EMC) to estimate total TSS masses per event and iii) a uniform distributed daily wastewater discharge combined with a constant TSS concentration. While the practical benefit of the model is clearly highlighted, the authors point out the simplified process description and its limited predictive power. Chen and Adams (2007) introduce a general probability distribution approach in which cumulated distribution functions for pollutant loads and event mean concentrations are obtained from probabilistic rainfall-runoff transformation. Sharifi et al. (2011) performed Monte-Carlo simulations and used corresponding results to assess the effects of stormwater best management practices on water quality for six toxic metals. As Rossi et al. (2005) they also assumed a power law relationship between runoff and pollutant concentrations during an event. However, they stochastically considered the exponent of the used power equation for the intra-event relationship, which in turn led to a large amount of pollutographs to be analyzed.

A refinement of the exponential washoff equation by incorporating stochastic fluctuations is analyzed by Daly et al. (2014). Here, the coefficient dominating the washoff process is assumed to be random and consequently addressed by adding gaussian noise. A good agreement to empirical distributions for TSS and TN (Total Nitrogen) is reported, which required large amount of data, though. Qin et al. (2013) obtained frequency distributions of i) event pollutant load, ii) event mean concentration and iii) peak concentration of COD from a continuous simulation of an urbanized catchment. Exponential equations for buildup and washoff were employed and calibrated with regard to continuous COD concentration measurement data using a genetic algorithm. It is however mentioned, that the predictive power is limited because the study site undergoes further developments. Annual loads for micropollutants have been estimated based on theoretical distribution functions of event mean concentration for three residential catchments by Hannouche et al. (2017).

1.2 Research gap

Stormwater quality models are known to be far from being reliable (Francey et al. 2010). The predictive capability of available stormwater quality models to replicate pollutographs is inferior to hydrographs (Niazi et al. 2017). Improving quality models is crucial to produce more reliable model results. In this respect, in-depth knowledge of processes is a key requirement which consequently demands measurement data.

In recent years much effort has been spent to investigate the influence of meteorological influences and catchment characteristics on stormwater quality based on samples at small sites (Alias et al. 2014, Egodawatta et al. 2012, Liu et al. 2013). Samples support the assessment of stormwater quality and the estimation of pollutant loads. However, due to low sampling frequency, intra-event dynamics are hardly revealed.

In this respect, the development of advanced on-line monitoring techniques in the past two decades allows both researchers and practitioners to get more insights of stormwater pollutant processes. High resolution online data supports the analysis of environmental, temporal and spatial influences on flushing characteristics of e.g. the parameter total suspended solids (TSS). Continuous signals of UV-Vis spectrometers or turbidity sensors are frequently used to study intra-event pollutant processes and to estimate event loads or event mean concentrations (Bertrand-Krajewski et al. 1998, Bertrand-Krajewski 2004, Caradot et al. 2015, Di Modugno et al. 2015, Gruber et al. 2004, Métadier and Bertrand-Krajewski 2012, Sun et al. 2015). Studies which employed on-line techniques generally presented heterogeneous data indicated by significant variability of pollutographs. This evidently demonstrates the complex nature of pollutant processes (Métadier and Bertrand-Krajewski 2012). However, it has not been investigated whether the process variability is also significant for small sites. It is believed that monitoring at small urban environments is required to isolate relevant pollutant processes and to reduce interfering influences of catchment size and environment. Consequently, applying continuous on-line monitoring techniques to monitor small sites creates a novel opportunity to study pollutant process at small sites.

Furthermore, stormwater pollutant processes are affected by stochastic influences which have to be considered (Shaw et al. 2010). As available models show poor performance to replicate long-term pollutant processes, alternative model approaches are required (Sage et al. 2015). The literature review of stormwater quality modelling (section 1.1.3) shows various approaches to take stochasticity of pollutant processes into account. While early studies primarily used probabilistic methods to overcome scarcity of stormwater quality data, recent studies using continuous quality data tend to admit the variability of natural pollutant processes by employing stochastic concepts. With regard to continuous long-term stormwater quality simulations, alternative modelling approaches presented incorporate stochasticity through i) probabilistic description and transformation of model input data (rainfall-runoff), ii) modification of empirical pollutant buildup/washoff equations, iii) distribution-based parameterization of intra-event dynamics and iv) probabilistic analysis of model results after calibration (post-processing).

It has however not been investigated, whether available stormwater quality models can be calibrated towards probabilistic pollutant characteristics. Using a distribution-based calibration proposes an additional alternative to incorporate pollutant stochasticity. In contrast to approaches already introduced, this method maintains existing model concepts and avoids expensive post-processing.

This however requires sufficient stormwater quality data, especially of event loads and concentration.

This work fundamentally aims towards new insights of stormwater quality processes and modelling which in turn improves urban stormwater management. Research questions identified address i) application of continuous online monitoring techniques at small sites, ii) process analyses using high resolution online data and iii) modelling with respect of natural pollutant stochasticity.

1.3 Objectives

According to the research gap identified in section 1.2, the main objective of this thesis is to develop a general applicable methodology to increase reliability of stormwater quality models.

High-resolution online data of stormwater quality are prerequisite and thus collected at common urban environments such as i) flat roof (FR), ii) parking lot (PL), iii) residential catchment (RC) and iv) high traffic street (HT). Compact monitoring stations equipped with quality probes and peripheral hardware are developed and locally installed. An innovative data management system is implemented to guarantee high-quality data. Data are subjected to extensive statistical analysis to assess correlations of environmental conditions and stormwater quality. Probabilistic analyses are conducted to respect random pollutant processes, primarily for the parameter total suspended solids (TSS). Parameters of the deterministic stormwater quality model SWMM are innovatively calibrated to account for pollutant stochasticity.

The first paper (**Paper I**, Leutnant et al. (2016)) introduces the experimental sites selected including the monitoring devices and sampling setup employed. Results of the long-term monitoring program and of the statistical analysis are given. Intra-event pollutant processes are described with Mass-Volume-Curves with respect to experimental site and season.

The second paper (**Paper II**, Leutnant et al. (2018c)) investigates the data further by means of probabilistic analysis. Theoretical distribution functions are fitted to approximate site-specific TSS event loads. Goodness-of-fit is assessed for both the entire event data, yearly grouped events and randomized sampled events to evaluate sensitivity and representativity of data acquired.

Paper III (Leutnant et al. 2018a) shortly communicates on an R package to support modelling with SWMM. The package fundamentally prepares **Paper IV** (Leutnant et al. 2018b) to allow for rapid and flexible prototyping of new model calibration schemes and assessment methods.

Finally, the fourth paper (**Paper IV**, Leutnant et al. (2018b)) presents an innovative distribution-based calibration approach for urban stormwater quality models. Its application is exemplified at the two experimental sites i) flat roof and ii) parking lot. Benefits, limits and requirements of the developed methodology are discussed.

More specifically, the objectives of this dissertation are to

- (i) develop and install monitoring stations to continuously observe stormwater runoff quality at small urban environments
- (ii) analyse environmental, climatic and anthropologic impacts on the pollutant processes using continuous turbidity measurement data
- (iii) evaluate pollutant characteristics with probabilistic methods
- (iv) develop a stormwater runoff quality modelling approach which accounts for natural stochasticity
- (v) apply and validate the modelling approach with measurement data from the experimental sites

2 Experimental sites and monitoring setup²

Chapter 2 introduces the experimental sites used to collect stormwater quality measurement data. Monitoring techniques, sampling setup and the developed measurement data management system are presented.

2.1 Experimental sites

A meaningful analysis of stormwater quality processes *accumulation* and *washoff* requires the selection of representative experimental sites. Relevant urban environments can be classified into i) roofs, ii) roads and iii) residential catchments. To identify possible sites for each class, spatial information of the city of Muenster and sewer system data were queried by means of geographic information system (GIS). The following seven criteria were defined and checked:

1. The catchment must be representative with respect to urban characteristics and pollutant loads (e.g. catchments with construction sites need to be excluded as they contribute unpredictable loads of contaminants).
2. The catchment must be drained with separated sewers with no additional infiltration water to specifically measure stormwater quality.
3. The catchment size should not exceed approx. 10 ha to isolate relevant processes and to minimize unknown process interferences.
4. The catchment should be in close proximity to the institute as logistical expenditures are required to be minimized.
5. Power and water supply is available.
6. Accessibility to sewer must be safe and simple.
7. Discharge measurement is free of interference and no backwater occurs.

After potential locations were GIS-based determined, each site was individually assessed by in-situ inspections. Criteria *accessibility* and *discharge measurement* were particularly restrictive since many sewers were not safely accessible or reliable flow measurements could not be installed. As a result, four sites were identified to reliably measure stormwater runoff and quality continuously.

The experimental sites selected are (i) a 50 m² flat roof (FR); (ii) a parking lot (PL) with approx. 2,350 m² and 78 parking spaces; (iii) a 9.4 ha residential catchment (RC) in a suburb of Muenster, Germany (separate sewer system); and (iv) a high-traffic (HT) street in the center of Muenster (2.5 ha, 30,000 vehicles per day). The roof is covered with bitumen sheeting and has an average slope of 2%. Runoff is drained via a downpipe with a nominal diameter of DN 110, whose inlet is arranged in the corner area. Surfaces of the parking lot are asphalt (55%), porous pavement (40%, 8% thereof being joints) and small vegetated pervious areas (5%) which do not contribute to runoff. The impervious area has a slope of 2.5%. Stormwater runoff is discharged via a DN 300 concrete sewer. The residential catchment consists of streets (25%), flat and steep roofs (25%), and pervious

² This chapter is partly composed of paragraphs from Leutnant et al. (2016)

area (50%). At site HT surfaces mainly consist of asphalt (60%), porous pavement (10%, 8% thereof being joints), flat and steep roofs (25%), and disconnected pervious area (5%). Figure 2-1 shows the location of experimental sites used in this thesis.

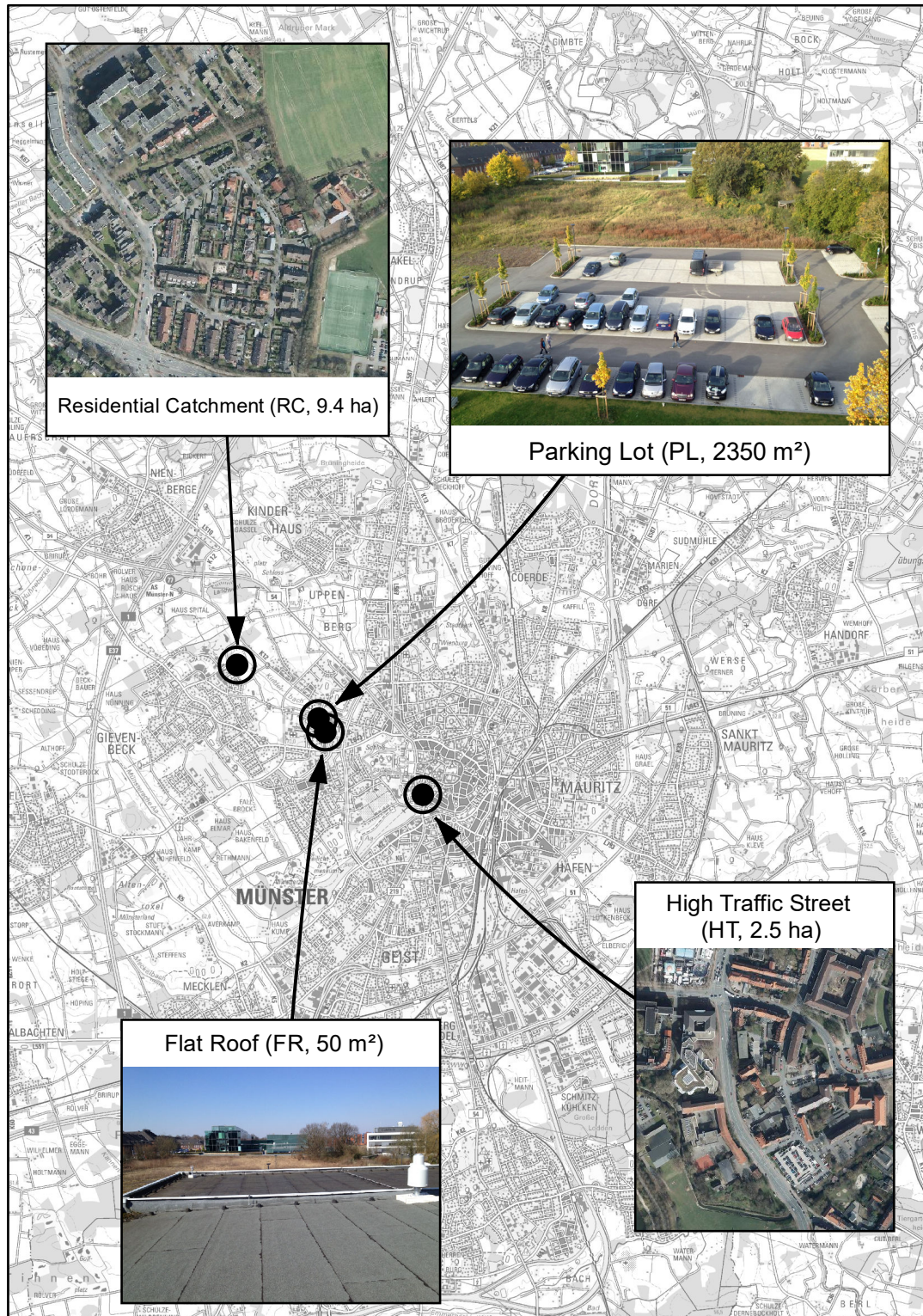


Figure 2-1. Location of experimental sites Flat Roof (FR), Parking Lot (PL), Residential Catchment (RC) and High Traffic Street (HT) in the City of Muenster, North Rhine-Westphalia, Germany.

2.2 Monitoring and sampling setup

Individual rain gauges of type Pluvio2 (OTT) are directly installed at FR, PL, and RC. Rainfall data from FR is also used for HT, being 2 km off FR. Runoff at FR runs from a downpipe into a horizontal measurement pipe (63 mm, PVC) in which an electromagnetic flowmeter (Promag50W25, Endress + Hauser) and quality sensors for turbidity, electrical conductivity, and pH (VisoTurb700IQ, Tetra-Con700IQ, and SensoLyt700IQ, WTW) are installed (Figure 2-2). Samples are taken from the measurement pipe with an automatic sampler (vacuum sampler ASP Station, Endress + Hauser). Sampling begins if runoff is above 0.03 L/s and repeats every 10 min. Each sample consists of five subsamples of about 200 mL. The capacity of the automatic sampler is 12 samples.



Figure 2-2. Installation of monitoring devices at site FR

The control section at PL is a 300 mm circular concrete pipe (length 55 m, slope 1.8%). Runoff is calculated from measured water level by the Manning-Strickler-equation because of uniform flow conditions and no backwater effects. Manning's roughness coefficient n was experimentally determined with artificial inflows and ranges between 0.015 and 0.017. At RC and HT runoff is calculated from mean flow velocity and water level (POA, NIVUS). The control section at RC is a 900 mm circular concrete pipe (length 46 m, slope 1.8%). Manning's roughness coefficient n was also identified with artificial inflows and is about 0.0105. At HT, flow sensors are installed in a 500 mm circular concrete pipe (length 30 m, slope 0.6%).

In contrast to FR, quality sensors at PL, RC, and HT are integrated in a horizontal measurement pipe (63 mm, PVC, length: 1.5 m) of an external monitoring station (Figure 2-3 and Figure 2-4). In case of an event, stormwater is pumped to the measurement pipe by a peristaltic pump (Delasco 2Z3, PCM) through a hose (20 mm, PVC) whose orifice is fixed in the middle of the stormwater pipe 1.5 cm above the ground (Figure 2-4).

The suction velocity in the hose is about 1.5 m s^{-1} with a corresponding flow of approx. 0.5 L s^{-1} . Stormwater flows with approx. 0.18 m/s through the measurement pipe and is later discharged to the sewer. At these sites, the sampling program starts if the water level in the stormwater pipe exceeds 1.5 cm . Samples of all sites are tested for total suspended solid (TSS) concentrations based on a standard method given in (US-EPA 1971), and fine solids less than $63 \mu\text{m}$ (TSS63) according to the protocol given in Dierschke and Welker (2015).

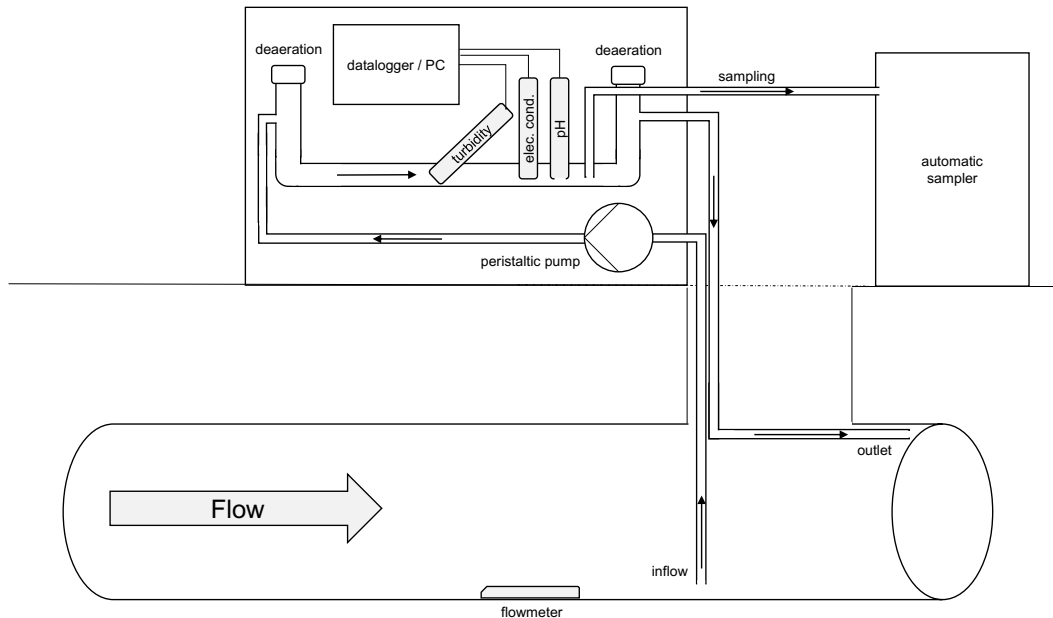


Figure 2-3. Schematic overview of the monitoring station developed (Leutnant et al. 2016).

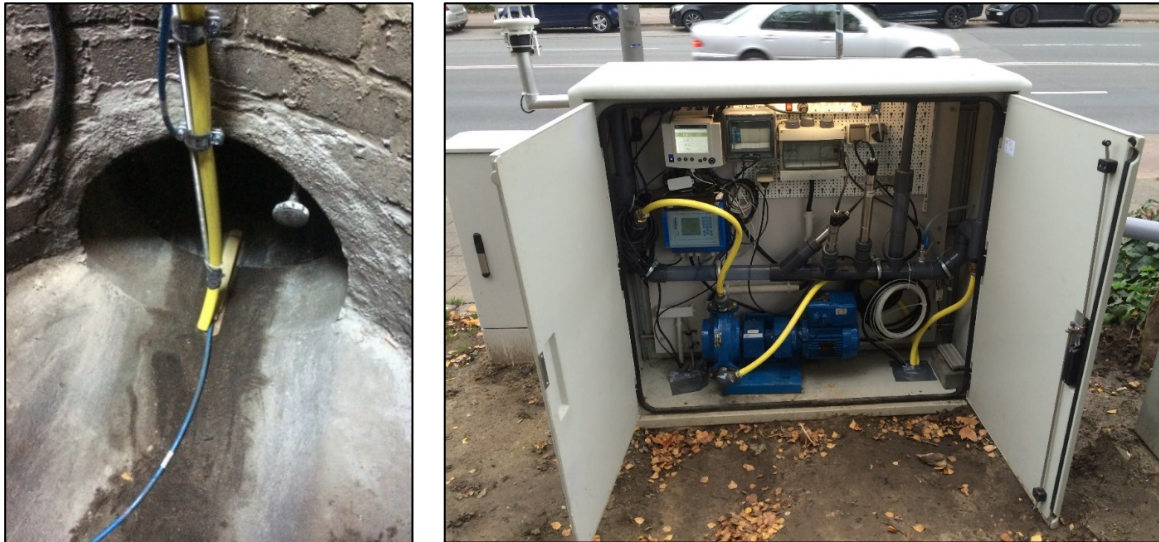


Figure 2-4. Installation of suction hose and flow meter in separated sewers (left) and compact monitoring station for urban stormwater runoff (right). Runoff is pumped by a peristaltic pump from the sewer into a measurement pipe equipped with quality sensors.

2.3 Data management

Monitoring urban stormwater quality include manifold, heterogeneous and spatially distributed data sources. Commonly, high-resolution online sensors and signal processing technologies are applied which have led to an increased amount of environmental data. This consequently requires an appropriate Information Technology (IT) infrastructure. Typically, this is defined and covered by core functions of Supervisory Control and Data Acquisition (SCADA) systems available (Campisano et al. 2013). However, available systems are mostly proprietary, cost-intensive and require a case-specific customization. Moreover, the use of different systems for data acquisition and provision for further analysis, such as time series analysis, validation or visualization, eventually lead to complex work flows and thus is prone to errors. In this respect, the open source language and environment for statistical computing R (R Core Team 2018) is becoming vastly popular for data management or visualization tasks. Its functions can easily be extended due to its flexible package-oriented concept. Using R for urban drainage data acquisition and further processing is seen to be an efficient alternative to address data challenges.

In this thesis, data of all monitoring stations were automatically processed and quality controlled with the *Online Supervisory Control and Urban Drainage Data Acquisition system with R* (OSCAR) (Leutnant et al. 2015). Applying an automated data processing system greatly reduces data maintenance costs and signals eventual errors or malfunctions promptly. As this thesis heavily relies on high quality data, a supportive data management and provision system is of high relevance. In fact, the amount of data to be analyzed is considerable which highlights the importance of an adequate data analysis environment.

All sensor signals were logged with a 1 min frequency. High-resolution online runoff and quality data is available for approx. 2.5 years for sites FR and RC, 1.5 years for PL, and 0.5 years HT, respectively (Table 2-1).

Table 2-1. Site-specific time range of stormwater quality measurement data acquired

| site | measurement data range | | |
|------|------------------------|--------------|-------|
| | from (yyyy-mm) | to (yyyy-mm) | years |
| FR | 2013-03 | 2015-11 | 2.5 |
| PL | 2013-05 | 2014-11 | 1.5 |
| RC | 2013-07 | 2015-11 | 2.5 |
| HT | 2015-10 | 2016-03 | 0.5 |

3 Methodology

The following chapter 3 presents the methods employed to address the objectives of this thesis. Initially, methods to prepare and analyse the measurement data are given. An extended probabilistic analysis concept is outlined. In addition, computational steps required are described. Furthermore, an alternative stormwater quality model calibration approach is introduced. As the approach was prototyped within the programming language R, the developed R package to auto-calibrate the stormwater management model SWMM is illustrated.

3.1 Analysis of monitoring data³

3.1.1 Continuous TSS time series from turbidity data

Total suspended solids (TSS) are a key parameter to assess emissions related to urban stormwater. Test methods to determine TSS concentrations in water samples are internationally standardized and approved (DIN 38409-2 1987, US-EPA 1971). Testing water samples according to the standards is considered elementary but requires substantial financial and labor resources. Investigating stormwater pollutant processes implies sampling at high frequency as stormwater pollutant processes are known to be highly dynamic. This in turn would lead to immense analytical costs as a high number of samples would be subjected to analysis.

Advanced online monitoring techniques have been developed and applied in the past two decades which allows both researchers and practitioners to get more insights of stormwater pollutant processes. In contrast to sampling, online sensors provide continuous signals and thus allow an analysis based on high resolution. With respect to the quality parameter TSS, UV-Vis spectrometers (Caradot et al. 2015, 2013, Gruber et al. 2004) or turbidity sensors (Bertrand-Krajewski 2004, Deletic 1998, Lacour et al. 2009a, Leutnant et al. 2016, Métadier and Bertrand-Krajewski 2012) are frequently used as surrogate. This means, the signal monitored needs to be converted by an appropriate correlation function to obtain the parameter of interest (“equivalent parameter”). Correlation functions are strongly dependent on the water matrix and need to be site-specifically estimated (Métadier and Bertrand-Krajewski 2012).

To obtain correlation functions, turbidity of selected samples was measured before TSS analysis. Initially, this has been conducted in the original sample bottle (PE, squared base, slightly transparent). Due to significant variance of the measured turbidity, a black cylindrical PE-HD bottle (diameter 10.8 cm, height 18.1 cm) has been used later. While measuring the turbidity, the sample is homogenized with a magnetic stirrer at 450 rpm. The five-minute mean of the turbidity is recorded and assigned to the TSS concentration. Calibration of turbidity probes was conducted with formazine primary standard solutions. TSS concentrations and

³ This section is partly composed of paragraphs from Leutnant et al. (2016)

the corresponding turbidity values were subjected to correlation analysis. Resulting linear regression equations are used to create continuous TSS time series from raw turbidity signals. It is to be noted, that the process of converting turbidity to TSS concentration introduces uncertainties which are thoroughly discussed in the literature (Bertrand-Krajewski 2004, Hannouche et al. 2011, Lepot et al. 2013).

3.1.2 Rainfall event definition

Site-specifically acquired rainfall time series (Table 2-1) are used to extract relevant rainfall events. An event is considered relevant if the minimum rainfall depth H exceeds 2 mm and maximum rainfall intensity in 60 minutes $I_{\max 60}$ exceeds 2.5 mm h⁻¹. Rainfall events below these criteria usually do not contribute to relevant runoff. Missing values in either runoff or turbidity data caused an event to be excluded.

3.1.3 Calculation of runoff and TSS event characteristics

Based on continuous runoff and TSS time series, event volumes (Vol), event loads (loads), and event mean concentrations (EMC) are calculated according to Equations 3-1 - 3-3 for the events selected.

$$\text{Event volume (m}^3\text{): } Vol = \sum_{i=1}^n Q_i \Delta t \quad 3-1$$

$$\text{Event load (kg): } Load = \sum_{i=1}^n Q_i C_i \Delta t \quad 3-2$$

$$\text{Event mean concentration (mg L}^{-1}\text{): } EMC = \frac{Load}{Vol} \quad 3-3$$

where i = index of time series, n = number of data points of an event, Q_i = runoff at index i , Δt = time interval (i.e., 1 min), and C_i = TSS concentration at index i .

3.1.4 Correlation analysis

To investigate the correlation of different event characteristics on TSS event load, Pearson's empirical correlation coefficient is used. It is calculated according to Equation 3-4 and compares the empirical covariance to the root of the product of the standard deviations. However, it should be noted that the correlation coefficient only describes linearity between two variables. Nonlinear relationships cannot be identified.

$$\text{correlation coefficient (-): } r = \frac{\sum_{i=1}^n (x_i - \bar{x})(y_i - \bar{y})}{\sqrt{\sum_{i=1}^n (x_i - \bar{x})^2 \sum_{i=1}^n (y_i - \bar{y})^2}} \quad 3-4$$

where y = observation of variable y , x = observation of variable x , \bar{y} = mean of observation of variable y , \bar{x} = mean of observation of variable x .

3.1.5 Analysis of TSS intra-event dynamics

Intra-event distributions of TSS loads are examined by means of mass-volume-curves (*MV-curves*) (Bertrand-Krajewski et al. 1998, Geiger 1987). *MV-curves* describe the proportion of transported mass at a given runoff volume proportion. This method is usually used to visualize transported mass proportions and to analyze the first-flush phenomenon. Knowledge of catchment-specific first-flush characteristics is crucial to design cost-effective treatment or storage structures. However, *MV-curves* tend to be site-specific and vary greatly from event to event (Métadier and Bertrand-Krajewski 2012). Aggregation of similar *MV-curves* is therefore required to extract relevant information. Lacour et al. (2009b) for example, divide *MV-curves* in three different zones to classify similar events. Zone A contains curves with a dominant first-flush effect, while curves in Zone C tend to be more last-flush affected. Curves in Zone B are near the bisecting line and show a runoff-proportional mass transport.

This thesis also uses *MV-curves* to characterize the two types of wash-off process, namely *source-limited* and *transport-limited* wash-off (Bai and Li 2013, Zhao et al. 2016). Source-limited runoff events have, in general, sufficient energy to wash off all available particles on the surface. This occurs if either mass on surface is rather limited or the kinetic energy of rainfall/runoff is high enough. Transport-limited events are not able to completely remove available masses. Typically, these events occur either if the available masses are adequately high or the kinetic energy of runoff is insufficient. *MV-curves* are calculated for the four study sites and compared. A seasonal differentiation is conducted. Instead of using zones to classify *MV-curves*, boxplots of the transported mass proportions are created at runoff volume quantiles. With calculated and visualized interquartile ranges (IQR), the event variability and main wash-off trends can be observed and characterized.

3.2 Probabilistic modelling of TSS event loads⁴

3.2.1 Theoretical distribution functions

Site-specific distributions of empirical TSS event loads are derived and used to approximate theoretical distribution functions given in Table 3-1. For this purpose, distribution functions of type i) Exponential, ii) Gamma, iii) Lognormal and iv) Weibull are selected, as they closely correspond to observed distributions. In particular, these functions are only defined for positive values ($x > 0$) so that they inherently reflect one of the main characteristics of the empirical data. Additionally, parameters of the theoretical distribution functions are listed in the table. While the Exponential distribution has only one parameter, the Gamma, Lognormal and Weibull distributions offer two parameters to be estimated.

⁴ This section is partly composed of paragraphs from Leutnant et al. (2018c)

Table 3-1. Theoretical distribution functions (Leutnant et al. 2018c)

| name (abbreviation) | formula | parameter |
|---------------------|---|--------------------------------------|
| Exponential (exp) | $F(x) = \begin{cases} 0, & x \leq 0 \\ 1 - e^{-\alpha x}, & x > 0 \end{cases}$ | α (rate) |
| Gamma (gamma) | $F(x) = \begin{cases} 0, & x \leq 0 \\ \frac{b^p}{\Gamma(p)} \times \int_0^x t^{p-1} e^{-bt} dt, & x > 0 \end{cases}$ | p (shape), b (rate) |
| Lognormal (lnorm) | $F(x) = \begin{cases} 0, & x \leq 0 \\ \frac{1}{\sigma\sqrt{2\pi}} \times \int_0^x \frac{1}{t} e^{-\frac{1}{2}\left(\frac{\ln t - \mu}{\sigma}\right)^2} dt, & x > 0 \end{cases}$ | μ (meanlog), σ (sdlog) |
| Weibull (weibull) | $F(x) = \begin{cases} 0, & x \leq 0 \\ 1 - e^{-\alpha x^\beta}, & x > 0 \end{cases}$ | α (scale), β (shape) |

To fit theoretical distribution functions to an empirical distribution, distribution parameters need to be optimized. In this thesis, parameters are estimated by maximum likelihood method (exact standard error model: $\mu = 0$, $\sigma = 1$) because this also enables to analyse the standard error of estimated parameter. The likelihood function in general can be stated as follows (Equation 3-5):

$$\mathcal{L}(\theta) = f(x_1, x_2, \dots, x_n | \theta) = \prod_{i=1}^n f(x_i | \theta) \quad 3-5$$

with x_i the n observation of variable X (i.e., TSS event loads) and $f(\cdot | \theta)$ the density function of the theoretical distribution function used. Parameters to be optimized are denoted by θ .

Since computation of likelihoods could result in very small numbers which may cause numerical precision problems, the logarithm of likelihoods (LL) is taken instead. Fitting of theoretical distribution functions and numerical goodness-of-fit computations were utilized with *R* (R Core Team 2018) and the package *fitdistrplus* (Delignette-Muller and Dutang 2015). Once optimal parameters are estimated, the goodness-of-fit is evaluated by Kolmogorov-Smirnov (KS) and Anderson-Darling (AD) test statistics which are calculated according to Equations 3-6 and 3-7 given in Table 3-2.

Table 3-2. Goodness-of-fit statistics used to evaluate the fitting (F_n denotes the empirical distribution function, F represents the fitted theoretical distribution function, *sup* abbreviates supremum which indicates the least element of x that is greater than or equal to all elements of x ("least upper bound")) (Leutnant et al. 2018c).

| statistic (abbreviation) | Formula | |
|--------------------------|--|-----|
| Kolmogorov-Smirnov (KS) | $D_n = \sup_x F_n(x) - F(x) $ | 3-6 |
| Anderson-Darling (AD) | $A^2 = n \int_{-\infty}^{\infty} \frac{(F_n(x) - F(x))^2}{F(x)(1 - F(x))} dF(x)$ | 3-7 |

In general, both tests are used to test whether a sample follows a specific distribution by calculating the maximum distance between empirical and theoretical distribution function. This means smaller test statistics indicate a lower numerical distance to the distribution analyzed. The AD test refines the KS test and gives more weight to the distribution tails. The tests are applied to decide whether the null hypothesis H_0 "The sample follows a specified distribution" can be accepted or must be rejected at a specified significance level. Alternatively, hypothesis H_A is defined as "the sample does not follow a specified distribution". Critical values for the acceptance decision of the KS test are calculated according to Equation 3-8 for sample sizes > 35 . For sample sizes below 35, critical values are obtained from Hedderich and Sachs (2012).

$$d_\alpha = \sqrt{\frac{-0.5 \ln \left(\frac{\alpha}{2}\right)}{\sqrt{n}}}, \text{ for } n > 35 \quad 3-8$$

with sampling size n and significance level α .

3.2.2 Monte-Carlo resampling to determine minimum sample size

A Monte-Carlo simulation based resampling strategy without replacement has been conducted to analyse the effect of different sample sizes on the quality of distribution fitting. Motivated by the idea to determine a minimum sample size required, the computational steps are as follows:

1. Estimating parameters of lognormal distribution function by maximum likelihood taking all samples into account.
2. Sampling k ($k \in \mathbb{N}, 0 < k \leq n$) events from all events n with 1000 repetitions. If less than 1000 repetitions are possible, all possible combinations are taken into account (Equation 3-9).

$$repetitions = MIN \left(\binom{n}{k}, 1000 \right) \quad 3-9$$

with population n and sample size k .

3. Computing of KS distance between empirical cumulative distribution function of sample and theoretical distribution function with estimated parameters for all repetitions.
4. Computing of mean, standard deviations of KS distances for all repetitions.

The results are then interpreted and visually compared to the critical values for the Kolmogorov-Smirnov test statistic at 90 % significance level.

3.3 Software environment for model calibration⁵

Calibration of stormwater quality models by means of an optimization algorithm is considered computational expensive as numerous simulation runs need to be executed. Having an efficient and flexible software environment is required to configure and control the optimization task. For calibrating the stormwater quality model SWMM, both commercial (cf. Niazi et al. 2017) and free software are available (Henrichs 2015). However, implementing user defined objective functions is limited. In addition, depending on simulation duration and time step, the size of model output files is potentially huge. An efficient processing of simulation results can be addressed with modern computer architectures and programming languages. In this respect, the free software environment for statistical computing and graphics R (R Core Team 2018) is frequently used by both scientists and engineers. Since R's capabilities can be extended by packages containing arbitrary functions, the development of alternative algorithms is promoted. In fact, a huge variety of add-on packages is already available which could be employed to address issues related to urban drainage modeling such as model parameter optimization (e.g. Ardia et al. 2016), visualization (Vanderkam et al. 2017, Wickham 2016), time series management (Ryan and Ulrich 2017) or statistical analysis. Consequently, the availability of these packages enables an efficient data management and supports modelling with SWMM.

To bridge the gap between SWMM and R, the *swmmr* package (Leutnant et al. 2018a) has been developed and used in this thesis. Core functions of the package comprise fast reading and writing of SWMM files, conversion between GIS data and the SWMM input file format as well as model data transformation to produce expressive visualization.

At its core, the package relies on the tidy data concept (Wickham 2014) which is expressed through a set of harmonized packages sharing common data representation principles ("tidyverse" - Wickham 2017). Although most tasks could have been addressed with *base R*⁶, packages from the "tidyverse" tend to simplify both the programming and the data analysis. For example, *swmmr* uses `tibbles` (Müller and Wickham 2017) instead of R's build-in `data.frame` class to represent SWMM model sections. This becomes apparent in functions which parse SWMM text files, i.e. `read_inp()`, `read_rpt()` and `read_lid_rpt()` (Table 3-3). Generally, these functions take the path to a corresponding SWMM file (`*.inp` or `*.rpt`) and parse its content to a named list of `tibbles` or a single `tibble`, respectively.

`read_inp()` creates an object of class `inp`, whose list element names are identical to the names of SWMM input sections available in lower letters (e.g. `options`,

⁵ This section is partly composed of paragraphs from Leutnant et al. (2018a)

⁶ *base R* refers to a set of default packages which R is actually based upon without any additional packages loaded.

subcatchments). `read_rpt()` creates a named list of class `rpt` containing summary sections from the report file of SWMM (e.g. `subcatchment_runoff_summary`). While both of the aforementioned functions maintain the original SWMM file structure, `read_lid_rpt()` interprets text files from specific LID elements. A single `tibble` or index-based time series data of class `xts` object is returned accordingly.

Reading simulation output data from the binary `.out` file is supported by `read_out()`. Because of the potentially huge size of `.out` data, the function design aims for fast data processing, enabled by embedded C++ code through `Rcpp` (Eddelbuettel and François 2011). Output data per system element and model variable is always represented as object of class `xts` and conveniently stored in a list environment.

The function `write_inp()` writes an `inp` object to disk, which addresses cases where an `inp` object has been modified within R and changes need to be saved back to disk (e.g. model parameter calibration). Thus, it takes an existing `inp` object and creates a model file on disk which can be read and run by SWMM. A SWMM simulation run can be initiated from the R console with `run_swmm()` which takes the path to an `.inp` file and calls the SWMM executable with the required file paths as arguments.

Moreover, *swmmr* uses the simple features class (`"sf"` - Pebesma 2018) to represent SWMM input sections with spatial reference (e.g. subcatchment). Conversion of sections is supported with corresponding `*_to_sf()` functions.

Based on the conversion of SWMM input sections to simple feature geometries, an `inp` object can be converted to the popular `.shp` file format with `inp_to_files()`. Additionally, `.txt` files containing simulation settings, storage and pumping curves are returned as well as files containing SWMM time series data. As a counterpart the function `shp_to_inp()` converts spatial data given in `.shp` files into an `inp` object.

Information on simulation settings, rainfall time series etc. can be given in `.txt` files to complete the model data. While the conversion to `sf` objects already enables common spatial analysis of SWMM model data in R, this also allows using the plotting interface of `ggplot2` through `geom_sf()`.

The R package presented has been submitted to the Comprehensive R Archive Network (CRAN⁷) and can also be installed from GitHub⁸, where users might inspect or contribute to the code basis. In addition, the reader is referred to three package vignettes which explain how to auto-calibrate a SWMM model with *swmmr* or how to convert GIS and SWMM model data with *swmmr*.

⁷ <https://cran.r-project.org/package=swmmr>

⁸ <https://github.com/dleutnant/swmmr>

Table 3-3. Functions for the R environment provided by `swmmr` (modified from Leutnant et al. 2018a).

| Name | Inputs | Description |
|-----------------------------|---|--|
| <code>run_swmm()</code> | paths of <code>.inp</code> , <code>.rpt</code> and <code>.out</code> file | Initiate a SWMM run from the R console |
| <code>read_inp()</code> | path of <code>.inp</code> file | Reads a SWMM model as list of tibbles (i.e. <code>inp</code> object) |
| <code>read_out()</code> | path of <code>.out</code> file | Reads SWMM simulation results (time series) as list of <code>xts</code> objects |
| <code>read_rpt()</code> | path of <code>.rpt</code> file | Reads SWMM simulation results (summary) as list of tibbles |
| <code>read_lid_rpt()</code> | path of LID report file | Reads a SWMM LID Report File as tibble or <code>xts</code> object |
| <code>write_inp()</code> | inp object (optionally modified) and filename | Writes an <code>inp</code> file to disk which can be read and run by SWMM |
| <code>*_to_sf()</code> | inp object | Converts SWMM objects as tibble with simple feature geometries (supported objects are junctions, links, orifices, out-falls, pumps, raingages, storages, subcatchments, weirs) |
| <code>inp_to_sf()</code> | inp object | Converts an entire <code>inp</code> object as list of tibbles with simple feature geometries |
| <code>inp_to_files()</code> | inp object, model name and directory path | Converts <code>.inp</code> to <code>.shp</code> and <code>.txt</code> files |
| <code>shp_to_inp()</code> | s. package manual | Converts <code>.shp</code> files as list of tibbles (i.e. <code>inp</code> object) |

3.4 Continuous modelling of stormwater quality⁹

3.4.1 Stormwater management model SWMM

In this thesis pollutant processes for buildup and washoff are modelled with the widely used exponential equations implemented in the stormwater management model SWMM5 (Rossman 2010). Buildup $B(t)$ is mathematically described as function of antecedent dry weather days t (Equation 3-10). Pollutant washoff $W(t)$ is expressed as function of current runoff rate $q(t)$ and available masses on surface $B(t)$ (Equation 3-11). Both functions offer two individual parameters to be calibrated. Additionally, the initial buildup B_0 at the beginning of simulation ($t=0$) needs to be estimated. Table 3-4 shows the parameter used for calibration. Corresponding parameter ranges were extracted from literature (Gamerith et al. 2013, Sage et al. 2015) and harmonized with authors experience.

$$B(t) = k * (1 - e^{-\alpha * t}) \quad 3-10$$

with buildup coefficient k ($g\ m^{-2}$), buildup exponent α (d^{-1}), t denotes number of preceding dry weather days.

$$W(t) = C_1 * q(t)^{C_2} * B(t) \quad 3-11$$

with washoff coefficient C_1 (-), washoff exponent C_2 (-), runoff rate q ($mm\ h^{-1}$), available pollutant masses on surface B ($g\ m^{-2}$) and time index t .

Table 3-4. Quality model parameter and corresponding ranges used for calibration (Leutnant et al. 2018b)

| parameter | description | unit | range |
|-----------|---|-------------|---------------|
| B_0 | masses available at the beginning of simulation ($t = 0$) | $g\ m^{-2}$ | [1; 5] |
| K | maximum possible buildup | $g\ m^{-2}$ | [0.0001; 2] |
| α | rate constant of buildup per day | d^{-1} | [0.0001; 0.2] |
| C_1 | washoff coefficient | - | [0.0001; 1] |
| C_2 | washoff exponent | - | [0.0001; 3] |

3.4.2 Concept of model calibration

SWMM models are calibrated using a distribution-based approach. Instead of replicating single-event characteristics or pollutographs, the approach aims to minimize the difference between observed and simulated TSS event load distribution. Since observed TSS event load distributions can be well approximated with theoretical distribution functions (Leutnant et al. 2018c), the calibration uses a parameterized lognormal distribution as reference.

The approach focuses probabilistic event load distribution and puts less emphasis on intra-event dynamics. Model results are therefore required to be analyzed

⁹ This section is partly composed of paragraphs from Leutnant et al. (2018b)

by means of Mass-Volume-Curves (MV-Curves) (Bertrand-Krajewski et al. 1998). Sites FR and PL are modelled only, as sufficient data to calibrate is available.

3.4.3 Parameter estimation and goodness-of-fit assessment

For both sites to be modelled, parameters affecting runoff generation and hydrograph characteristics are initially calibrated by means of the multi-objective algorithm NSGA-2 (Deb et al. 2000). The algorithm allows to optimize multiple objectives simultaneously and identifies pareto-optimal solutions from which a compromise can be drawn. Here, a single objective is defined as an event-specific Nash-Sutcliffe-Efficiency (NSE) (Nash and Sutcliffe 1970). 8 rainfall-runoff events were taken into account which consequently yields 8 objectives to be optimized. The compromise solution follows the L2-metric (Deb 2008) which calculates the euclidean distance of all pareto-optimal solutions to an ideal solution. The solution with smallest euclidean distance is considered as compromise. Model parameters i) surface roughness, ii) depression storage and iii) characteristic width of the overland flow are considered for calibration. The calibration yielded an average event-specific NSE of 0.73 for site FR and 0.72 for site PL (results of water quantity calibration are not further discussed in this thesis).

Once optimized parameters of runoff calibration are estimated, model parameters for pollutant buildup and washoff (Table 3-4) are optimized. The calibration aim is to fit the simulated TSS event loads distribution to the parameterized lognormal distribution. For this purpose, the Kolmogorov-Smirnov (KS) statistic D_n which numerically describes the equality of two distributions and tests whether a sample follows a specific distribution (Hedderich and Sachs 2012) is used as objective function. This means the smaller the KS statistic D_n gets, the higher the goodness-of-fit of the calibration. The KS statistic ranges from $0 \leq D_n \leq 1$. As this calibration only considers a single objective, a single objective optimization algorithm is used. A differential evolution algorithm (Price et al. 2005) implemented by Ardia et al. (2016) is applied. The following computation steps are performed:

1. Simulation with a new set of parameters generated by the optimization algorithm.
2. Determine and split events from simulation time series which satisfy selection criteria (Table 3-5). An event starts when runoff starts and ends if the maximum runoff within a predefined window is 0.
3. Computation of runoff volume and TSS load per event.
4. Selection of events which exceeds a minimum runoff volume (Table 3-5). This step is introduced because the small size of the catchments leads to a significant number of events with numerically low runoff volume which would result in disproportionately weights to these events.
5. Computation of cumulative TSS event load distribution function for the events remaining.
6. Computation of Kolmogorov-Smirnov Distance D_n according to Equation 3.

$$D_n = \sup_x |F_{SWMM}(x) - F_{lognormal(\mu,\sigma)}(x)| \quad 3-12$$

with F_{SWMM} being the simulated cumulative TSS event load distribution function and $F_{lognormal}$ the site-specific parameterized lognormal distribution function.

7. Repeat steps 1 – 7 to minimize D_n until convergence.

Table 3-5. Summary of simulation period and rainfall-runoff event selection criteria

| | flat roof | parking lot |
|--|----------------------|-----------------------|
| simulation duration (observation period) | 2013/03 – 2015/11 | 2013/04 – 2014/10 |
| simulation duration (a) | 2.7 | 1.6 |
| days with rainfall ≥ 2 mm d ⁻¹ | 250 | 137 |
| event selection criteria | | |
| event window (min) | | 480 |
| min. runoff volume (L) | 19 (~0.4 percentile) | 465 (~0.2 percentile) |
| events selected (-) | 224 | 107 |

The goodness-of-fit of the calibrated stormwater quality model is numerically assessed and visually evaluated through a direct comparison of the simulated distribution function and the parameterized lognormal distribution function for TSS event loads. Residuals of the simulated event loads and observed event loads are computed. Simulated intra-event dynamics are analyzed by means of Mass-Volume-Curves (MV-Curves).

3.4.4 Concept of model validation

The calibration uses measurement data from site-specific stormwater quality observation period. Estimated parameters are expected to be valid beyond this period. Model validation therefore uses all available rainfall data from the 5 years period (2013/03 – 2018/04). Equality of simulated TSS event load distributions from the 5 years period and the observation period are evaluated using Kolmogorov-Smirnov's distance $KS D_N$ (cf. Equation 3-6).

3.4.5 Model parameter uncertainty analysis

The differential evolution algorithm applied belongs to the class of genetic algorithms which minimize an objective function by evolving a population of candidate solutions through successive generations (Ardia et al. 2016). In this study, the configuration of evolution strategy and mutating operators (crossover probability and differential weighting factor) follows the developers recommendations. However, the maximum number of iterations is set to 400 and the number of population members (i.e. parameter sets per iteration) is set to 100, which result in 40.000 simulation runs per model in total. For estimating model parameter uncertainties, simulation results are divided into behavioral and non-behavioral groups. Parameter sets which yield to the best 20 % solutions are attributed behavioral and subjected to statistical analysis.

3.4.6 Estimation of annual TSS loads¹⁰

The calibrated stormwater quality models are finally used to estimate annual TSS event loads and event mean concentrations originated from the study sites. Annual TSS event loads are estimated by considering all event loads from a moving window of 12 consecutive months to account for natural rainfall variability. Using the extended rainfall series, the simulation period comprises ~5 years with 62 months which yields 50 (62 – 12) moving years.

3.5 Summary of methods applied

The methods applied in this thesis are visually summarized in Figure 3-1. Based on continuous stormwater quality measurement data, event characteristics are initially determined and characterized. TSS concentrations and event loads are calculated and statistically analyzed. Afterwards, characteristics are probabilistically described and finally used for model calibration.

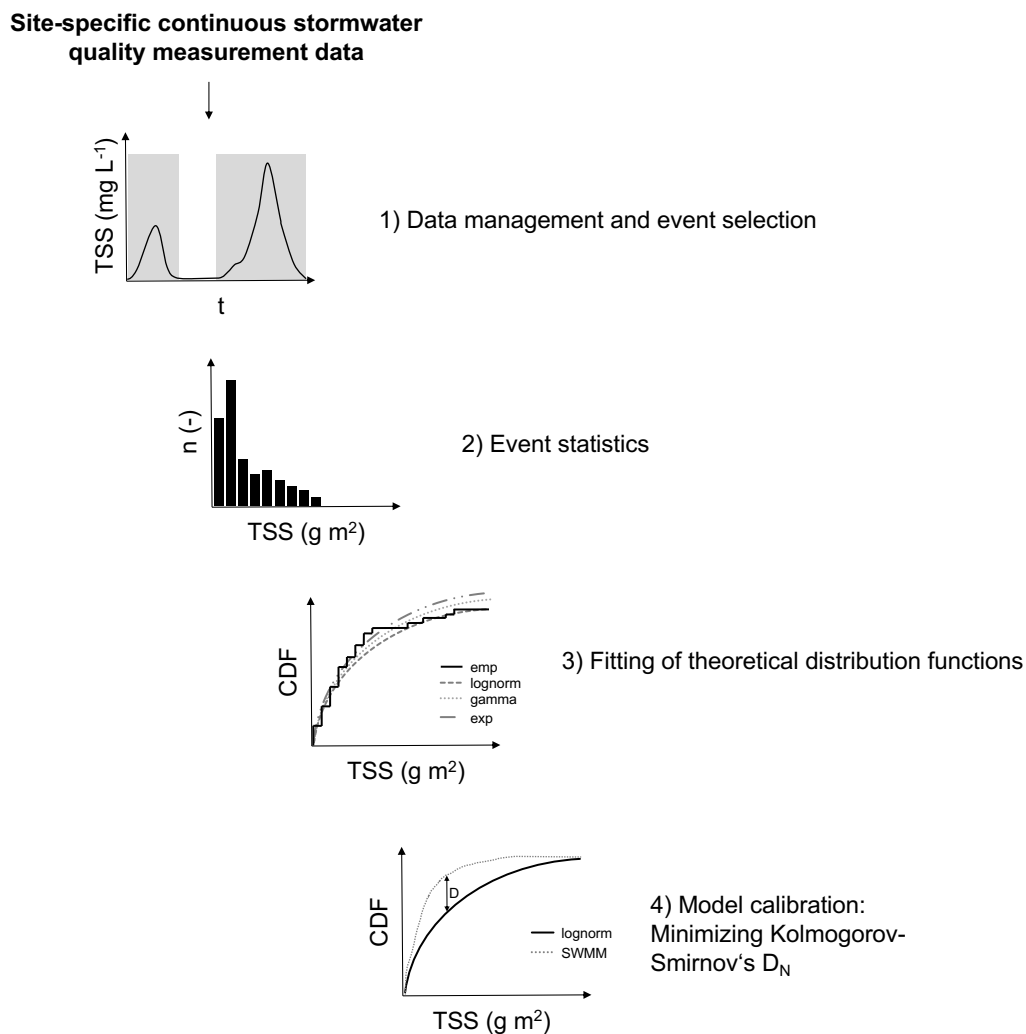


Figure 3-1. Overview of methods used in this thesis

¹⁰ This section is partly composed of paragraphs from Leutnant et al. (2018b)

4 Results and discussion

Chapter 4 presents results of this thesis. First, descriptive statistics of events observed are discussed. Intra-event processes are interpreted by means of Mass-Volume-Curves. Probabilistic TSS event load distributions are site-specifically inferred. Results of the developed calibration approach are shown. Finally, simulated annual loads for selected sites are given.

4.1 Stormwater quality analysis¹¹

4.1.1 TSS sample statistics

Table 4-1 summarizes TSS sample statistics at the four study sites. Statistics were also calculated for the dataset excluding outliers. Due to non-normality of the dataset, outliers are conservatively considered and defined as points beyond the mean \pm four times the standard deviation. Mean and standard deviation are iteratively computed while potential outliers are excluded.

At site FR, 193 samples were analyzed from 40 events. With the 0.75 percentile being 14.2 mg L^{-1} , the flat roof clearly shows low TSS potential and distributions are similar to other findings (Dierschke and Welker 2013, Förster 1999, Kobencic 2002).

For site RC, 269 samples of 39 events were taken. The distribution of TSS concentration also reveals low TSS contribution. Compared to the results of Brombach et al. (2005), values are lower than TSS concentrations of a separated sewer system in Germany. The mean value of 114.3 mg L^{-1} and the standard deviation of 339 mg L^{-1} indicates high variation. However, these statistics are strongly influenced by the maximum value of 3645 mg L^{-1} . The 0.9 percentile being at 205 mg L^{-1} confirms this.

140 samples from 38 events were analyzed for site PL. TSS concentration ranges from 7.3 mg L^{-1} to 1842 mg L^{-1} , with the median at 170 mg L^{-1} .

At HT, 92 samples of 17 events were collected. Compared to other studies at high-trafficked streets (Helmreich et al. 2010), the TSS statistics are significantly lower. For example, the median of 77.4 mg L^{-1} is less than half as the median in their study (175 mg L^{-1}).

¹¹ This chapter is partly composed of paragraphs from Leutnant et al. (2016)

Table 4-1. Site-specific TSS sample statistics (FR: flat roof, RC: residential catchment, PL: parking lot, HT: high-traffic street) (Leutnant et al. 2016).

| Site | Outlier excl. | n | Events | TSS (mg L ⁻¹) | | | | | | | | |
|------|---------------|----------------------|--------|---------------------------|-------|--------|--------|--------|-------|------|------|-----|
| | | | | Min | 0.1-P | 0.25-P | Median | 0.75-P | 0.9-P | Max | Mean | Sd |
| FR | no | 193 | 40 | 0.6 | 2 | 4 | 7 | 14 | 46 | 674 | 22 | 60 |
| | yes | 182 | 39 | 0.6 | 2 | 4 | 7 | 12 | 28 | 85 | 12 | 16 |
| RC | no | 269 | 39 | 1.4 | 6 | 10 | 21 | 73 | 205 | 3646 | 114 | 340 |
| | yes | 256 | 39 | 1.4 | 6 | 9 | 19 | 63 | 133 | 569 | 56 | 92 |
| PL | no | 140 | 38 | 7.3 | 20 | 59 | 169 | 335 | 551 | 1842 | 248 | 278 |
| | yes | 139 | 38 | 7.3 | 20 | 59 | 168 | 334 | 547 | 1189 | 237 | 244 |
| HT | no | 92 | 17 | 2.9 | 26 | 53 | 77 | 99 | 129 | 237 | 79 | 41 |
| | yes | no outliers detected | | | | | | | | | | |

4.1.2 Relationship between TSS and turbidity

To create continuous TSS data from online turbidity data, correlation functions are determined. Due to the change of bottle type in which the turbidity was measured, correlation functions were established with only a subset of all samples presented in Table 4-2. The range of the sample subset is within the range of all samples with outliers being excluded. Only the maximum value at site RC is slightly higher (580.1 mg L⁻¹ compared to 569.1 mg L⁻¹) and therefore still used for analysis. Both linear and non-linear relationships were tested. Since non-linear functions did not significantly outperform linear functions, only linear regression coefficients are listed in Table 4-3. The goodness-of-fit of the linear regression is visually verified and numerically expressed by r-squared. With the lowest r-squared being at 0.68, all linear regression models show a good fit of the underlying dataset.

Table 4-2. Site-specific TSS sample statistics of samples used for turbidity correlation (FR: flat roof, RC: residential catchment, PL: parking lot, HT: high-traffic street) (Leutnant et al. 2016).

| Site | n | Events | TSS (mg L ⁻¹) | | | | | | | | |
|------|----|--------|---------------------------|-----------|------------|--------|------------|-----------|-----|------|-----|
| | | | Min | 0.1-Perc. | 0.25-Perc. | Median | 0.75-Perc. | 0.9-Perc. | Max | Mean | Sd |
| FR | 36 | 4 | 2 | 3 | 4 | 5 | 9 | 23 | 43 | 9 | 10 |
| RC | 60 | 7 | 2 | 9 | 18 | 42 | 65 | 150 | 580 | 71 | 108 |
| PL | 96 | 33 | 2 | 7 | 18 | 41 | 98 | 137 | 460 | 67 | 77 |
| HT | 85 | 16 | 1 | 19 | 41 | 67 | 82 | 103 | 141 | 64 | 32 |

Table 4-3. Linear regression coefficients for correlation of TSS and turbidity ($TSS = f(turbidity) = a + b * turbidity$, FR: flat roof, RC: residential catchment, PL: parking lot, HT: high-traffic street) (Leutnant et al. 2016).

| Site | a | b | R ² |
|------|-------|------|----------------|
| FR | -3.52 | 1.89 | 0.835 |
| RC | -20.9 | 3.69 | 0.823 |
| PL | 1.97 | 0.84 | 0.683 |
| HT | 7.93 | 0.97 | 0.681 |

4.1.3 Event database

An overview of the event database with continuous measurement data is given in Table 4-4. It contains the number of total observed events and the number of events which are excluded from further analysis. Events are rejected if either selection criteria are violated or if measurement data is doubtful. In this respect, sites FR and RC show a high number of events with doubtful data. This is mainly caused by almost constantly low turbidity values ($FNU < 15$) in the course of an event. For site FR this can be justified with few particles in the runoff. At site RC, this is also caused by pumping difficulties. Gaps due to measurement failures of runoff and quality sensors are rarely present. Turbidity gaps are only observed if stormwater contained substances which caused intensive foaming in the measurement pipe. However, in total, 65 events were analyzed at FR, 23 at site RC, 46 at PL, and 16 at HT. Descriptive statistics of selected event characteristics are given in Table 4-5. Figure 4-6 depicts empirical cumulative distribution functions and boxplots of site-specific monitored TSS event loads.

Table 4-4. Description of event database with continuous monitoring data (FR: flat roof, RC: residential catchment, PL: parking lot, HT: high-traffic street) (Leutnant et al. 2016).

| Site | Total Observed Events | Events Violating Selection Criteria | Events with Doubtful Data | Valid Events | Valid Events/ Total Observed Events |
|------|-----------------------|-------------------------------------|---------------------------|--------------|-------------------------------------|
| FR | 415 | 275 | 75 | 65 | 16% |
| RC | 324 | 199 | 102 | 23 | 7% |
| PL | 152 | 87 | 19 | 46 | 37% |
| HT | 40 | 11 | 13 | 16 | 40% |

Table 4-5. Descriptive statistic data (min, 0.1-, 0.25-, 0.5-, 0.75-, 0.9-percentiles, max, mean, standard deviation) of site-specific event characteristics; rainfall depth: H, max. rainfall intensity in 60 minutes ($I_{\max60}$), max runoff (Q_{\max}), runoff volume (Vol), TSS loads (Loads), and TSS event mean concentrations (EMC) (FR: flat roof, RC: residential catchment, PL: parking lot, HT: high-traffic street) (Leutnant et al. 2016).

| Parameter | Site | Min | 0.1-P | 0.25-P | Median | 0.75-P | 0.9-P | Max | Mean | Sd |
|------------------------------------|------|------|-------|--------|--------|--------|-------|------|------|------|
| H (mm) | FR | 2.0 | 2.1 | 3.1 | 4.3 | 7.3 | 9.6 | 22.7 | 5.6 | 3.8 |
| | RC | 2.2 | 3.8 | 4.3 | 7.1 | 13.4 | 18.9 | 29.1 | 9.8 | 7.2 |
| | PL | 2.1 | 2.6 | 3.1 | 5.1 | 10.0 | 18.8 | 31.0 | 8.0 | 6.9 |
| | HT | 2.3 | 3.2 | 3.6 | 6.2 | 8.7 | 17.5 | 21.8 | 8.0 | 5.9 |
| $I_{\max60}$ (mm h ⁻¹) | FR | 2.6 | 2.8 | 3.3 | 4.6 | 8.2 | 15.2 | 49.4 | 7.4 | 8.1 |
| | RC | 2.5 | 2.7 | 3.0 | 3.7 | 5.2 | 6.6 | 10.4 | 4.4 | 2.1 |
| | PL | 2.5 | 2.7 | 2.9 | 5.5 | 10.4 | 18.7 | 44.9 | 8.6 | 8.2 |
| | HT | 1.1* | 1.3 | 1.8 | 2.3 | 2.6 | 4.7 | 7.5 | 2.7 | 1.7 |
| Vol (m ³) | FR | 0.0 | 0.0 | 0.1 | 0.2 | 0.3 | 0.4 | 1.2 | 0.2 | 0.2 |
| | RC | 18 | 46 | 65 | 116 | 233 | 428 | 716 | 192 | 191 |
| | PL | 1 | 3 | 3 | 6 | 12 | 30 | 71 | 12 | 14 |
| | HT | 81 | 105 | 122 | 166 | 336 | 581 | 784 | 269 | 211 |
| Q_{\max} (L s ⁻¹) | FR | 0.0 | 0.0 | 0.1 | 0.1 | 0.3 | 0.4 | 1.6 | 0.2 | 0.3 |
| | RC | 9 | 10 | 16 | 29 | 95 | 148 | 216 | 61 | 67 |
| | PL | 1 | 2 | 4 | 8 | 13 | 23 | 55 | 11 | 11 |
| | HT | 13 | 16 | 20 | 27 | 52 | 82 | 133 | 41 | 33 |
| Loads (kg ha ⁻¹) | FR | 0.0 | 0.0 | 0.1 | 0.2 | 1.7 | 4.9 | 19.4 | 1.7 | 3.6 |
| | RC | 0.1 | 0.3 | 0.6 | 0.9 | 3.5 | 7.4 | 9.4 | 2.6 | 2.9 |
| | PL | 0.1 | 0.5 | 0.9 | 1.3 | 2.6 | 6.3 | 11.1 | 2.3 | 2.6 |
| | HT | 1.6 | 3.1 | 3.6 | 8.0 | 13.6 | 29.2 | 47.5 | 12.6 | 12.7 |
| EMC (mg L ⁻¹) | FR | 0 | 1 | 3 | 9 | 35 | 94 | 250 | 33 | 55 |
| | RC | 4 | 11 | 18 | 50 | 92 | 152 | 364 | 77 | 94 |
| | PL | 5 | 13 | 24 | 49 | 80 | 112 | 254 | 60 | 49 |
| | HT | 27 | 38 | 54 | 120 | 172 | 242 | 297 | 125 | 84 |

*Note: Event is considered valid although the $I_{\max60}$ criteria is violated.

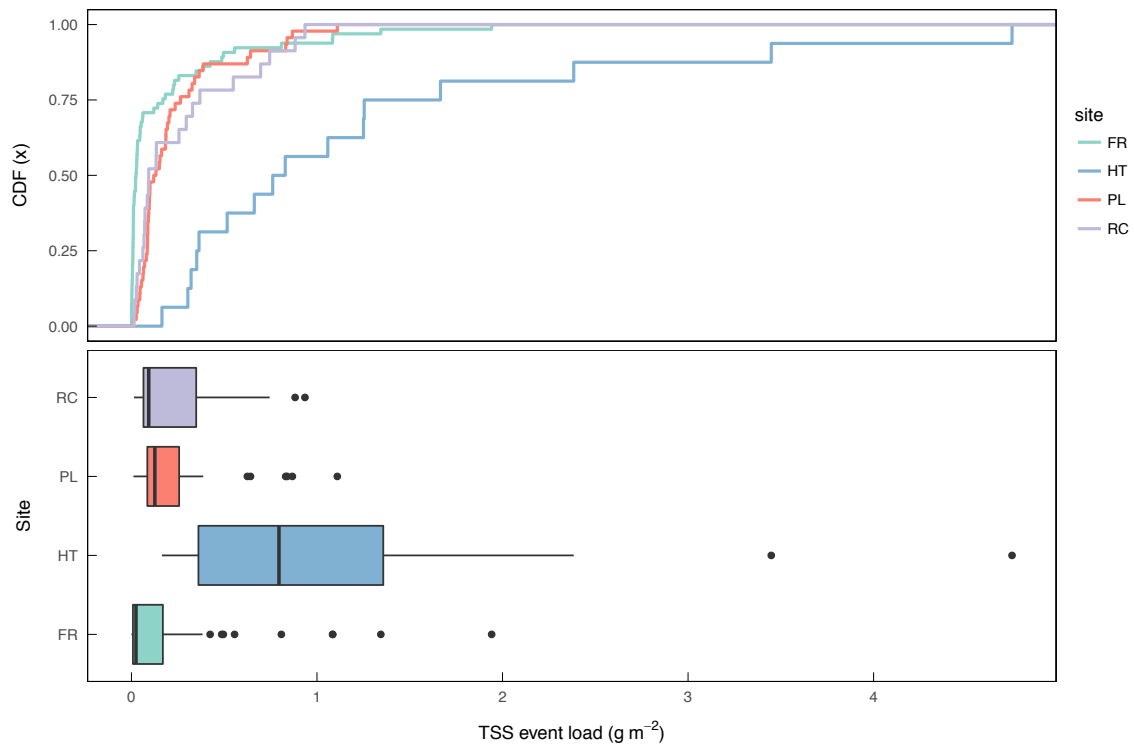


Figure 4-1. Empirical cumulative distribution functions and boxplots of site-specific monitored TSS event loads (FR: Flat Roof, HT: High Traffic Street, PL: Parking Lot, RC: Residential Catchment) (Leutnant et al. 2018c).

4.1.4 Correlation analysis

Table 4-6 shows Pearson correlation coefficients for TSS loads and selected variables at the four study sites. A strong correlation of rainfall intensities and mean/max runoff to TSS loads can be observed at site FR. This effect is also evident but less intense at sites PL and HT. However, the variable I_{mean} (mean rainfall intensity) has only a strong influence at FR (0.8). Rainfall depths seem to be strongly correlated to TSS loads at site HT, only. The overall rainfall duration does not correlate with TSS loads at any site. Correlation of the variables runoff volume (Vol) and antecedent dry weather periods (ADWP) to TSS loads can be noticed only at site HT and PL, respectively.

Table 4-6. Site-specific Pearson correlation coefficients (FR: flat roof, RC: residential catchment, PL: parking lot, HT: high-traffic street) for TSS loads and selected variables: rainfall depth, duration, and intensities (H , D_p , I_{mean} : I_{max60}), runoff characteristics (Q_{mean} , Q_{max} , volume), and antecedent dry weather period (ADWP). Bold values indicate correlation coefficients > 0.5 (Leutnant et al. 2016).

| Site | H | D_p | I_{mean} | I_{max1} | I_{max5} | I_{max60} | Q_{mean} | Q_{max} | Vol | ADWP |
|------|-------------|-------|-------------------|-------------------|-------------------|--------------------|-------------------|------------------|-------------|-------------|
| FR | 0.39 | -0.09 | 0.80 | 0.68 | 0.80 | 0.82 | 0.90 | 0.88 | 0.37 | 0.20 |
| RC | 0.19 | -0.03 | 0.40 | 0.47 | 0.43 | 0.26 | 0.45 | 0.35 | 0.29 | -0.06 |
| PL | 0.50 | 0.08 | 0.48 | 0.69 | 0.69 | 0.63 | 0.49 | 0.64 | 0.38 | 0.56 |
| HT | 0.80 | 0.30 | 0.41 | 0.73 | 0.74 | 0.64 | 0.62 | 0.59 | 0.78 | -0.06 |

From the correlation analysis it is stated, that firstly rainfall intensity ($I_{\max 5}$, $I_{\max 60}$) has a strong influence on TSS loads at small catchments with a high proportion of impervious surfaces (FR, PL, HT). Secondly, this effect decreases with increasing catchment size. Thirdly, in residential catchments which consist of multiple subcatchments (e.g., roofs, streets, parking lots) the correlation between rainfall event characteristics and TSS loads is strongly attenuated. The low correlation of the antecedent dry weather period suggests that this parameter is inappropriate to describe the pollutant build-up. However, in this study, the average antecedent dry weather period is about three days. This means pollutants are mostly accumulated shortly after an event and therefore exposed to other influential processes such as wind-driven processes (cf. 1.1.2).

4.1.5 Intra-event TSS load distributions

Intra-event distributions of TSS load are studied with site-specific MV-curves (Figure 4-2). Clearly, all sites show large variability of intra-event TSS load distribution which confirms findings of other studies (Métadier and Bertrand-Krajewski 2012, Sun et al. 2015) also for microscale sites. However, from the four study sites it can be observed that the more curves are taken into account the variability increases. Therefore, boxplots at runoff volume quantiles are used to depict the main tendency of wash-off behavior. This enables a visual comparison between site and season-specific MV-curves.

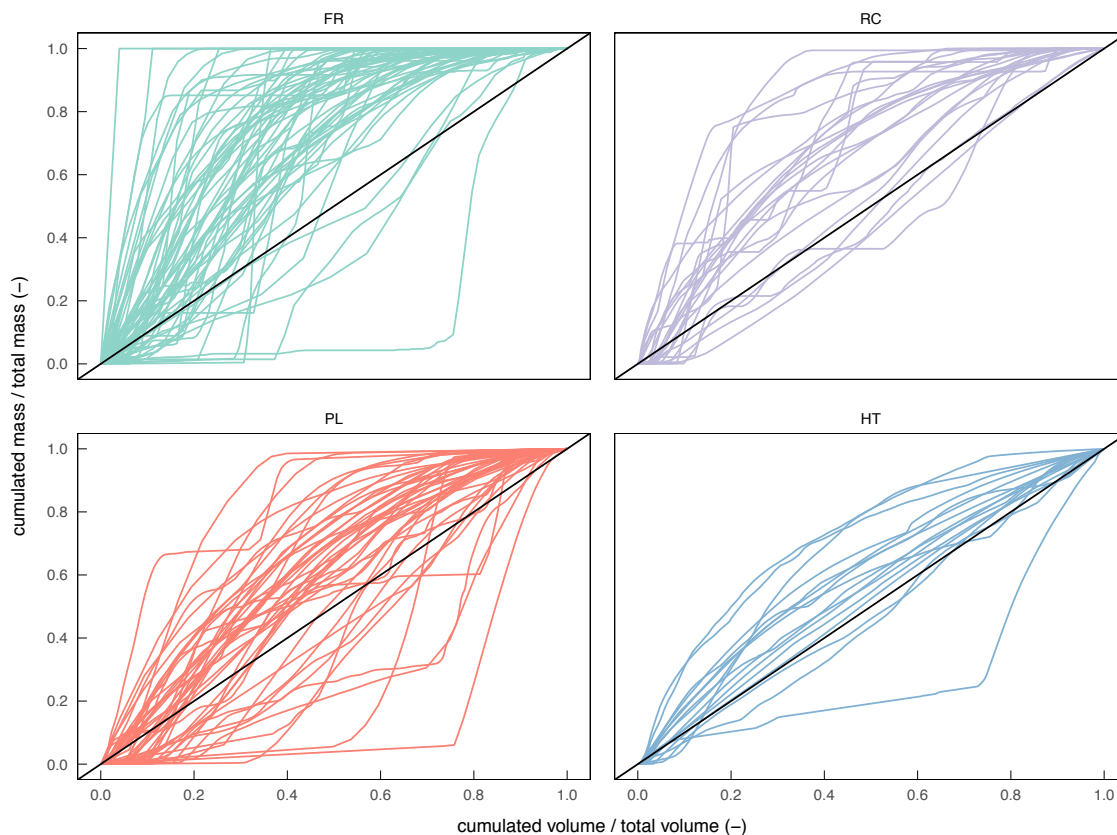


Figure 4-2. Site-specific MV-curves (FR: flat roof, RC: residential catchment, PL: parking lot, HT: high-traffic street) (modified from Leutnant et al. (2016)).

Figure 4-3 shows boxplots of *MV*-curve distributions at given runoff volume quantiles for each of the study sites. At site FR, in most cases a large portion of pollution loads tend to be washed-off in the first period of an event. In addition, distances between the first and third quartile (interquartile range, IQR) increases until 20% of runoff volume and decreases afterwards. This generally indicates a decreasing event variability. In this respect, after 60% of runoff volume, most pollutants are already washed off. With regard to site PL and RC, the IQR rises until 20% of runoff volume and almost constantly continues up to 60% of runoff volume. At site HT, the IQR is merely changing in the first 80% of runoff volume. Although, the number of events taken into account is likely to affect the interquartile ranges, *MV*-curves from site HT are noticeably closer to the bisecting line than *MV*-curves from site FR. Similarly, *MV*-curves from PL are closer to the bisecting line compared to the *MV*-curves from site RC.

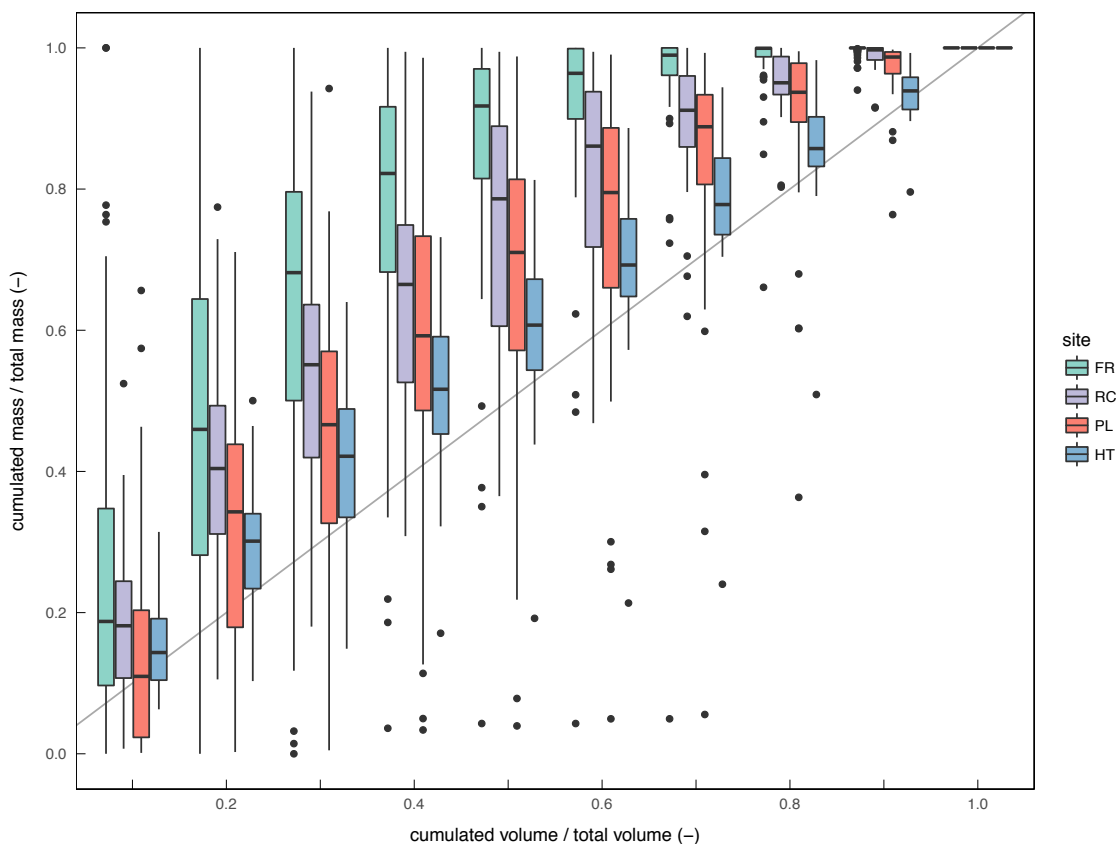


Figure 4-3. Site-specific boxplots of *MV*-curve distributions at runoff volume quantiles (FR: flat roof, RC: residential catchment, PL: parking lot, HT: high-traffic street). Box ranges correspond to the first and third quartiles. Median is indicated by a solid black horizontal line. Whiskers comprise lowest/highest value within $1.5 \times$ inter-quartile range. Outliers exceed whiskers' ends and are indicated by solid black dots (modified from Leutnant et al. (2016)).

Analysis of *MV*-curves suggests, that firstly, small urban catchments analysed generally show a more pronounced first-flush effect and only a few events with a delayed wash-off process. Secondly, the wash-off process at FR seems to be source limited because of the majority of particles are washed-off after 60% of

runoff volume and the IQR is significantly low at the end of the events. Thirdly, in contrast, PL and HT show a more transport-limited wash-off because the IQR is closer to the bisecting line at the end of the events. Finally, it is assumed, that RC's wash-off processes are influenced by a composition of subcatchment-specific (i.e., roofs, streets, and parking lots) wash-off characteristics, which is explained by the intermediate position of RC in comparison to FR, HT, and PL. In fact, runoff from different surfaces is superposed and therefore pollution transport processes are mixed.

4.1.6 Seasonal intra-event TSS load distributions

Figure 4-4 shows *MV*-curve distributions for different seasons. At FR, the *MV*-curves start steeper in spring, summer, and autumn periods, which indicates a more pronounced first flush. Contrarily, in winter, the *MV*-curves show a less dominant wash-off behavior at the beginning of the events. At site PL, the variability is highest during spring and autumn periods. Events during summer months show similar wash-off behavior, which is indicated by relatively low IQR. The three events in the winter are characterized by a delayed wash-off but cannot be statistically interpreted due to small number of events available. *MV*-curve distributions at site RC are comparable to PL with highest variability during spring and autumn months. Pollutants tend to be washed-off in the first periods of an event. For site HT, monitored events are available in the autumn and winter months, only. Both seasons show comparable washoff behavior, which is characterized by washoff almost proportional to runoff, low IQR, and close distance to the bisecting line.

From seasonal *MV*-curves it can be observed, first, that *MV*-curve distributions at FR show the largest variability in the first 50% of runoff volume throughout the seasons except for spring. The delayed wash-off process during winter months can be caused by a low pollutant potential on surfaces, coarser particles with high densities, or by events with low rain intensities. Second, variability of *MV*-curve distribution, in general, is largest during autumn, especially for sites FR, RC, and PL. It can be assumed that this is mainly caused by high variability of rainfall intensities in conjunction with varying pollutant masses available at surface. It must also be noted, that only few events were monitored during the winter months, which must be taken into account for further statistical analysis.

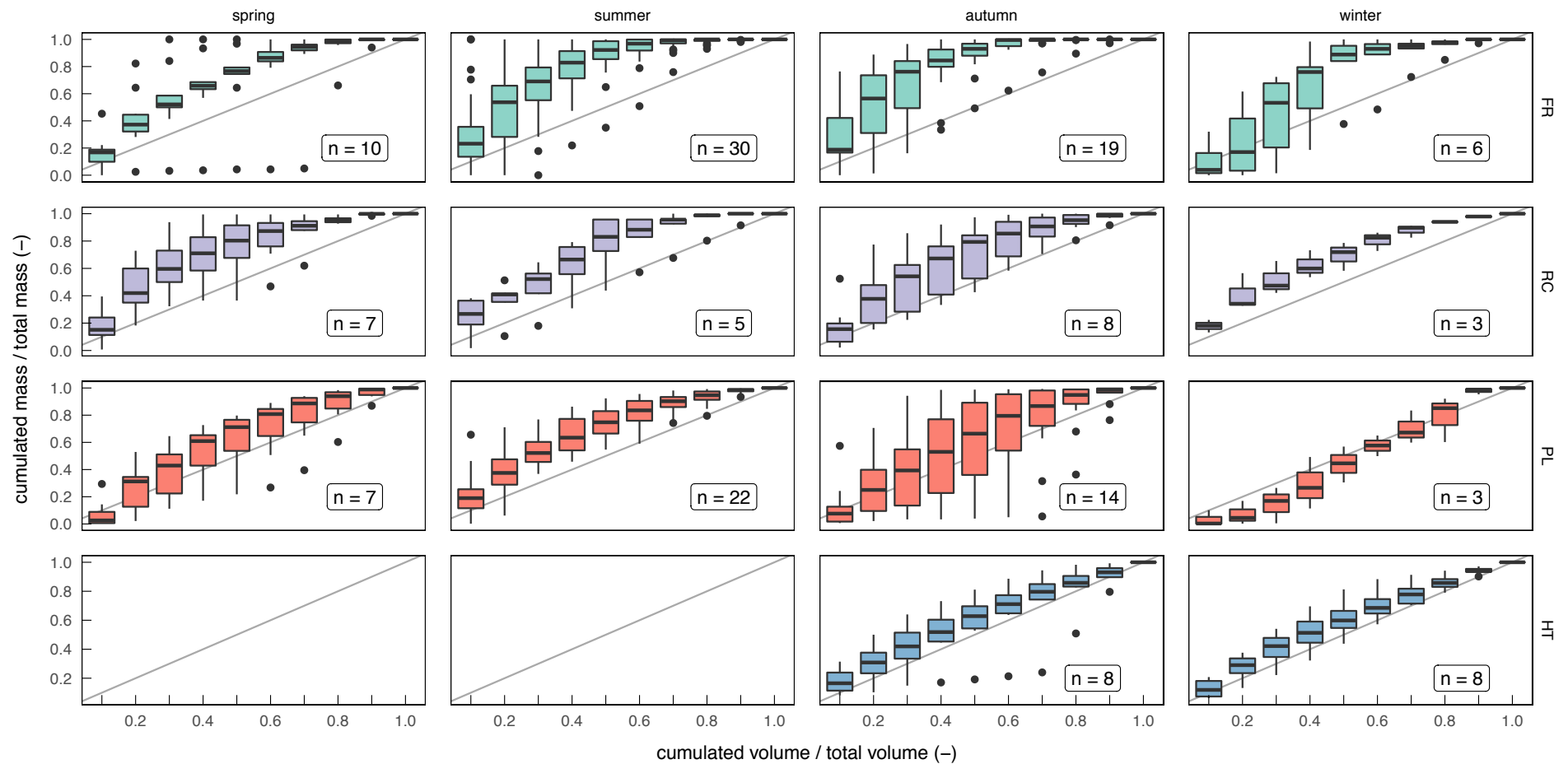


Figure 4-4. Seasonal- (horizontal) and site- (vertical) specific boxplots of MV-curve distributions at runoff volume quantiles (FR: flat roof, RC: residential catchment, PL: parking lot, HT: high-traffic street). Box ranges correspond to the first and third quartiles. Median is indicated by a solid black horizontal line. Whiskers comprise lowest/highest value within $1.5 \times$ inter-quartile range (IQR). Outliers exceed whiskers' ends and are indicated by solid black dots (modified from Leutnant et al. (2016)).

4.2 Probabilistic modelling of TSS event loads¹²

4.2.1 Derived theoretical distribution functions

Results of fitting theoretical distribution functions to the empirical TSS event load distribution are presented in Table 4-7. It shows site- and distribution-specific goodness-of-fit values and estimated parameters. Figure 4-5 illustrates the approximation with lognormal distribution function for all sites.

Table 4-7. Results of fitting empirical TSS load distribution functions to theoretical distribution functions (FR: Flat Roof, HT: High Traffic Street, PL: Parking Lot, RC: Residential Catchment, LL: LogLikelihood, AD: Anderson-Darling statistic A^2 , KS: Kolmogorov-Smirnov statistic D_n) (Leutnant et al. 2018c).

| site | distr. | goodness-of-fit | | | parameter estimates (standard error) | | | | |
|------|---------|-----------------|--------|--------|--------------------------------------|------------------|------------------|------------------|------------------|
| | | LL | AD | KS | rate | shape | meanlog | sdlog | scale |
| FR | exp | 48.66 | 29.074 | 0.442* | 5.747 (0.713) | - | - | - | - |
| | gamma | 88.29 | 2.254 | 0.186* | 1.994 (0.504) | 0.347 (0.049) | - | - | - |
| | Inorm | 89.9 | 0.806 | 0.099 | - | - | -3.69 (0.301) | 2.429 (0.213) | - |
| | weibull | 92.05 | 1.123 | 0.131 | - | 0.484 (0.046) | - | - | 0.077 (0.021) |
| HT | exp | -19.64 | 0.379 | 0.153 | 0.797 (0.199) | - | - | - | - |
| | gamma | -19.25 | 0.394 | 0.136 | 1.068 (0.412) | 1.341 (0.428) | - | - | - |
| | Inorm | -18.18 | 0.192 | 0.128 | - | - | -0.19 (0.228) | 0.912 (0.161) | - |
| | weibull | -19.46 | 0.382 | 0.137 | - | 1.121 (0.208) | - | - | 1.316 (0.312) |
| PL | exp | 21.69 | 1.168 | 0.126 | 4.356 (0.642) | - | - | - | - |
| | gamma | 22.03 | 1.279 | 0.157 | 5.093 (1.175) | 1.169 (0.218) | - | - | - |
| | Inorm | 25.31 | 0.398 | 0.116 | - | - | -1.96 (0.146) | 0.987 (0.103) | - |
| | weibull | 21.72 | 1.203 | 0.137 | - | 1.030 (0.111) | - | - | 0.233 (0.035) |
| RC | exp | 7.91 | 1.011 | 0.222 | 3.833 (0.799) | - | - | - | - |
| | gamma | 8.1 | 0.681 | 0.189 | 3.283 (1.120) | 0.857 (0.219) | - | - | - |
| | Inorm | 9.07 | 0.38 | 0.131 | - | - | -2.03 (0.259) | 1.243 (0.183) | - |
| | weibull | 8.23 | 0.586 | 0.174 | - | 0.882 (0.142) | - | - | 0.244 (0.061) |

* rejecting H_0

¹² This section is partly composed of paragraphs from Leutnant et al. (2018)

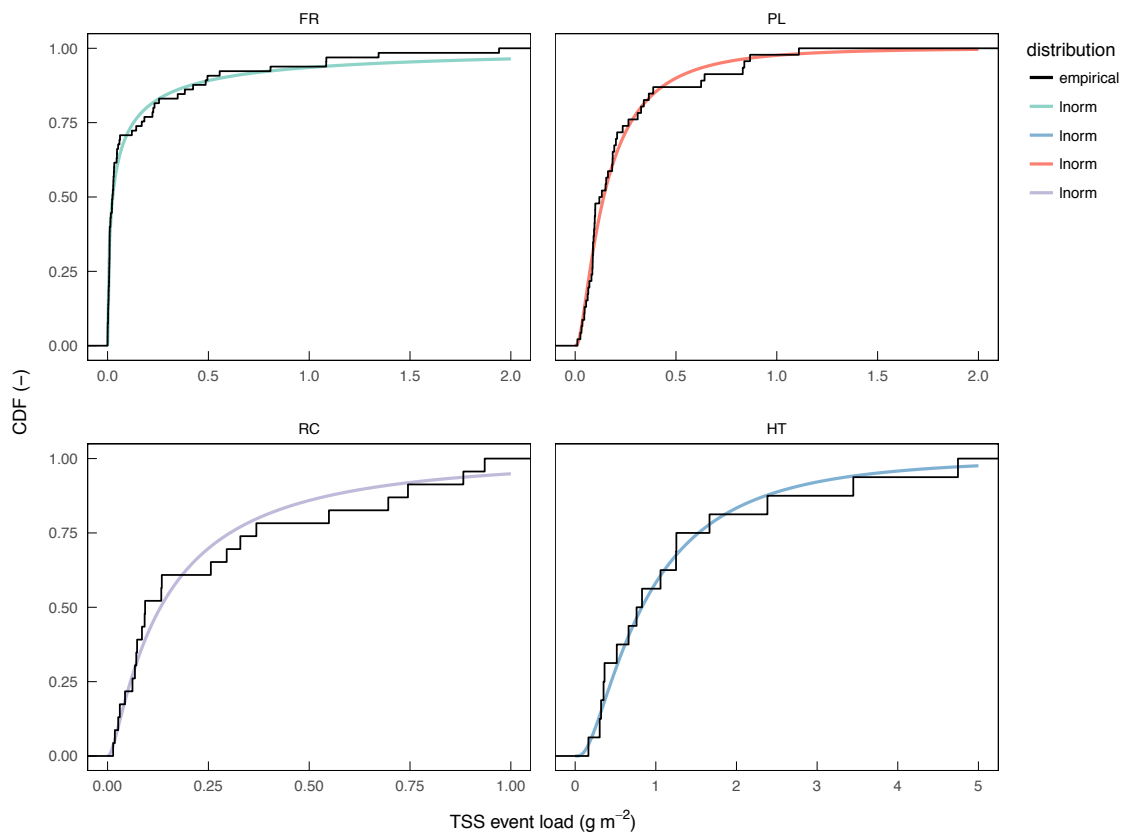


Figure 4-5. Site-specific approximation of empirical TSS event load distribution functions with lognormal distribution function at all sites (Leutnant et al. 2018c).

Table 4-8 shows results of fitting the lognormal distribution to TSS event load distributions grouped by year. Sites FR and PL are considered only as they provide sufficient samples per group. The goodness-of-fit is given for each individual group and compared to the original sample from all years. Additionally, the goodness-of-fit is visualised in Figure 4-6.

Table 4-8. Results of fitting empirical TSS load distribution functions grouped by year to lognormal distribution function (FR: Flat Roof, HT: High Traffic Street, PL: Parking Lot, LL: LogLikelihood, AD: Anderson-Darling statistic A^2 , KS: Kolmogorov-Smirnov statistic D_n) (Leutnant et al. 2018c).

| site | year | n | distr. | goodness-of-fit | | | parameter estimates (standard error) | |
|------|-----------|----|--------|-----------------|-------|-------|---|---------------|
| | | | | LL | AD | KS | meanlog | sdlog |
| FR | all years | 65 | Inorm | 89.9 | 0.806 | 0.099 | -3.69 (0.301) | 2.429 (0.213) |
| | 2015 | 25 | Inorm | 24.54 | 0.64 | 0.138 | -2.99 (0.359) | 1.80 (0.254) |
| | 2014 | 17 | Inorm | 41.63 | 0.288 | 0.142 | -5.04 (0.786) | 3.24 (0.556) |
| | 2013 | 23 | Inorm | 32.52 | 0.365 | 0.12 | -3.45 (0.388) | 1.86 (0.274) |
| PL | all years | 46 | Inorm | 25.31 | 0.398 | 0.116 | -1.96 (0.146) | 0.987 (0.103) |
| | 2014 | 30 | Inorm | 23.76 | 0.616 | 0.167 | -2.08 (0.161) | 0.88 (0.114) |
| | 2013 | 16 | Inorm | 2.93 | 0.243 | 0.105 | -1.72 (0.281) | 1.12 (0.199) |

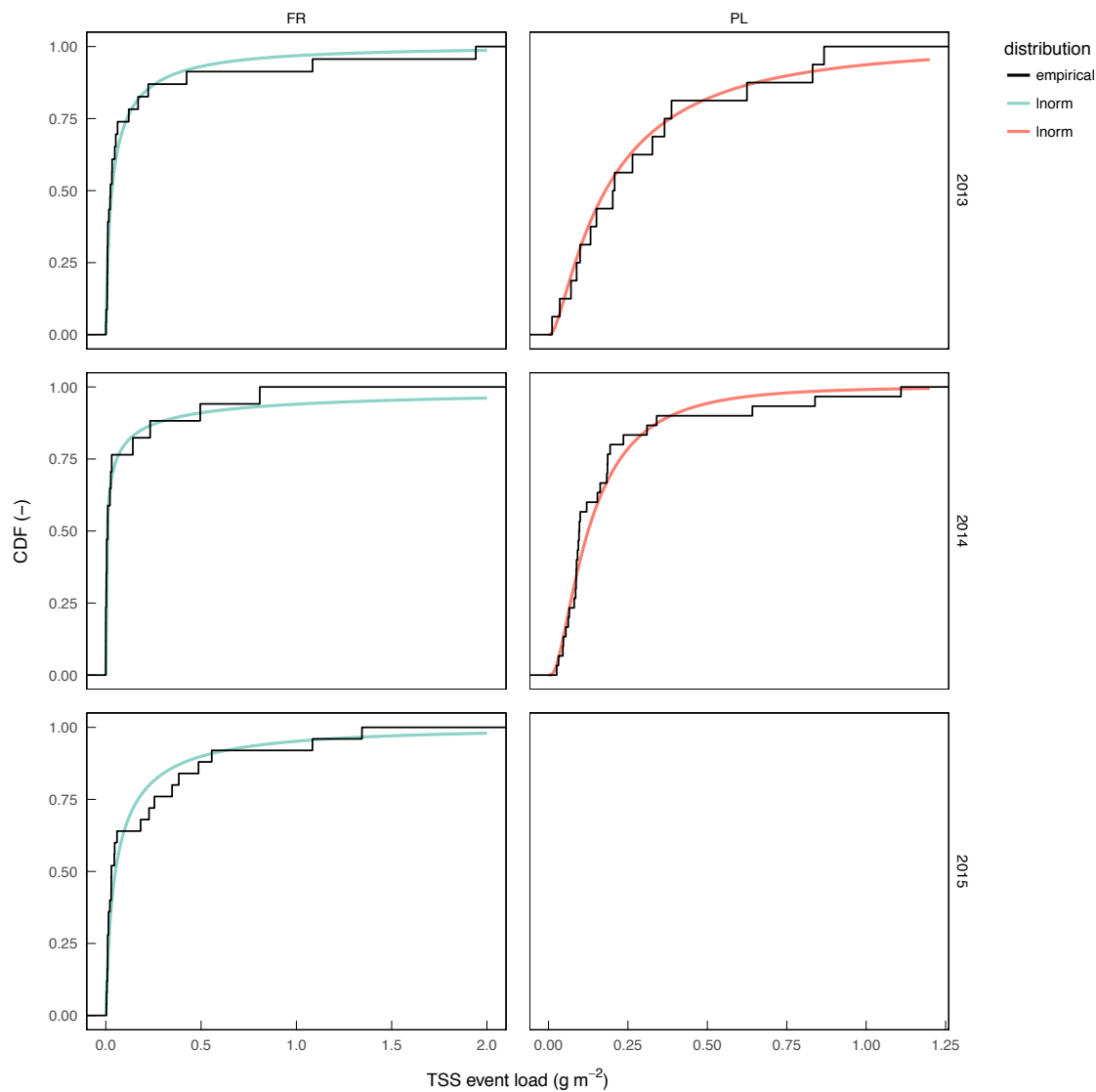


Figure 4-6. Approximation of empirical TSS event load distribution function grouped by year with lognormal distribution function at site FR and PL (Leutnant et al. 2018c).

All selected theoretical distribution functions were able to approximate the empirical distribution with statistical significance except for the Exponential and the Gamma distribution at site FR (H_0 gets rejected). These two functions are not able to reflect the initially steep gradient and subsequent moderate gradient of the empirical distribution. The Exponential function has the least flexibility among the analysed functions because it only provides one parameter to be fitted. This explains the poor approximation results. Thus, a statistical significant description of TSS event distributions requires at least a two-parameter distribution.

Using the Weibull distribution which basically extends the Exponential distribution function with an additional parameter, clearly improves the fitting. The application of Weibull and Gamma distribution lead to comparable results which is indicated by similar goodness-of-fit measures. Highest goodness-of-fit is obtained with the lognormal distribution that accordingly approximates the underlying dataset best.

The goodness-of-fit of the lognormal distribution however, varies between sites. On the one hand, this might be caused by insufficient samples, which lead to more pronounced steps in the empirical distribution function. On the other hand, this also could reflect a site-specific behavior, which is expressed by the shape of distribution function. While the monitored small roof catchment has significantly more events with low loads, this effect is attenuated for the other catchments. The differences in the results of the two-parameter functions are marginal which demonstrates the functions are general able to replicate the empirical distribution. Comparing the fitted parameters also indicates that distributions of site PL and RC are comparable which is confirmed by their empirical distribution functions (cf. Figure 4-1).

The results of distribution fitting grouped by year shows that also subsamples can be well approximated by lognormal distribution. According to the KS statistic, for both sites the year 2013 has been fitted best. Only the AD statistic of the year 2014 for site FR indicates a slightly better fit which is caused by a relative low maximum load in this year (2013: 1.94 gm^{-2} , 2014: 0.8 gm^{-2} , 2015: 1.34 gm^{-2}). The optimized parameters of the lognormal distribution for both sites highlight the individuality of each year as they strongly vary. This is also expressed by the spread of goodness-of-fit values. Consequently, this indicates the sensitivity of the sampling characteristics which is induced by the utilized database. In the present study the database available does not cover all events of an entire year mainly due to measurement issues and predefined rainfall-runoff criteria for event selection (Leutnant et al. 2016). However, rainfall-runoff events are affected by numerous environmental variables and generally occur randomly in time, space and intensity. Therefore, although the event database grouped by year undoubtedly is incomplete, the approach reflects natural variability in which the number of events per year and their characteristics change. Robust fitting of a theoretical distribution function should therefore prioritize sample size over sampling period (cf. 4.2.2).

4.2.2 Minimum sample size

The results obtained from the Monte-Carlo-based sampling are visualised in Figure 4-7. It shows the mean (colored solid line) and regions of one and two standard deviations (grey shaded areas) of Kolmogorov-Smirnov's statistic as function of sample size for site FR and PL. Furthermore, critical values for the 90 % significance level are illustrated (black solid line).

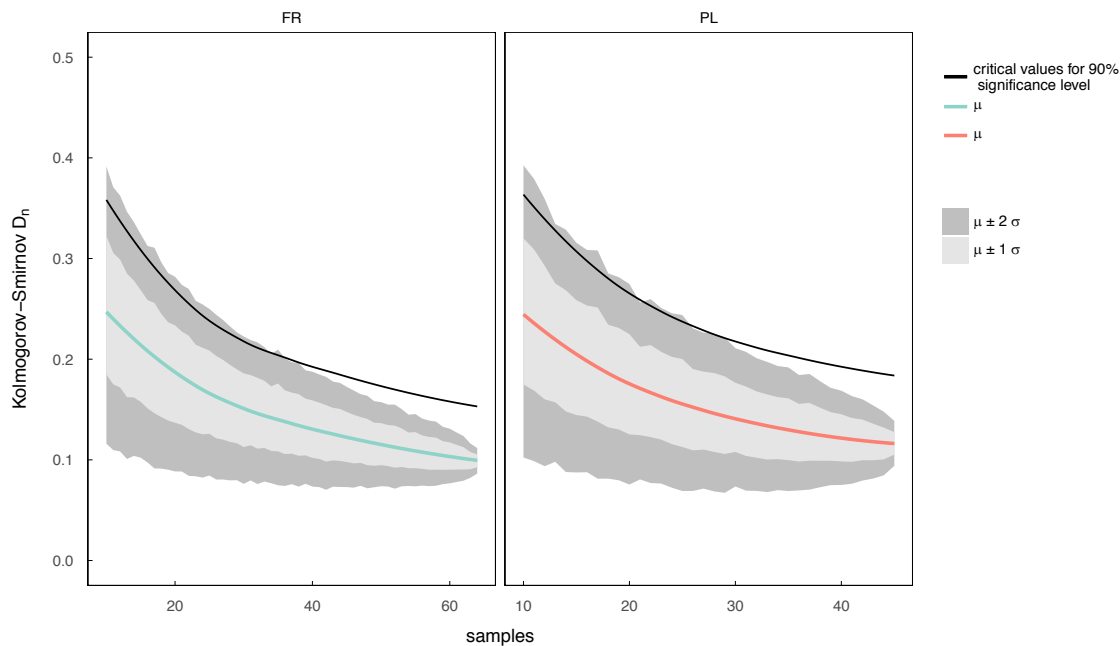


Figure 4-7. Mean and regions of one and two standard deviations of Kolmogorov-Smirnov's statistic as function of sample size from Monte-Carlo-based sampling for sites FR and PL. Critical values for 90% confidence are indicated as black solid line (Leutnant et al. 2018c).

The results of the Monte-Carlo analysis show, that the mean of the calculated goodness-of-fit values improves with increasing sample size and approximates to the value obtained when all samples are taken into account (FR: 0.099, PL: 0.12). The standard deviation decreases with increasing sampling size by implication. With respect to critical values for 90% confidence level, accepting the null hypothesis H_0 ("The data follow the lognormal distribution") generally requires Kolmogorov-Smirnov's D_n to be approximately below the $\mu + 2\sigma$ threshold which is satisfied for minimum sample sizes of roughly 40 at site FR and of roughly 30 at site PL. It can be legitimately assumed that simulated KS statistics follow a normal distribution which according to the *empirical rule*¹³ consequently implies that more than approximately 95 % of samples lead to KS statistics lower than 0.188 at site FR and 0.211 at site PL. Narrowing the uncertainty range to the upper limit of $\mu + \sigma$ threshold results in KS statistics of 0.159 at site FR and 0.176 at site PL (approx. more than 68% of samples are within this range).

Generally, the simulated dataset confirms that the more samples are taken into account, the more precise the estimates get which as a matter of fact is the basic assumption for any statistical significance test. In order to determine the minimum sample size which leads to accepting the null hypothesis H_0 with high probability, it is suggested to choose at least the minimum of 40 samples because of i) the chance of having a sample which can be statistically represented by the lognormal distribution is high (>95 %) and ii) the mean of KS statistic in this case only

¹³ The empirical rule states that for a normal distribution 99.7% of the data fall within three standard deviations, 95% are within two standard deviations and 68 % fall within one standard deviation (Hedderich and Sachs 2012).

slightly differs from the optimal value taking all samples into account ($0.131 > 0.099$ at site FR and $0.122 > 0.12$ at site PL). However, the choice of criteria remains subjective and might be adapted as further data becomes available. Of course, using more data to approximate the lognormal distribution may probably lead to more appropriate fitting results, but this requires to provide more samples which in turn needs more measurement data. The criteria proposed therefore are presenting a compromise solution between measurement duration and quality of approximation.

4.3 Distribution-based calibration of SWMM¹⁴

4.3.1 Calibration results

Calibration results for both sites are shown in Table 4-9. Statistics for both model parameters and the Kolmogorov-Smirnov-based objective function are given. The best fit parameter sets yielded to an objective function of roughly 0.05 for both models.

Table 4-9. Calibrated model parameters and corresponding uncertainty statistics (FR: Flat Roof, PL: Parking lot, sd: standard deviation, CoV: Coefficient of Variation, KS D_n : Kolmogorov-Smirnov distance) (Leutnant et al. 2018b).

| site | statistic | objective function | | parameter | | | |
|------|-----------|--------------------|----------------------------|------------------------|-----------------------------|------------|------------|
| | | KS D_n | B_0 g m ⁻² | k g m ⁻² | α d ⁻¹ | C_1 - | C_2 - |
| FR | best fit | 0.053 | 2.713 | 1.899 | 0.022 | 0.017 | 2.040 |
| | mean | 0.056 | 3.437 | 1.706 | 0.024 | 0.021 | 2.070 |
| | sd | 0.003 | 0.608 | 0.201 | 0.005 | 0.006 | 0.054 |
| | CoV | 0.053 | 0.177 | 0.118 | 0.212 | 0.277 | 0.026 |
| PL | best fit | 0.049 | 4.545 | 0.891 | 0.194 | 0.472 | 1.120 |
| | mean | 0.050 | 4.726 | 0.882 | 0.204 | 0.470 | 1.103 |
| | sd | 0.002 | 0.257 | 0.053 | 0.021 | 0.043 | 0.070 |
| | CoV | 0.032 | 0.054 | 0.061 | 0.105 | 0.091 | 0.063 |

According to the low Kolmogorov-Smirnov statistic D_n of approx. 0.05 for both sites (Table 4-9), the best-fit parameter sets obtained by the distribution-based calibration approach lead to well-approximated parameterized lognormal distributions. From a statistical perspective which also takes the number of samples into account, it can be legitimately assumed that both distributions (lognormal and simulated TSS event loads) follow the same distribution. Both KS statistics are below the critical values at 90% significance level (0.082 for site FR and 0.118 at site PL).

¹⁴ This section is partly composed of paragraphs from Leutnant et al. (2018b)

Cumulative distribution functions of simulated TSS event loads are depicted for both models in Figure 4-8 (FR) and Figure 4-9 (PL). Simulation results are opposed to the parameterized lognormal distribution function used for calibration and the original empirical distribution function from observation. Additionally, absolute residuals between observed and simulated TSS event loads are presented on the right-hand side of the figures. For site FR, the mean of TSS event loads residuals is -0.0087 g m^{-2} (sd: 0.19; min: -0.41 ; max: 0.94), at site PL, the mean of TSS event loads residuals is 0.065 g m^{-2} (sd: 0.19; min: -0.27 ; max: 0.74).

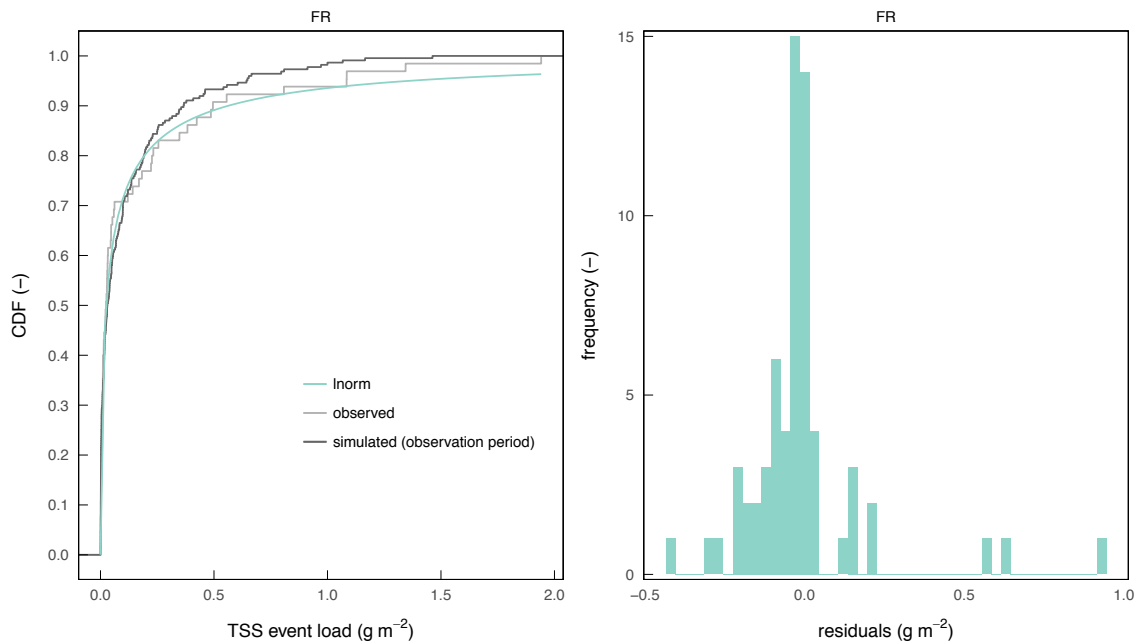


Figure 4-8. Cumulative distribution functions of lognormal, observed and simulated TSS event loads (left) and distribution of residuals between observed and simulated event loads (right) at site Flat roof (Leutnant et al. 2018b).

At site FR, the calibrated model replicates the distribution function until the 0.8-percentile with a high goodness-of-fit (Figure 4-8). Events exceeding this value are generally underestimated by the model and lead to lower simulated event loads than suggested by the lognormal distribution. Since the KS statistic represents the maximum distance between two cumulative distribution functions, maximum 5% of the events with more than the 0.8-percentile of event loads are underestimated.

The results for site PL show a similar effect (Figure 4-9). Here, the model shows a good fitting of the distribution function until the 0.9-percentile which accordingly implies that maximum 5% of the events with more than the 0.9-percentile of event loads are underestimated.

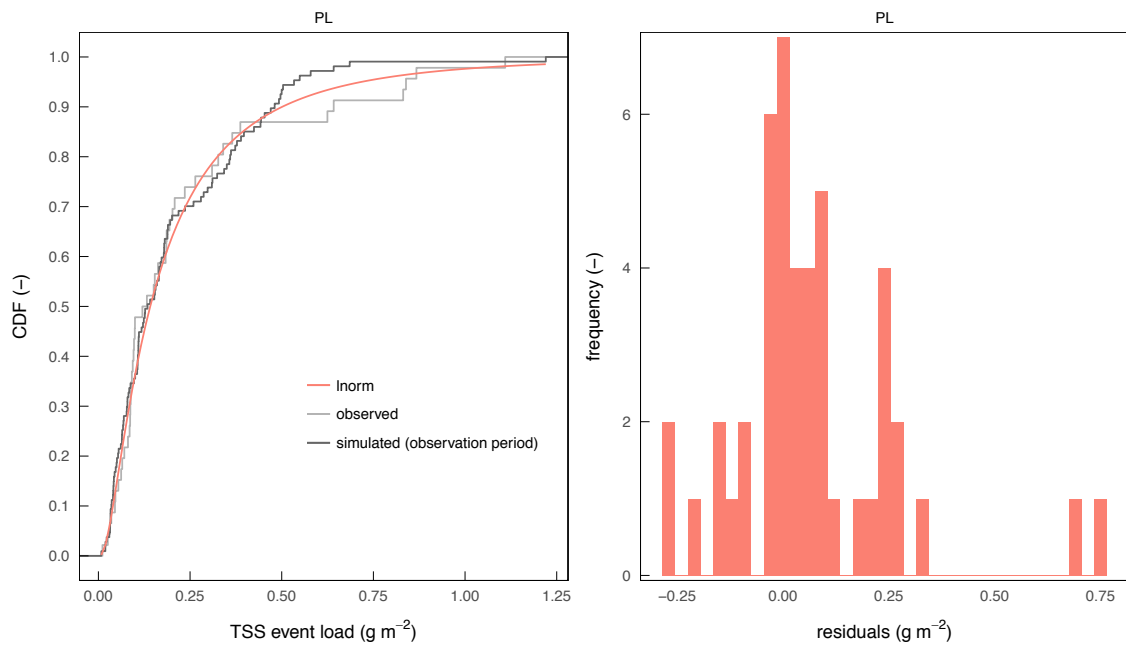


Figure 4-9. Cumulative distribution functions of lognormal, observed and simulated TSS event loads (left) and distribution of residuals between observed and simulated event loads (right) at site Flat roof (Leutnant et al. 2018b).

Both calibrated models tend to underestimate events with high TSS loads which indicates that the calibration approach and the objective function applied is heavily influenced by events with low TSS event load which as a matter of fact is the case for the majority of events for both sites. Applying an alternative goodness-of-fit measure as objective function which also emphasize the upper tailing of a distribution function could lead to superior model performance. This however remains unclear as the applied pollutant model itself also induces limitations to replicate natural pollutant processes (Bertrand-Krajewski 2007, Sage et al. 2015, Shaw et al. 2010).

Table 4-10 compares the total TSS event loads of simulated and observed TSS event loads. At site FR, the calibrated model yields to 11.9 gm⁻² (+5%), site PL gives 7.57 gm⁻² (-28%).

Table 4-10. Observed and simulated total TSS event loads (Leutnant et al. 2018b).

| site | events | total TSS event loads (g m ⁻²) | | |
|------|--------|--|-----------|--------------------|
| | | observed | simulated | relative deviation |
| FR | 65 | 11.3 | 11.9 | + 5 % |
| PL | 46 | 10.6 | 7.57 | - 28 % |

The fact, that events with high TSS event loads are underestimated affects the goodness-of-fit concerning the total TSS event load of the events observed (Table 4-10). This is especially evident at site PL, where the total TSS event load is underestimated by roughly 28 %. Events with more than 0.5 g m⁻² are poorly

represented (cf. Figure 4-9). At site FR, the relative deviation is only about 5 %. This signals that the error is compensated by events whose simulated TSS event load is higher than the observed (intersection at approx. 0.1 g m⁻², cf. Figure 4-8).

Distributions of simulated and observed TSS event mean concentrations are given in Table 4-11. A notably high agreement of mean EMC is obtained for both sites (FR: 33 mg L⁻¹, PL: 62 mg L⁻¹). It can also be observed that EMC percentiles of simulation for site FR are slightly higher than observed percentiles until the 0.75-Percentile. Site PL shows the opposite behavior: EMC percentiles of simulation are slightly lower than observed percentiles until the 0.5-Percentile. However, in both cases, the maximum observed EMC are strongly underestimated which again suggests an inappropriate accumulation process model to account for random influences (e.g. traffic induced pollutant emissions (Gunawardena et al. 2018)).

Table 4-11. Observed (obs) and simulated (sim) TSS event mean concentrations (Leutnant et al. 2018b).

| site | source | N | TSS event mean concentration (mg L ⁻¹) | | | | | | | | |
|------|--------|----|--|-----------|------------|--------|-----------|-----------|-------|------|------|
| | | | Min | 0.1-Perc. | 0.25-Perc. | Median | 0.75-Perc | 0.9-Perc. | Max | Mean | Sd |
| FR | obs | 65 | <0.1 | 1.2 | 2.8 | 9.0 | 35.1 | 94.0 | 249.9 | 33.2 | 54.6 |
| | sim | 65 | 1.2 | 5.8 | 9.6 | 20.6 | 35.5 | 82.6 | 178.2 | 33.4 | 36.5 |
| PL | obs | 46 | 4.7 | 13.2 | 24.4 | 49.4 | 80.1 | 112.4 | 253.7 | 60.3 | 49.3 |
| | sim | 46 | 0.2 | 4.6 | 13.9 | 45.4 | 98.8 | 156.6 | 161.6 | 62.9 | 54.7 |

Observed and simulated MV-Curves are shown in Figure 4-10. Simulated MV-Curves are calculated for both the stormwater quality observation period and the 5 years period using all available rainfall data.

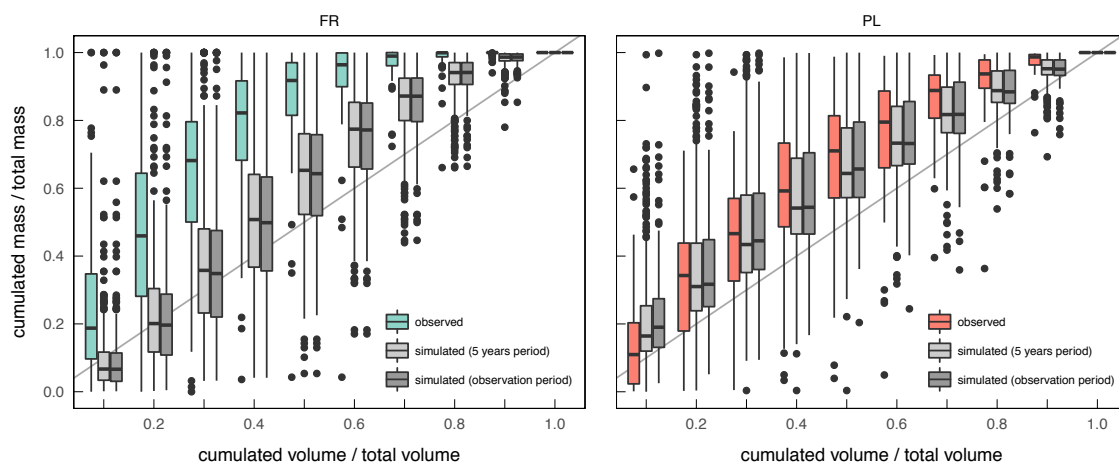


Figure 4-10. Comparison of observed and simulated Mass-Volume-Curves for sites Flat Roof (left) and Parking Lot (right) (Leutnant et al. 2018b).

Mass-Volume-Curves (Figure 4-10, left) for site FR reveal, that intra-event processes simulated do not reflect the observed dynamics in general. Especially, the

prevailing first-flush characteristic is not appropriately replicated. Instead simulated washoff tends to occur proportionally to runoff.

In contrast, statistics of simulated intra-event processes at site PL (Figure 4-10, right) correspond well to the data observed. It can be seen that the calibrated model also tends to generate wash proportional to runoff. The high agreement of observed and simulated MV-Curves at site PL is obtained since observed MV-Curves already show a more runoff proportional washoff behavior. Although the general characteristic at site PL is satisfactorily represented, the results from both sites indicate that the observed intra-event dynamic can hardly be deterministically described by the model for a continuous simulation period. As pointed out in previous studies by (Sage et al. 2015, Shaw et al. 2010) pollutant buildup and washoff is highly affected by stochastic inputs which consequently limits the goodness-of-fit of replicating intra-event dynamics.

Simulated distribution functions from the observation period (calibration) are compared to the results using the 5 years period (validation) in Figure 4-11. Corresponding goodness-of-fit is given in Table 4-12. At site FR, the difference between both distributions is marginal implying the observation period being highly representative. The KS statistic of 0.062 from validation only slightly differs from calibration (KS: 0.053) which indicates a successful model validation. In contrast, the distribution function from validation at site PL underestimates the assumed lognormal distribution constantly. This is also expressed by a higher KS statistic of 0.073. The distance between calibration and validation period is slightly higher (KS: 0.083) indicating a less successful model validation. However, it is noticeable that the simulated TSS event distribution of observation period falls below the lognormal distribution between 0.25 g m^{-2} and 0.4 g m^{-2} and exceeds the lognormal distribution for event loads higher 0.5 g m^{-2} . This indicates the observation period being less representative as the number of events is significantly lower.

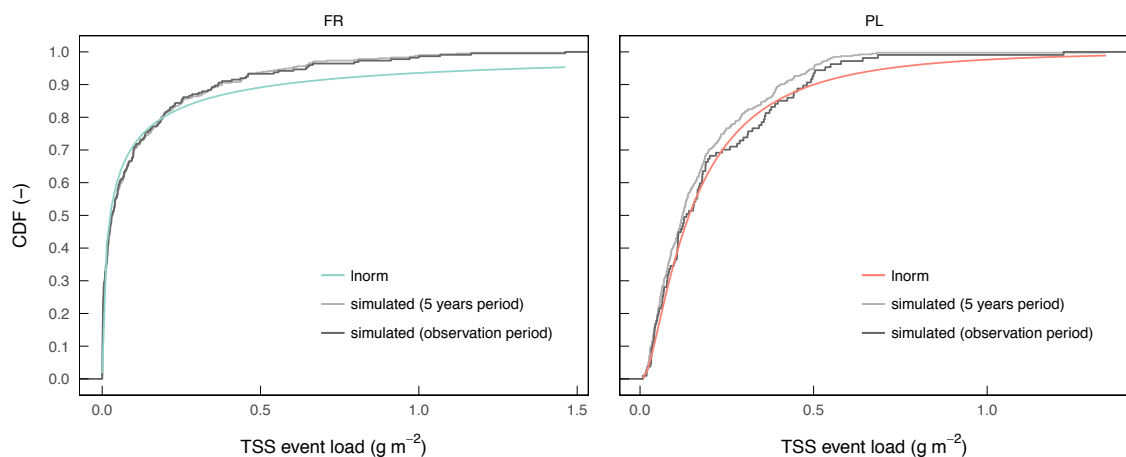


Figure 4-11. Cumulative distribution functions of lognormal and simulated TSS event loads for the observation period (calibration) and the 5 years period (validation) for sites Flat Roof (left) and Parking Lot (right) (Leutnant et al. 2018b).

Table 4-12. Goodness-of-fit matrix for observation period (calibration) and 5 years period (validation) (FR: Flat Roof, PL: Parking lot, KS Dn: Kolmogorov-Smirnov distance) (Leutnant et al. 2018b).

| site | | KS D _N | | |
|------|--------------------|-------------------|-------------------------|----------------|
| | | Inorm | observation pe- riod | 5 years period |
| FR | Inorm | - | | |
| | observation period | 0.053 | - | |
| | 5 years period | 0.062 | 0.035 | - |
| PL | Inorm | - | | |
| | observation period | 0.049 | - | |
| | 5 years period | 0.073 | 0.083 | - |

4.3.2 Annual TSS loads¹⁵

Calibrated and validated models were finally used to estimate annual TSS loads (Table 4-13) which is of special interests for practical purposes. In the present study, the estimated mean annual TSS loads for site FR is $9.9 \text{ g m}^{-2} \text{ a}^{-1}$ (sd: 0.75) which according to Dierschke (2014) represents a roof with “low to normal” load contribution. Annual TSS loads for site PL was estimated at $13.7 \text{ g m}^{-2} \text{ a}^{-1}$ (sd: 1.17) which is significant lower than reported from measurements by Allen Burton and Pitt (2001) ($\sim 40 \text{ g m}^{-2} \text{ a}^{-1}$). As already stated, the model disregards traffic related stochastic inputs, which could explain the low annual TSS loads estimated. Consequently, the result must be carefully interpreted. Nevertheless, the result highlights the need to especially account for load intensive events either through an alternative objective function or modification of the model concept.

Table 4-13. Simulated annual TSS loads (FR: Flat Roof, PL: Parking lot) (Leutnant et al. 2018b).

| site | n (moving years within 5 years period) | annual TSS loads ($\text{g m}^{-2} \text{ a}^{-1}$) | |
|------|---|---|------|
| | | mean | sd |
| FR | 50 | 9.9 | 0.75 |
| PL | 50 | 13.7 | 1.17 |

¹⁵ This section is partly composed of paragraphs from Leutnant et al. (2018b)

5 Conclusions and outlook¹⁶

In this thesis, a long-term monitoring campaign was conducted to analyze stormwater pollutant processes at four common urban catchments. Stormwater quality data from i) a flat roof (FR), ii) a parking lot (PL), iii) a residential catchment with a separated sewer system (RC) and iv) a high traffic street (HT) were collected. Small catchments were especially selected to isolate relevant pollutant processes and to reduce interfering influences of catchment size and environment surrounded. With primary focus on the quality parameter total suspended solids (TSS), turbidity signals were used as a surrogate to derive continuous TSS time series. Regression functions required were site-specifically determined and applied to convert raw turbidity data. As continuous stormwater quality data of small urban environments (< 10 ha) have not been captured in-situ before, this data innovatively allows to investigate pollutant processes.

Continuous monitoring data were used to create a site-specific event database. Besides rainfall and runoff characteristics, the database contains TSS event loads and TSS event mean concentrations for each event.

5.1 Stormwater quality processes at small sites

A correlation analysis was conducted to investigate the relationship between meteorological attributes and TSS event loads. Using Pearson's correlation coefficient, a strong relationship between rainfall intensity and TSS event load for small catchments with a high proportion of impervious surfaces was revealed. Contrarily, the correlation at site RC was observed to be less significant.

The antecedent dry weather period was shown to be low correlated which generally questions its sole application to describe pollutant build-up.

Intra-event pollutant processes were analyzed by means of Mass-Volume-Curves (MV-Curves). For the first-time, MV-curves were grouped at runoff quantiles which allows to identify general washoff characteristics.

This analysis revealed that the washoff process at site FR tends to be source-limited while sites PL and HT show a transport-limited behavior. Washoff at site RC is assumed to be influenced by superposed runoff from multiple subcatchments.

Nevertheless, a seasonal analysis of site-specific MV-curve distributions highlighted the large variability of pollutant processes, even for small catchments.

Consequently, influences are multifaceted and demand for further probabilistic analyses.

Furthermore, the event database was further used to derive site-specific empirical distribution functions of TSS event loads. Aiming towards a universal probabilistic description of TSS event load distributions, a set of theoretical distribution

¹⁶ This chapter is partly composed of paragraphs from Leutnant et al. (2018a, 2016, 2018c, 2018b)

functions were used to describe the empirical data. The goodness-of-fit was evaluated by Kolmogorov-Smirnov's test statistic and the minimum sample size required to achieve satisfying fittings was investigated.

From the analysis, it was found that the lognormal distribution function is most expressive to approximate empirical TSS event load distributions at all experimental sites. Successfully derived and fitted distribution functions provide a closed-form characterization of TSS event loads, consequently allowing to intra- and extrapolate of probabilistic event characteristics not observed. The minimum sample analysis demonstrated that a robust fitting should generally prioritize sample size over sampling period. About 40 events are required to reasonably fit the lognormal distribution. Using more samples potentially improves the goodness-of-fit but subsequently requires to extend the duration of cost-intensive monitoring campaigns.

When applying the concept of probabilistic description of TSS event loads based on theoretical distribution function, the results of this analysis may also support the evaluation of stormwater runoff quality monitoring campaigns with respect to their duration-to-information ratio. Data from an ongoing monitoring campaign may be used to update the parameters of the theoretical distribution function which in turn can be analyzed in terms of their relative change. If changes are not significant the duration of monitoring might be shortened. However, the minimum sample size should be taken into account (cf. section 4.2.2).

Also, the fitted distribution functions provide an excellent basis to calibrate urban stormwater quality models by focusing on probabilistic TSS event load characteristics. This finding especially led to the development of an innovative calibration approach of stormwater quality models, presented in the last part of this thesis.

5.2 Stormwater quality modelling

Modelling stormwater quality processes historically showed poor performance because of i) unsuitable model concepts for pollutant buildup and washoff and ii) lack of calibration data. With respect to more appropriate model concepts, it is assumed that pollutant stochasticity needs to be considered.

The presented calibration approach for existing conceptual stormwater quality models primarily aims at replicating TSS event load distributions by using a parameterized lognormal distribution function as objective function. This implies that instead of replicating occurrence and extent with chronologic precision, TSS event loads are considered probabilistically. In this way pollutant stochasticity is taken into account.

The approach developed was successfully demonstrated with stormwater quality models of site FR and PL for which reliable lognormal distribution functions were previously determined. Both models have been successfully calibrated, indicated by the low Kolmogorov-Smirnov distance measure. Distribution functions from simulation were validated with 5 years rainfall data. The maximum deviation between lognormal and simulated TSS event load distribution is 5%. A notably high agreement of observed and simulated mean of event mean concentrations

(μEMC) was achieved for both sites (FR: 33.2 vs. 33.4 mg L^{-1} , PL: 60.3 vs. 62.9 mg L^{-1}).

Finally, calibrated stormwater quality models allows to estimate annual TSS loads. This is of special interest from a practical point of view as annual TSS loads is a key parameter for emission control in several stormwater management guidelines. The average annual loads for site FR are 9.9 $\text{g m}^{-2} \text{a}^{-1}$ and 13.7 $\text{g m}^{-2} \text{a}^{-1}$ for site parking lot.

5.3 Outlook

This work focused the quality of urban stormwater runoff being a major source of nonpoint pollutants. An in-depth understanding of pollutant processes promotes an appropriate design of treatment measures which in turn results in environmental and economic benefits.

To gain further insights, online measurement techniques were applied to observe natural processes. A significant correlation of turbidity and TSS was fundamental for this thesis. However, the correlation was initially found to be lower than other studies reported (e.g. Al Ali et al. 2017). While this is assumed to be caused by the composition of stormwater (stormwater matrix), this clearly highlights the uncertainty affected to this method. In fact, turbidity is influenced by various parameters such as particle distribution, shape and color. Consequently, knowing the site-specific stormwater matrix with respect to its particle characteristics would allow to improve the correlation. This should also include the proportion of organic and mineral contaminants. In this respect UV-Vis spectrometer probes may provide more information as the adsorbance of multiple frequencies is measured. However, this highlights again the importance of sampling which is essential to establish the regression function. Sampling from small sites has been found to be challenging as runoff is usually low. The applied vacuum sampler occasionally stopped sampling under these conditions as inflow was insufficient. In case of small sites, a more appropriate sampling strategy designed for low-flow might increase the sampling robustness.

More physically-based models to replicate pollutant buildup and washoff processes will potentially increase the reliability of model results. While the washoff process got recently more attention by international research (Hong et al. 2016a, 2016b, 2016c, Shaw et al. 2006), this was not observed for pollutant buildup (Gunawardena et al. 2018). A systematic analysis, possibly supported by comprehensive measurement campaigns and modern data analysis techniques, is assumed to be required to improve knowledge on atmospheric deposition and traffic related pollution. However, random influences from e.g. construction sites will still remain and could hardly be described deterministically. But this can be minimized if monitoring sites are carefully chosen.

The objective function used for calibration employs the Kolmogorov-Smirnov statistic. While this goodness-of-fit criterion captivates by its simplicity, it has been shown, that events with high TSS event loads tend to be underestimated. A more behavioral distance measure which also accounts for events with high loads remains open for future research. Moreover, the calibration approach developed still needs to be tested on larger catchments which consists of multiple subcatchments with different land use. Additionally, it could be of interest whether conceptual model parameters for pollutant processes are correlated to parameters of the theoretical distribution function or catchment characteristics.

Using a theoretical distribution instead of an empirical distribution allows to calibrate stormwater quality models even if data is incomplete as the theoretical distribution is continuously defined. The approach developed is assumed to be general applicable and especially powerful if distribution functions get generalizable on a catchment-scale. This however requires additional measurement data. In this thesis data from four common types of urban catchments were collected and used. The transferability of the methods applied and developed has not been verified yet. Comparing the parameterized lognormal distributions with data from similar catchment would be of high relevance.

The empirical concepts for pollutant buildup and washoff are known to be mostly inappropriate. However, in contrast to more physically-based models, its usage is simple, fast and only little additional data is required. With the calibration approach developed, the calibrated model aims to simulate probabilistic TSS event loads over long-term condition. Conversely, stormwater quality shows seasonal variability (cf. 1.1.2) which is currently not taken into account. Additional research on seasonal pollutant distribution might improve the calibration scheme. For example, events within a load intensive season might get additional weights. Also, model parameters might follow a seasonal pattern.

This thesis used a broad field of methods aiming to observe, understand and replicate stormwater quality processes. Methods were linked from topics of online monitoring techniques, data management, data analysis and modelling. The requirements are undoubtedly immense and introduce its own complexity. This must be taken into account, especially when considering a broader application. An appropriate measurement data management system is crucial and strongly advised as the amount of data is expected to increase significantly in the next years.

6 References

- Al Ali, S., Bonhomme, C., Dubois, P., and Chebbo, G. (2017): Investigation of the wash-off process using an innovative portable rainfall simulator allowing continuous monitoring of flow and turbidity at the urban surface outlet. *Science of The Total Environment*, **609**, S. 17–26.
- Alias, N., Liu, A., Goonetilleke, A., and Egodawatta, P. (2014): Time as the critical factor in the investigation of the relationship between pollutant wash-off and rainfall characteristics. *Ecological Engineering*, **64**, S. 301–305.
- Allen Burton, G. and Pitt, R. (2001): *Stormwater Effects Handbook: A Toolbox for Watershed Managers, Scientists, and Engineers*. : CRC Press.
- Amodio, M., Catino, S., Dambruoso, P. R., de Gennaro, G., Di Gilio, A., Giungato, P., Laiola, E., Marzocca, A., Mazzone, A., Sardaro, A., and Tutino, M. (2014): Atmospheric Deposition: Sampling Procedures, Analytical Methods, and Main Recent Findings from the Scientific Literature. *Advances in Meteorology*, **2014**, S. 1–27.
- Ardia, D., Mullen, K. M., Peterson, B. G., and Ulrich, J. (2016): *DEoptim: Differential Evolution in R*.
- Aryal, R. K., Furumai, H., Nakajima, F., and Boller, M. (2005): Dynamic behavior of fractional suspended solids and particle-bound polycyclic aromatic hydrocarbons in highway runoff. *Water Research*, **39**(20), S. 5126–5134.
- Aryal, R., Vigneswaran, S., Kandasamy, J., and Naidu, R. (2010): Urban stormwater quality and treatment. *Korean Journal of Chemical Engineering*, **27**(5), S. 1343–1359.
- Bai, S. and Li, J. (2013): Sediment Wash-Off from an Impervious Urban Land Surface. *Journal of Hydrologic Engineering*, **18**(5), S. 488–498.
- Barbosa, A. E., Fernandes, J. N., and David, L. M. (2012): Key issues for sustainable urban stormwater management. *Water Research*, **46**(20), S. 6787–6798.
- Beck, H. J. and Birch, G. F. (2012): Spatial and Temporal Variance of Metal and Suspended Solids Relationships in Urban Stormwater—Implications for Monitoring. *Water, Air, & Soil Pollution*, **223**(3), S. 1005–1015.
- Beck, H. J. and Birch, G. F. (2013): The magnitude of variability produced by methods used to estimate annual stormwater contaminant loads for highly urbanised catchments. *Environmental Monitoring and Assessment*, **185**(6), S. 5209–5220.
- Bender, G. H. and Terstriep, H. L. (1984): Effectiveness of street sweeping in urban runoff pollution control. *The Science of the Total Environment*, **33**, S. 185–192.

- Bertrand-Krajewski, J. L., Chebbo, G., and Saget, A. (1998): Distribution of pollutant mass vs volume in stormwater discharges and the first flush phenomenon. *Water Research*, **32**(8), S. 2341–2356.
- Bertrand-Krajewski, J.-L. (2004): TSS concentration in sewers estimated from turbidity measurements by means of linear regression accounting for uncertainties in both variables. *Water Science and Technology*, **50**(11), S. 81–88.
- Bertrand-Krajewski, J.-L. (2007): Stormwater pollutant loads modelling: epistemological aspects and case studies on the influence of field data sets on calibration and verification. *Water Science and Technology*, **55**(4), S. 1–17.
- Bilotta, G. S. and Brazier, R. E. (2008): Understanding the influence of suspended solids on water quality and aquatic biota. *Water Research*, **42**(12), S. 2849–2861.
- Bonhomme, C. and Petrucci, G. (2017): Should we trust build-up/wash-off water quality models at the scale of urban catchments?. *Water Research*, **108**, S. 422–431.
- Bratieres, K., Fletcher, T. D., Deletic, A., and Zinger, Y. (2008): Nutrient and sediment removal by stormwater biofilters: A large-scale design optimisation study. *Water Research*, **42**(14), S. 3930–3940.
- Brezonik, P. L. and Stadelmann, T. H. (2002): Analysis and predictive models of stormwater runoff volumes, loads, and pollutant concentrations from watersheds in the Twin Cities metropolitan area, Minnesota, USA. *Water Research*, **36**(7), S. 1743–1757.
- Brombach, H., Weiss, G., and Fuchs, S. (2005): A new database on urban runoff pollution: comparison of separate and combined sewer systems. *Water Science and Technology*, **51**(2), S. 119–128.
- Campisano, A., Ple, J. C., Muschalla, D., Pleau, M., and Vanrolleghem, P. A. (2013): Potential and limitations of modern equipment for real time control of urban wastewater systems. *Urban Water Journal*, **10**(5), S. 300–311.
- Caradot, N., Sonnenberg, H., Riechel, M., Matzinger, A., and Rouault, P. (2013): The influence of local calibration on the quality of UV-VIS spectrometer measurements in urban stormwater monitoring. *Water Practice and Technology*, **8**(3–4).
- Caradot, N., Sonnenberg, H., Rouault, P., Gruber, G., Hofer, T., Torres, A., Pesci, M., and Bertrand-Krajewski, J.-L. (2015): Influence of local calibration on the quality of online wet weather discharge monitoring: feedback from five international case studies. *Water Science & Technology*, **71**(1), S. 45.

- Charters, F. J., Cochrane, T. A., and O'Sullivan, A. D. (2015): Particle size distribution variance in untreated urban runoff and its implication on treatment selection. *Water Research*, **85**, S. 337–345.
- Chebbo, G. and Bachoc, A. (1992): Characterization of Suspended-Solids in Urban Wet Weather Discharges. *Water Science and Technology*, **25**(8), S. 171–179.
- Chen, J. and Adams, B. J. (2007): A derived probability distribution approach to stormwater quality modeling. *Advances in Water Resources*, **30**(1), S. 80–100.
- Daly, E., Bach, P. M., and Deletic, A. (2014): Stormwater pollutant runoff: A stochastic approach. *Advances in Water Resources*, **74**, S. 148–155.
- Davis, B. and Birch, G. (2010): Comparison of heavy metal loads in stormwater runoff from major and minor urban roads using pollutant yield rating curves. *Environmental Pollution*, **158**(8), S. 2541–2545.
- Deb, K. (2008): *Multi-Objective Optimization using Evolutionary Algorithms*. Chichester: John Wiley & Sons, LTD.
- Deb, K., Agrawal, S., and Pratap, A. (Eds.) (2000): *A Fast Elitist Non-dominated Sorting Genetic Algorithm for Multi-objective Optimization: NSGA-II*. Vol. 1917, New York: Springer.
- Delestre, O., Darboux, F., James, F., Lucas, C., Laguerre, C., and Cordier, S. (2017): FullSWOF: Full Shallow-Water equations for Overland Flow. *The Journal of Open Source Software*, **2**(20), S. 448.
- Deletic, A. (1998): The first flush load of urban surface runoff. *Water Research*, **32**(8), S. 2462–2470.
- Deletic, A. B. and Maksimovic, Č. T. (1998): Evaluation of water quality factors in storm runoff from paved areas. *Journal of Environmental Engineering*, **124**(9), S. 869–879.
- Deletic, A. and Orr, D. W. (2005): Pollution Buildup on Road Surfaces. *Journal of Environmental Engineering*, **131**(1), S. 49–59.
- Delignette-Muller, M. L. and Dutang, C. (2015): fitdistrplus: An R package for fitting distributions. *Journal of Statistical Software*, **64**(4), S. 1–34.
- Di Modugno, M., Gioia, A., Gorgoglione, A., Iacobellis, V., la Forgia, G., Piccinni, A., and Ranieri, E. (2015): Build-Up/Wash-Off Monitoring and Assessment for Sustainable Management of First Flush in an Urban Area. *Sustainability*, **7**(5), S. 5050–5070.
- Dierschke, M. (2014): *Methodischer Ansatz zur Quantifizierung von Feinpartikeln (PM63) in Niederschlagsabflüssen in Abhängigkeit von der Herkunftsfläche ("Methodical approach for quantifying of fine particles (PM63) in rainfall runoffs depending on the surface of origin")*. Dissertation (in German). University of Kaiserslautern.

- Dierschke, M. and Welker, A. (2013): Feine Feststoffe (PM63) in Dachabflüssen. *Gwf Wasser-Abwasser*, **154**(11), S. 1242–1249.
- Dierschke, M. and Welker, A. (2015): Bestimmung von Feststoffen in Niederschlagsabflüssen. *Gwf Wasser-Abwasser*, **156**(4), S. 440–446.
- DIN 38409-2 (1987): Summarische Wirkungs- und Stoffkenngrößen (Gruppe H) - Bestimmung der abfiltrierbaren Stoffe und des Glührückstandes (H 2).
- Dotto, C. B. S., Deletic, A., and Fletcher, T. D. (2009): Analysis of parameter uncertainty of a flow and quality stormwater model. *Water Science & Technology*, **60**(3), S. 717.
- Dotto, C. B. S., Kleidorfer, M., Deletic, A., Rauch, W., McCarthy, D. T., and Fletcher, T. D. (2011): Performance and sensitivity analysis of stormwater models using a Bayesian approach and long-term high resolution data. *Environmental Modelling & Software*, **26**(10), S. 1225–1239.
- Eddelbuettel, D. and François, R. (2011): Rcpp: Seamless R and C++ Integration. *Journal of Statistical Software*, **40**(8), S. 1–18.
- Egodawatta, P., Miguntanna, N. S., and Goonetilleke, A. (2012): Impact of roof surface runoff on urban water quality. *Water Science and Technology*, **66**(7), S. 1527–1533.
- Egodawatta, P., Thomas, E., and Goonetilleke, A. (2007): Mathematical interpretation of pollutant wash-off from urban road surfaces using simulated rainfall. *Water Research*, **41**(13), S. 3025–3031.
- Egodawatta, P., Ziyath, A. M., and Goonetilleke, A. (2013): Characterising metal build-up on urban road surfaces. *Environmental Pollution*, **176**, S. 87–91.
- Fallah Shorshani, M., Bonhomme, C., Petrucci, G., André, M., and Seigneur, C. (2014): Road traffic impact on urban water quality: a step towards integrated traffic, air and stormwater modelling. *Environmental Science and Pollution Research*, **21**(8), S. 5297–5310.
- Förster, J. (1999): Variability of roof runoff quality. *Water Science and Technology*, **39**(5), S. 137–144.
- Francey, M., Fletcher, T. D., Deletic, A., and Duncan, H. (2010): New Insights into the Quality of Urban Storm Water in South Eastern Australia. *Journal of Environmental Engineering-Asce*, **136**(4), S. 381–390.
- Gamerith, V., Neumann, M. B., and Muschalla, D. (2013): Applying global sensitivity analysis to the modelling of flow and water quality in sewers. *Water Research*, **47**(13), S. 4600–4611.
- Geiger, W. F. (1987): Flushing effects in combined sewer systems. In: *Proceedings of the 4th International Conference in Urban Storm Drainage.*, S. 40–46, Lausanne, Switzerland.

- Goonetilleke, A., Thomas, E., Ginn, S., and Gilbert, D. (2005): Understanding the role of land use in urban stormwater quality management. *Journal of Environmental Management*, **74**(1), S. 31–42.
- Grottker, M. (1987): Runoff quality from a street with medium traffic loading. *Science of The Total Environment*, **59**(0), S. 457–466.
- Gruber, G., Winkler, S., and Pressl, A. (2004): Quantification of pollution loads from CSOs into surface water bodies by means of online techniques. *Water Science and Technology*, **50**(11), S. 73–80.
- Gunawardena, J., Egodawatta, P., Ayoko, G. A., and Goonetilleke, A. (2012): Role of traffic in atmospheric accumulation of heavy metals and polycyclic aromatic hydrocarbons. *Atmospheric Environment*, **54**, S. 502–510.
- Gunawardena, J., Egodawatta, P., Ayoko, G. A., and Goonetilleke, A. (2013): Atmospheric deposition as a source of heavy metals in urban stormwater. *Atmospheric Environment*, **68**, S. 235–242.
- Gunawardena, J. M. A., Liu, A., Egodawatta, P., Ayoko, G. A., and Goonetilleke, A. (2018): Influence of Traffic and Land Use on Urban Stormwater Quality - implications for urban stormwater treatment design. Singapore: Springer Singapore.
- Gunawardena, J., Ziyath, A. M., Egodawatta, P., Ayoko, G. A., and Goonetilleke, A. (2014): Mathematical relationships for metal build-up on urban road surfaces based on traffic and land use characteristics. *Chemosphere*, **99**, S. 267–271.
- Hannouche, A., Chebbo, G., Joannis, C., Gasperi, J., Gromaire, M.-C., Moille-ron, R., Barraud, S., and Ruban, V. (2017): Stochastic evaluation of annual micropollutant loads and their uncertainties in separate storm sewers. *Environmental Science and Pollution Research*, **24**(36), S. 28205–28219.
- Hannouche, A., Chebbo, G., Ruban, G., Tassin, B., Lemaire, B. J., and Joannis, C. (2011): Relationship between turbidity and total suspended solids concentration within a combined sewer system. *Water Science and Technology*, **64**(12), S. 2445–2452.
- Harremoës, P. (1988): Stochastic models for estimation of extreme pollution from urban runoff. *Water Research*, **22**(8), S. 1017–1026.
- Hedderich, J. and Sachs, L. (2012): *Angewandte Statistik: Methodensammlung mit R. 14., überarb. und erg. Aufl*, Heidelberg: Springer.
- Helmreich, B., Hilliges, R., Schriewer, A., and Horn, H. (2010): Runoff pollutants of a highly trafficked urban road – Correlation analysis and seasonal influences. *Chemosphere*, **80**(9), S. 991–997.

- Henrichs, M. (2015): Einfluss von Unsicherheiten auf die Kalibrierung urbanhydrologischer Modelle ("Influence of uncertainties on the calibration of urban hydrological models"). Dissertation (in German). Technische Universität Dresden, Dresden.
- Herngren, L. F. (2005): Build-up and wash-off process kinetics of PAHs and heavy metals on paved surfaces using simulated rainfall. PhD. .
- Hong, Y., Bonhomme, C., and Chebbo, G. (2016a): Development and Assessment of the Physically-Based 2D/1D Model "TRENNOE" for Urban Stormwater Quantity and Quality Modelling. *Water*, **8**(12), S. 606.
- Hong, Y., Bonhomme, C., Le, M.-H., and Chebbo, G. (2016b): A new approach of monitoring and physically-based modelling to investigate urban wash-off process on a road catchment near Paris. *Water Research*, **102**, S. 96–108.
- Hong, Y., Bonhomme, C., Le, M.-H., and Chebbo, G. (2016c): New insights into the urban washoff process with detailed physical modelling. *Science of The Total Environment*, **573**, S. 924–936.
- Hvitved-Jacobsen, T., Vollertsen, J., and Nielsen, A. H. (2010): Urban and highway stormwater pollution : concepts and engineering. Boca Raton, FL: CRC Press/Taylor & Francis.
- Iserloh, T., Fister, W., Seeger, M., Willger, H., and Ries, J. B. (2012): A small portable rainfall simulator for reproducible experiments on soil erosion. *Soil and Tillage Research*, **124**(0), S. 131–137.
- Kobencic, R. (2002): Verunreinigung des Regenwasserabflusses von Dachflächen. Diplomarbeit. TU Graz, Graz.
- Krein, A. and Schorer, M. (2000): Road runoff pollution by polycyclic aromatic hydrocarbons and its contribution to river sediments. *Water Research*, **34**(16), S. 4110–4115.
- Lacour, C., Joannis, C., and Chebbo, G. (2009a): Assessment of annual pollutant loads in combined sewers from continuous turbidity measurements: Sensitivity to calibration data. *Water Research*, **43**(8), S. 2179–2190.
- Lacour, C., Joannis, C., Gromaire, M.-C., and Chebbo, G. (2009b): Potential of turbidity monitoring for real time control of pollutant discharge in sewers during rainfall events. *Water Science & Technology*, **59**(8), S. 1471.
- Le, M.-H., Cordier, S., Lucas, C., and Cerdan, O. (2015): A faster numerical scheme for a coupled system modeling soil erosion and sediment transport. *Water Resources Research*, **51**(2), S. 987–1005.
- Lee, H., Lau, S.-L., Kayhanian, M., and Stenstrom, M. K. (2004): Seasonal first flush phenomenon of urban stormwater discharges. *Water Research*, **38**(19), S. 4153–4163.

- Lepot, M., Aubin, J. B., and Bertrand-Krajewski, J. L. (2013): Accuracy of different sensors for the estimation of pollutant concentrations (total suspended solids, total and dissolved chemical oxygen demand) in wastewater and stormwater. *Water Sci Technol*, **68**(2), S. 462–71.
- Leutnant, D., Döring, A., and Uhl, M. (2018a): swmmr - An R package to interface SWMM. *Environmental Modelling & Software*, **submitted on March 7th**.
- Leutnant, D., Henrichs, M., Muschalla, D., and Uhl, M. (2015): OSCAR - An online supervisory control and urban drainage data acquisition system with R. In: T. Maere, S. Tik, S. Duchesne, and P. Vanrolleghem (Eds.): *Proceedings of the 10th International Conference on Urban Drainage Modelling*, S. 135–138, Quebec, Kanada.
- Leutnant, D., Muschalla, D., and Uhl, M. (2016): Stormwater Pollutant Process Analysis with Long-Term Online Monitoring Data at Micro-Scale Sites. *Water*, **8**(7), S. 299.
- Leutnant, D., Muschalla, D., and Uhl, M. (2018b): Distribution-based Calibration of a Stormwater Quality Model. *Water*, **submitted on April 26th**.
- Leutnant, D., Muschalla, D., and Uhl, M. (2018c): Statistical Distribution of TSS Event Loads From Small Urban Environments. *Water*, **submitted on April 12th**.
- Li, Y., Jia, Z., Wijesiri, B., Song, N., and Goonetilleke, A. (2017): Influence of traffic on build-up of polycyclic aromatic hydrocarbons on urban road surfaces: A Bayesian network modelling approach. *Environmental Pollution*.
- Liu, A., Egodawatta, P., Guan, Y., and Goonetilleke, A. (2013): Influence of rainfall and catchment characteristics on urban stormwater quality. *Science of The Total Environment*, **444**, S. 255–262.
- Liu, A., Goonetilleke, A., and Egodawatta, P. (2012): Taxonomy for rainfall events based on pollutant wash-off potential in urban areas. *Ecological Engineering*, **47**, S. 110–114.
- Liu, A., Liu, L., Li, D., and Guan, Y. (2015): Characterizing heavy metal build-up on urban road surfaces: Implication for stormwater reuse. *Science of The Total Environment*, **515–516**, S. 20–29.
- Makepeace, D. K., Smith, D. W., and Stanley, S. J. (1995): Urban stormwater quality: Summary of contaminant data. *Critical Reviews in Environmental Science and Technology*, **25**(2), S. 93–139.
- Markiewicz, A., Björklund, K., Eriksson, E., Kalmykova, Y., Strömvall, A.-M., and Siopi, A. (2017): Emissions of organic pollutants from traffic and roads: Priority pollutants selection and substance flow analysis. *Science of The Total Environment*, **580**, S. 1162–1174.

- Métadier, M. and Bertrand-Krajewski, J.-L. (2012): The use of long-term on-line turbidity measurements for the calculation of urban stormwater pollutant concentrations, loads, pollutographs and intra-event fluxes. *Water Research*, **46**(20), S. 6836–6856.
- Miguntanna, N. P., Goonetilleke, A., Egodawatta, P., and Kokot, S. (2010): Understanding nutrient build-up on urban road surfaces. *Journal of Environmental Sciences*, **22**(6), S. 806–812.
- Miguntanna, N. P., Liu, A., Egodawatta, P., and Goonetilleke, A. (2013): Characterising nutrients wash-off for effective urban stormwater treatment design. *Journal of Environmental Management*, **120**, S. 61–67.
- Müller, K. and Wickham, H. (2017): *tibble: Simple Data Frames*.
- Mummullage, S., Egodawatta, P., Ayoko, G. A., and Goonetilleke, A. (2016): Sources of hydrocarbons in urban road dust: Identification, quantification and prediction. *Environmental Pollution*, **216**, S. 80–85.
- Murphy, L. U., Cochrane, T. A., and O’Sullivan, A. (2015): Build-up and wash-off dynamics of atmospherically derived Cu, Pb, Zn and TSS in stormwater runoff as a function of meteorological characteristics. *Science of The Total Environment*, **508**, S. 206–213.
- Muschalla, D., Schneider, S., Gameraith, V., Gruber, G., and Schroter, K. (2008): Sewer modelling based on highly distributed calibration data sets and multi-objective auto-calibration schemes. *Water Science and Technology*, **57**(10), S. 1547–1554.
- Muthusamy, M., Tait, S., Schellart, A., Beg, M. N. A., Carvalho, R. F., and de Lima, J. L. M. P. (2018): Improving understanding of the underlying physical process of sediment wash-off from urban road surfaces. *Journal of Hydrology*, **557**, S. 426–433.
- Nash, J. E. and Sutcliffe, J. V. (1970): River flow forecasting through conceptual models part I - A discussion of principles. *Journal of Hydrology*, **10**(3), S. 282–290.
- Niazi, M., Nietch, C., Maghrebi, M., Jackson, N., Bennett, B. R., Tryby, M., and Massoudieh, A. (2017): Storm Water Management Model: Performance Review and Gap Analysis. *Journal of Sustainable Water in the Built Environment*, **3**(2), S. 04017002.
- Osman Akan, A. (1988): Derived Frequency Distribution for Storm Runoff Pollution. *Journal of Environmental Engineering*, **114**(6), S. 1344–1351.
- Pebesma, E. (2018): *sf: Simple Features for R*.
- Petrucci, G., Gromaire, M.-C., Shorshani, M. F., and Chebbo, G. (2014): Non-point source pollution of urban stormwater runoff: a methodology for source analysis. *Environmental Science and Pollution Research*, **21**(17), S. 10225–10242.

- Price, K. V., Storn, R. M., and Lampinen, J. A. (2005): *Differential evolution: a practical approach to global optimization*. Berlin ; New York: Springer.
- Qin, H., Tan, X., Fu, G., Zhang, Y., and Huang, Y. (2013): Frequency analysis of urban runoff quality in an urbanizing catchment of Shenzhen, China. *Journal of Hydrology*, **496**, S. 79–88.
- R Core Team (2018): *R: A Language and Environment for Statistical Computing*. Vienna, Austria: R Foundation for Statistical Computing.
- Rossi, L., Chèvre, N., Fankhauser, R., Margot, J., Curdy, R., Babut, M., and Barry, D. A. (2013): Sediment contamination assessment in urban areas based on total suspended solids. *Water Research*, **47**(1), S. 339–350.
- Rossi, L., Krejci, V., Rauch, W., Kreikenbaum, S., Fankhauser, R., and Gujer, W. (2005): Stochastic modeling of total suspended solids (TSS) in urban areas during rain events. *Water Research*, **39**(17), S. 4188–4196.
- Rossmann, L. A. (2010): *Storm Water Management Model - User's Manual Version 5.0.*, S. 285, Cincinnati, OH, USA: United States Environmental Protection Agency (US EPA).
- Ryan, J. A. and Ulrich, J. M. (2017): *xts: eXtensible Time Series*.
- Sage, J., Bonhomme, C., Al Ali, S., and Gromaire, M.-C. (2015): Performance assessment of a commonly used “accumulation and wash-off” model from long-term continuous road runoff turbidity measurements. *Water Research*, **78**(0), S. 47–59.
- Sansalone, J. J. and Buchberger, S. G. (1997): Characterization of solid and metal element distributions in urban highway stormwater. *Water Science and Technology*, **36**(8–9), S. 155–160.
- Sartor, J. D. and Boyd, G. B. (1972): *Water pollution aspects of street surface contaminants*. No. EPA-R2-72/081 : US Environmental Protection Agency, Washington, DC, USA,.
- Scholz, K. (1995): *Stochastische Simulation urbanhydrologischer Prozesse* (“Stochastic simulation of urban hydrological processes”). Dissertation (in German). University of Hannover.
- Sharifi, S., Massoudieh, A., and Kayhanian, M. (2011): A Stochastic Stormwater Quality Volume-Sizing Method with First Flush Emphasis. *Water Environment Research*, **83**(11), S. 2025–2035.
- Shaw, S. B., Stedinger, J. R., and Walter, M. T. (2010): Evaluating Urban Pollutant Buildup/Wash-Off Models Using a Madison, Wisconsin Catchment. *Journal of Environmental Engineering*, **136**(2), S. 194–203.
- Shaw, S. B., Walter, M. T., and Steenhuis, T. S. (2006): A physical model of particulate wash-off from rough impervious surfaces. *Journal of Hydrology*, **327**(3–4), S. 618–626.

- Shen, Z., Liu, J., Aini, G., and Gong, Y. (2016): A comparative study of the grain-size distribution of surface dust and stormwater runoff quality on typical urban roads and roofs in Beijing, China. *Environmental Science and Pollution Research*, **23**(3), S. 2693–2704.
- Sun, S., Barraud, S., Castebrunet, H., Aubin, J.-B., and Marmonier, P. (2015): Long-term stormwater quantity and quality analysis using continuous measurements in a French urban catchment. *Water Research*, **85**, S. 432–442.
- United Nations (2015): *World Urbanization Prospects: The 2014 Revision, (ST/ESA/SER.A/366)*. : Department of Economic and Social Affairs, Population Division.
- US-EPA (1971): *Methods for the Chemical Analysis of Water and Wastes (MCAWW). Method No. 160.2: Residue, Non-Filterable (Gravimetric, Dried at 103-105°C) (EPA/600/4-79/020)*.
- Vanderkam, D., Allaire, J. J., Owen, J., Gromer, D., Shevtsov, P., and Thieurmel, B. (2017): *dygraphs: Interface to “Dygraphs” Interactive Time Series Charting Library*.
- Wang, S., He, Q., Ai, H., Wang, Z., and Zhang, Q. (2013): Pollutant concentrations and pollution loads in stormwater runoff from different land uses in Chongqing. *Journal of Environmental Sciences*, **25**(3), S. 502–510.
- Welker, A. (2004): *Schadstoffströme im urbanen Wasserkreislauf - Aufkommen und Verteilung, insbesondere in den Abwasserentsorgungssystemen (“Pollutant flows in the urban water cycle - abundance and distribution, especially in urban drainage systems”)*. Habilitation (in German). University of Kaiserslautern, Kaiserslautern.
- Wickham, H. (2014): Tidy Data. *Journal of Statistical Software*, **59**(10).
- Wickham, H. (2016): *ggplot2: Elegant Graphics for Data Analysis*. : Springer-Verlag New York.
- Wickham, H. (2017): *tidyverse: Easily Install and Load the “Tidyverse.”*
- Wijesiri, B., Egodawatta, P., McGree, J., and Goonetilleke, A. (2015): Process variability of pollutant build-up on urban road surfaces. *Science of The Total Environment*, **518–519**(0), S. 434–440.
- Wijesiri, B., Egodawatta, P., McGree, J., and Goonetilleke, A. (2016): Influence of uncertainty inherent to heavy metal build-up and wash-off on stormwater quality. *Water Research*, **91**, S. 264–276.
- Yang, Y.-Y. and Toor, G. S. (2017): Sources and mechanisms of nitrate and orthophosphate transport in urban stormwater runoff from residential catchments. *Water Research*, **112**, S. 176–184.
- Zafra, C., Temprano, J., and Suárez, J. (2017): A simplified method for determining potential heavy metal loads washed-off by stormwater runoff from

- road-deposited sediments. *Science of The Total Environment*, **601–602**, S. 260–270.
- Zhao, H., Chen, X., Hao, S., Jiang, Y., Zhao, J., Zou, C., and Xie, W. (2016): Is the wash-off process of road-deposited sediment source limited or transport limited?. *Science of The Total Environment*, **563–564**, S. 62–70.
- Zhao, H., Jiang, Q., Xie, W., Li, X., and Yin, C. (2018): Role of urban surface roughness in road-deposited sediment build-up and wash-off. *Journal of Hydrology*, **560**, S. 75–85.
- Zhao, J., Chen, Y., Hu, B., and Yang, W. (2015): Mathematical Model for Sediment Wash-Off from Urban Impervious Surfaces. *Journal of Environmental Engineering*, **142**(4), S. 04015091.

Part B

Paper I - Stormwater Pollutant Process Analysis with Long-Term Online Monitoring Data at Micro-Scale Sites

Article

Stormwater Pollutant Process Analysis with Long-Term Online Monitoring Data at Micro-Scale Sites

Dominik Leutnant ^{1,*}, Dirk Muschalla ² and Mathias Uhl ¹

¹ Institute for Water Resources Environment (IWARU), Muenster University of Applied Sciences, Corrensstr. 25, Muenster 48149, Germany; uhl@fh-muenster.de

² Institute of Urban Water Management and Landscape Water Engineering, Graz University of Technology, Stremayrgasse 10/I, 8010 Graz, Austria; d.muschalla@tugraz.at

* Correspondence: leutnant@fh-muenster.de; Tel.: +49-251-83-65274

Academic Editor: Brigitte Helmreich

Received: 31 May 2016; Accepted: 1 July 2016; Published: 20 July 2016

Abstract: Stormwater runoff quality was measured with online turbidity sensors at four common types of small urban subcatchments: (i) a flat roof; (ii) a parking lot; (iii) a residential catchment; and (iv) a high-traffic street. Samples were taken to estimate site-specific correlations between total suspended solids (TSS) and turbidity. Continuous TSS time series were derived from online turbidity measurements and were used to estimate event loads and event mean concentrations. Rainfall runoff event characteristics were subjected to correlation analysis to TSS loads. Significant correlations were found for rainfall intensities at sites with high imperviousness and decrease with increasing catchment size. Antecedent dry weather periods are only correlated at the parking lot site. Intra-event TSS load distributions were studied with $M(V)$ -curves. $M(V)$ -curves are grouped at runoff quantiles and statistically described with boxplots. All sites show, in general, a more pronounced first-flush effect. While wash-off of the flat roof tends to be source-limited, the parking lot and high-traffic street sites show a more transport-limited behavior. Wash-off process of the residential catchment appears to be influenced by a composition of different subcatchments.

Keywords: stormwater quality; online monitoring; stormwater pollutant processes; micro scale

1. Introduction

Stormwater runoff from urban environments is a significant source of pollutants which impacts the quality of receiving waters. Effective measures require realistic estimations of stormwater pollutants to adequately protect the receiving water. Usually, stormwater quality models are applied to support the implementation of urban drainage strategies. Current stormwater quality model concepts are based upon empirical equations or simple regression functions to replicate the complex nature of pollutant accumulation and wash-off. Although, these approaches offer a set of parameters for model calibration, quality models often show poor performance when simulating long-term conditions [1,2]. As a result, model outputs are highly uncertain. Improving quality models is therefore crucial to produce more reliable model results. In this respect, in-depth knowledge of processes is a key requirement which consequently demands measurement data. In recent years much effort has been spent to investigate the influence of meteorological influences and catchment characteristics on stormwater quality based on samples at small sites [3–5]. Additionally, online turbidity measurements have been successfully used for intra-event analyses in larger catchments [6,7].

With aiming towards new insights of stormwater quality processes this work combines both approaches by using online turbidity measurements at microscale sites to analyze stormwater pollutant processes. Results of a long-term monitoring campaign at four common types of urban

subcatchments—(i) a flat roof; (ii) a parking lot; (iii) a residential catchment; and (iv) a high-traffic street—are presented. It is believed that monitoring at small urban environments is required to isolate relevant pollutant processes and to reduce interfering influences of catchment size and environment.

2. Materials and Methods

2.1. Experimental Sites

Stormwater runoff and quality was continuously monitored at four microscale experimental sites: (i) a 50 m² flat roof FR; (ii) a parking lot PL with approx. 2350 m²; (iii) a 9.4 ha residential catchment RC in a suburb of Muenster, Germany (separate sewer system); and (iv) a high-traffic HT street in the center of Muenster (2.5 ha, 30,000 vehicles per day). The 2% sloped roof is thoroughly covered with bitumen sheeting. Surfaces of the parking lot are asphalt (55%), porous pavement (40%, 8% thereof being joints) and small vegetated pervious areas (5%) which do not contribute to runoff. The impervious area has a slope of 2.5%. The residential catchment consists of streets (25%), flat and steep roofs (25%), and pervious area (50%). At site HT surfaces mainly consist of asphalt (60%), porous pavement (10%, 8% thereof being joints), flat and steep roofs (25%), and disconnected pervious area (5%).

2.2. Monitoring and Sampling Setup

Rainfall gauges are located at FR, PL, and RC (Pluvio2, OTT). Rainfall data from FR is also used for HT, being 2 km off FR. Runoff at FR runs from a downpipe into a horizontal measurement pipe (63 mm, PVC) in which an electromagnetic flowmeter (Promag50W25, Endress + Hauser) and quality sensors for turbidity, electrical conductivity, and pH (VisoTurb700IQ, TetraCon700IQ, and SensoLyt700IQ, WTW) are installed. Samples are taken from the measurement pipe with an automatic sampler (vacuum sampler ASP Station, Endress + Hauser). Sampling begins if runoff is above 0.03 L/s and repeats every 10 min. Each sample consists of five subsamples of about 200 mL. The capacity of the automatic sampler is 12 samples.

The control section at PL is a 300 mm circular concrete pipe (length 55 m, slope 1.8%). Runoff is calculated from measured water level by the Manning-Strickler-equation because of uniform flow conditions and no backwater effects. Manning's roughness coefficient n was experimentally determined with artificial inflows and ranges between 0.015 and 0.017. At RC and HT runoff is calculated from mean flow velocity and water level (POA, NIVUS). The control section at RC is a 900 mm circular concrete pipe (length 46 m, slope 1.8%). Manning's roughness coefficient n was also identified with artificial inflows and is about 0.0105. At HT, flow sensors are installed in a 500 mm circular concrete pipe (length 30 m, slope 0.6%).

In contrast to FR, quality sensors at PL, RC, and HT are integrated in a horizontal measurement pipe (63 mm, PVC, length: 1.5 m) of an external monitoring station (Figure 1). In case of an event stormwater is pumped to the measurement pipe by a peristaltic pump (Delasco 2Z3, PCM) through a hose (20 mm, PVC) whose orifice is fixed in the middle of the stormwater pipe 1.5 cm above the ground. The suction velocity in the hose is about 1.5 m/s with a corresponding flow of approx. 0.5 L/s. Stormwater flows with approx. 0.18 m/s through the measurement pipe and is later discharged to the sewer.

At these sites, the sampling program starts if the water level in the stormwater pipe exceeds 1.5 cm. Samples of all sites are tested for total suspended solid (TSS) concentrations based on a standard method given in [8], and fine solids less than 63 μm (TSS63) according to the protocol given in [9].

An online measurement data management system was applied to supervise all monitoring stations and to reduce data loss [10].

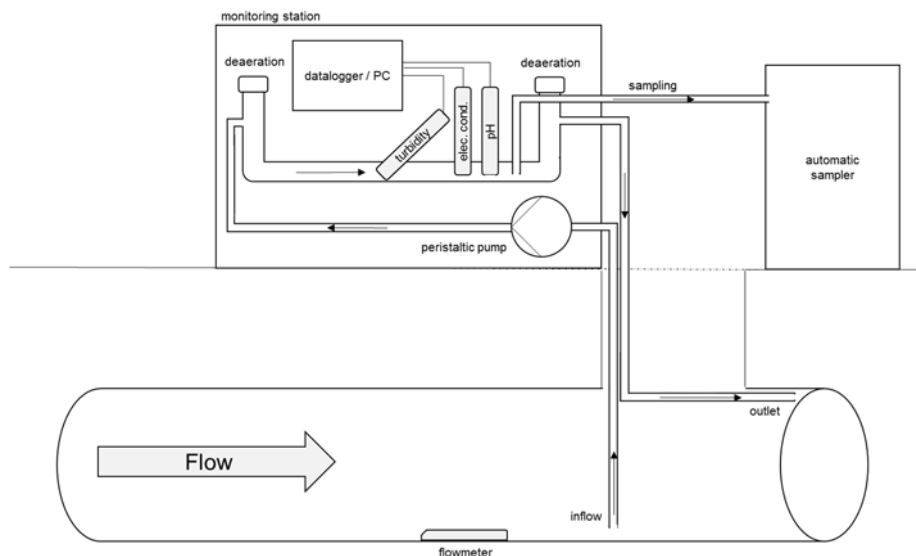


Figure 1. Schematic overview of the monitoring station.

2.3. Calculation of Continuous TSS Time Series

The turbidity of selected samples was measured to estimate the correlation to TSS. Initially, this has been conducted in the original sample bottle (PE, squared base, slightly transparent). Due to significant variance of the measured turbidity, a black cylindrical PE-HD bottle (diameter 10.8 cm, height 18.1 cm) has been used later. While measuring the turbidity, the sample is homogenized with a magnetic stirrer at 450 rpm. The five-minute mean of the turbidity is recorded. Calibration of turbidity probes was conducted with formazine primary standard solutions. TSS concentrations and the corresponding turbidity values were subjected to correlation analysis. The resulting linear regression equations are used to create continuous TSS time series from raw turbidity signals. Discussing the uncertainties through this conversion would exceed the scope of this paper and are therefore not presented here. The reader is referred to the literature [11–13].

2.4. Data and Analysis

All sensor signals were logged with a 1 min interval. High-resolution online runoff and quality data is available for approx. 2.5 years (FR and RC), 1.5 years (PL), and 0.5 years (HT), respectively. Rainfall runoff events were statistically analyzed using rainfall, runoff, and pollutant characteristics. Events with a minimum rainfall depth of $H > 2$ mm, maximum rainfall intensity in 60 min of $I_{\max 60} > 2.5$ mm/h, and complete runoff/turbidity data are selected, only. Rainfall events below these criteria usually do not contribute to relevant runoff and are therefore excluded. Based on continuous runoff and TSS time series data, event volumes, event loads, and event mean concentrations are calculated according to Equations (1)–(3). Furthermore, event characteristics were subjected to correlation analysis with special emphasis to TSS loads.

$$\text{Event volume (m}^3\text{)} : Vol = \sum_{i=1}^n Q_i t \quad (1)$$

$$\text{Event load (kg)} : Load = \sum_{i=1}^n Q_i C_i t \quad (2)$$

$$\text{Event mean concentration (mg/l)} : EMC = \frac{Load}{Vol} \quad (3)$$

where i = index of time series, n = number of data points of an event, Q_i = runoff at index i , Δt = time interval (i.e., 1 min), and C_i = TSS concentration at index i .

The intra-event distribution of TSS loads are examined by means of mass-volume-curves ($M(V)$ -curves, [14,15]). $M(V)$ -curves describe the proportion of transported mass at a given runoff volume proportion. This method is usually used to visualize transported mass proportions and to analyze the first-flush phenomenon. Knowledge of catchment-specific first-flush characteristics is crucial to designing cost-effective treatment or storage structures. However, $M(V)$ -curves tend to be site-specific and vary greatly from event to event [6]. Aggregation of similar $M(V)$ -curves is therefore required to extract relevant information. [16] for example, divide $M(V)$ -curves in three different zones to classify similar events. Zone A contains curves with a dominant first-flush effect, while curves in Zone C tend to be more last-flush affected. Curves in Zone B are near the bisecting line and show a runoff-proportional mass transport.

In this paper, $M(V)$ -curves are also used to characterize the two types of wash-off process, namely source-limited and transport-limited wash-off [17,18]. Source-limited runoff events have, in general, sufficient energy to wash off all available particles on the surface. This occurs if either masses on the surface are rather limited or the kinetic energy of rainfall/runoff is high enough. Transport-limited events are not able to completely remove available masses. Typically, these events occur either if the available masses are adequately high or the kinetic energy of runoff is insufficient.

$M(V)$ -curves are calculated for the four study sites and compared. A seasonal differentiation is included. Instead of using zones, boxplots of the transported mass proportions are created at runoff volume quantiles to group $M(V)$ -curves. With calculated and visualized interquartile ranges (IQR), the event variability and main wash-off trends can be observed and characterized.

3. Results

3.1. TSS Sample Statistics

Table 1 summarizes TSS sample statistics at the four study sites. Statistics were also calculated for the dataset excluding outliers. Due to non-normality of the dataset, outliers are conservatively considered and defined as points beyond the mean \pm four times the standard deviation. Mean and standard deviation are iteratively computed while potential outliers are excluded.

At site **FR**, 193 samples were analyzed from 40 events. With the 0.75 percentile being 14.2 mg/L, the flat roof clearly shows low TSS potential and distributions are similar to other findings [19–21].

For site **RC**, 269 samples of 39 events were taken. The distribution of TSS concentration also reveals low TSS contribution. Compared to the results of [22], values are lower than TSS concentrations of a separated sewer system in Germany. The mean value of 114.3 mg/L and the standard deviation of 339 mg/L indicates high variation. However, these statistics are strongly influenced by the maximum value of 3645 mg/L. The 0.9 percentile being at 205 mg/L confirms this. 140 samples from 38 events were analyzed for site **PL**. TSS concentration ranges from 7.3 mg/L to 1842 mg/L, with the median at 170 mg/L. At **HT**, 92 samples of 17 events were collected. Compared to other studies at high-trafficked streets [23], the TSS statistics are significantly lower. For example, the median of 77.4 mg/L is less than half as the median in their study (175 mg/L).

Table 1. Site-specific TSS sample statistics.

| Site | Outlier Excluded | <i>n</i> | Events | TSS (mg/L) | | | | | | | | |
|------|------------------|----------|--------|----------------------|-----------|------------|--------|------------|-----------|--------|-------|-------|
| | | | | Min | 0.1-Perc. | 0.25-Perc. | Median | 0.75-Perc. | 0.9-Perc. | Max | Mean | Sd |
| FR | no | 193 | 40 | 0.6 | 2.2 | 3.7 | 6.7 | 14.2 | 45.5 | 674.1 | 22.4 | 60.2 |
| | yes | 182 | 39 | 0.6 | 2.2 | 3.7 | 6.5 | 11.7 | 27.8 | 85.1 | 11.8 | 15.5 |
| RC | no | 269 | 39 | 1.4 | 5.6 | 9.7 | 21.0 | 73.0 | 205.2 | 3645.7 | 114.3 | 339.7 |
| | yes | 256 | 39 | 1.4 | 5.5 | 9.4 | 18.7 | 63.4 | 132.7 | 569.1 | 55.6 | 91.5 |
| PL | no | 140 | 38 | 7.3 | 19.7 | 58.6 | 169.2 | 335.1 | 550.5 | 1842.0 | 248.3 | 278.1 |
| | yes | 139 | 38 | 7.3 | 19.6 | 58.5 | 168.4 | 333.8 | 546.8 | 1189.4 | 236.8 | 243.7 |
| HT | no | 92 | 17 | 2.9 | 26.1 | 53.3 | 77.4 | 98.6 | 129.2 | 237.1 | 79.1 | 41.2 |
| | yes | | | no outliers detected | | | | | | | | |

3.2. Relationship between TSS and Turbidity

To create continuous TSS data from online turbidity data, correlation functions are determined. Due to the change of bottle type in which the turbidity was measured, correlation functions were established with only a subset of all samples presented in Table 2. The range of the sample subset is within the range of all samples with outliers being excluded. Only the maximum value at site RC is slightly higher (580.1 mg/L compared to 569.1 mg/L) and therefore still used for analysis. Both linear and non-linear relationships were tested. Since non-linear functions did not significantly outperform linear functions, only linear regression coefficients are listed in Table 3. The goodness-of-fit of the linear regression is visually verified and numerically expressed by r-squared. With the lowest r-squared being at 0.68, all linear regression models show a good fit of the underlying dataset.

Table 2. Site-specific TSS sample statistics of samples used for turbidity correlation.

| Site | <i>n</i> | Events | TSS (mg/L) | | | | | | | | |
|------|----------|--------|------------|-----------|------------|--------|------------|-----------|-------|------|-------|
| | | | Min | 0.1-Perc. | 0.25-Perc. | Median | 0.75-Perc. | 0.9-Perc. | Max | Mean | Sd |
| FR | 36 | 4 | 1.9 | 2.8 | 3.7 | 5.2 | 9.4 | 22.6 | 43.3 | 9.0 | 9.7 |
| RC | 60 | 7 | 2.3 | 8.9 | 17.8 | 41.6 | 65.2 | 150.1 | 580.1 | 70.7 | 107.8 |
| PL | 96 | 33 | 2.3 | 6.5 | 18.2 | 40.9 | 97.5 | 137.2 | 459.9 | 67.4 | 77.3 |
| HT | 85 | 16 | 0.5 | 19.0 | 41.0 | 67.1 | 82.1 | 103.2 | 140.7 | 63.7 | 31.7 |

Table 3. Linear regression coefficients for correlation of TSS and turbidity ($TSS = f(\text{turbidity}) = a + b * \text{turbidity}$).

| Site | <i>a</i> | <i>b</i> | <i>R</i> ² |
|------|----------|----------|-----------------------|
| FR | −3.52 | 1.89 | 0.835 |
| RC | −20.9 | 3.69 | 0.823 |
| PL | 1.97 | 0.84 | 0.683 |
| HT | 7.93 | 0.97 | 0.681 |

3.3. Event Database

An overview of the event database with continuous measurement data is given in Table 4. It contains the number of total observed events and the number of events which are excluded from further analysis. Events are rejected if either selection criteria are violated or if measurement data is doubtful. In this respect, sites FR and RC show a high number of events with doubtful data. This is mainly caused by almost constantly low turbidity values ($FNU < 15$) in the course of an event. For site FR this can be justified with few particles in the runoff. At site RC, this is also caused by pumping difficulties. Gaps due to measurement failures of runoff and quality sensors are rarely present. Turbidity gaps are only observed if stormwater contained substances which caused intensive foaming in the measurement pipe. However, in total, 65 events were analyzed at FR, 23 at site RC, 46 at PL, and 16 at HT. Descriptive statistics of selected event characteristics are given in Table 5.

Table 4. Description of event database with continuous monitoring data.

| Site | Total Observed Events | Events Violating Selection Criteria | Events with Doubtful Data | Valid Events | Valid Events/Total Observed Events |
|------|-----------------------|-------------------------------------|---------------------------|--------------|------------------------------------|
| FR | 415 | 275 | 75 | 65 | 16% |
| RC | 324 | 199 | 102 | 23 | 7% |
| PL | 152 | 87 | 19 | 46 | 37% |
| HT | 40 | 11 | 13 | 16 | 40% |

Table 5. Descriptive statistic data (min, 0.1-, 0.25-, 0.5-, 0.75-, 0.9-percentiles, max, mean, standard deviation) of site-specific event characteristics; rainfall depth: H, max. rainfall intensity in 60 minutes ($I_{\max60}$), max runoff (Q_{\max}), runoff volume (Vol), TSS loads (Loads), and TSS event mean concentrations (EMC).

| Site | Min | 0.1-Perc. | 0.25-Perc. | Median | 0.75-Perc. | 0.9-Perc. | Max | Mean | Sd | Min | 0.1-Perc. | 0.25-Perc. | Median | 0.75-Perc. | 0.9-Perc. | Max | Mean | Sd |
|------|-------------------------|-----------|------------|--------|------------|-----------|-------|-------|-------|---------------------|-----------|------------|--------|------------|-----------|-------|------|------|
| - | H (mm) | | | | | | | | | $I_{\max60}$ (mm/h) | | | | | | | | |
| FR | 2.0 | 2.1 | 3.1 | 4.3 | 7.3 | 9.6 | 22.7 | 5.6 | 3.8 | 2.6 | 2.8 | 3.3 | 4.6 | 8.2 | 15.2 | 49.4 | 7.4 | 8.1 |
| RC | 2.2 | 3.8 | 4.3 | 7.1 | 13.4 | 18.9 | 29.1 | 9.8 | 7.2 | 2.5 | 2.7 | 3.0 | 3.7 | 5.2 | 6.6 | 10.4 | 4.4 | 2.1 |
| PL | 2.1 | 2.6 | 3.1 | 5.1 | 10.0 | 18.8 | 31.0 | 8.0 | 6.9 | 2.5 | 2.7 | 2.9 | 5.5 | 10.4 | 18.7 | 44.9 | 8.6 | 8.2 |
| HT | 2.3 | 3.2 | 3.6 | 6.2 | 8.7 | 17.5 | 21.8 | 8.0 | 5.9 | 1.1 * | 1.3 | 1.8 | 2.3 | 2.6 | 4.7 | 7.5 | 2.7 | 1.7 |
| - | Vol (m ³) | | | | | | | | | Q_{\max} (L/s) | | | | | | | | |
| FR | 0.02 | 0.02 | 0.1 | 0.2 | 0.3 | 0.4 | 1.2 | 0.2 | 0.2 | 0.01 | 0.01 | 0.1 | 0.1 | 0.3 | 0.4 | 1.6 | 0.2 | 0.3 |
| RC | 18.2 | 45.5 | 65.2 | 116.3 | 233.5 | 428.5 | 715.8 | 192.0 | 191.0 | 8.9 | 10.5 | 15.9 | 28.8 | 95.4 | 148.4 | 215.7 | 61.3 | 66.5 |
| PL | 1.4 | 2.6 | 3.4 | 5.7 | 11.8 | 29.7 | 71.2 | 11.6 | 13.8 | 1.0 | 2.3 | 4.0 | 7.8 | 13.1 | 23.3 | 54.9 | 11.1 | 11.3 |
| HT | 81.2 | 105.5 | 121.5 | 166.3 | 336.1 | 581.4 | 784 | 268.5 | 211.4 | 13.5 | 16.3 | 19.8 | 27.5 | 52.3 | 81.8 | 133.1 | 40.7 | 32.9 |
| - | Loads (kg/ha) | | | | | | | | | EMC (mg/L) | | | | | | | | |
| FR | 0.0 | 0.0 | 0.1 | 0.2 | 1.7 | 4.9 | 19.4 | 1.7 | 3.6 | 0 | 1 | 3 | 9 | 35 | 94 | 250 | 33 | 55 |
| RC | 0.1 | 0.3 | 0.6 | 0.9 | 3.5 | 7.4 | 9.4 | 2.6 | 2.9 | 4 | 11 | 18 | 50 | 92 | 152 | 364 | 77 | 94 |
| PL | 0.1 | 0.5 | 0.9 | 1.3 | 2.6 | 6.3 | 11.1 | 2.3 | 2.6 | 5 | 13 | 24 | 49 | 80 | 112 | 254 | 60 | 49 |
| HT | 1.6 | 3.1 | 3.6 | 8.0 | 13.6 | 29.2 | 47.5 | 12.6 | 12.7 | 27 | 38 | 54 | 120 | 172 | 242 | 297 | 125 | 84 |

Note: * Event is considered valid although the $I_{\max60}$ criteria is violated.

3.4. Correlation Analysis

Table 6 shows Pearson correlation coefficients for TSS loads and selected variables at the four study sites. A strong correlation of rainfall intensities and mean/max runoff to TSS loads can be observed at site FR. This effect is also evident but less intense at sites PL and HT. However, the variable I_{mean} (mean rainfall intensity) has only a strong influence at FR (0.8). Rainfall depths seem to be strongly correlated to TSS loads at site HT, only. The overall rainfall duration does not correlate with TSS loads at any site. Correlation of the variables runoff volume (Vol) and antecedent dry weather periods (ADWP) to TSS loads can be noticed only at site HT and PL, respectively.

Table 6. Site-specific Pearson correlation coefficients (FR: flat roof, RC: residential catchment, PL: parking lot, HT: high-traffic street) for TSS loads and selected variables: rainfall depth, duration, and intensities ($H, D_p, I_{mean}:I_{max60}$), runoff characteristics (Q_{mean}, Q_{max} , volume), and antecedent dry weather period (ADWP). Bold values indicate correlation coefficients >0.5.

| Site | | H | D_p | I_{mean} | I_{max1} | I_{max5} | I_{max60} | Q_{mean} | Q_{max} | Vol | ADWP |
|------|-------|-------------|-------|-------------|-------------|-------------|-------------|-------------|-------------|-------------|-------------|
| FR | Loads | 0.39 | -0.09 | 0.80 | 0.68 | 0.80 | 0.82 | 0.90 | 0.88 | 0.37 | 0.20 |
| RC | | 0.19 | -0.03 | 0.40 | 0.47 | 0.43 | 0.26 | 0.45 | 0.35 | 0.29 | -0.06 |
| PL | | 0.50 | 0.08 | 0.48 | 0.69 | 0.69 | 0.63 | 0.49 | 0.64 | 0.38 | 0.56 |
| HT | | 0.80 | 0.30 | 0.41 | 0.73 | 0.74 | 0.64 | 0.62 | 0.59 | 0.78 | -0.06 |

3.5. Intra-Event TSS Load Distributions

Intra-event distributions of TSS load are studied with site-specific $M(V)$ -curves (Figure 2). Clearly, all sites show large variability of intra-event TSS load distribution which confirms findings of other studies [6,7] also for microscale sites. However, from the four study sites it can be observed that the more curves are taken into account the variability increases. Therefore, boxplots at runoff volume quantiles are used to depict the main tendency of wash-off behavior. This enables a visual comparison between site and season-specific $M(V)$ -curves.

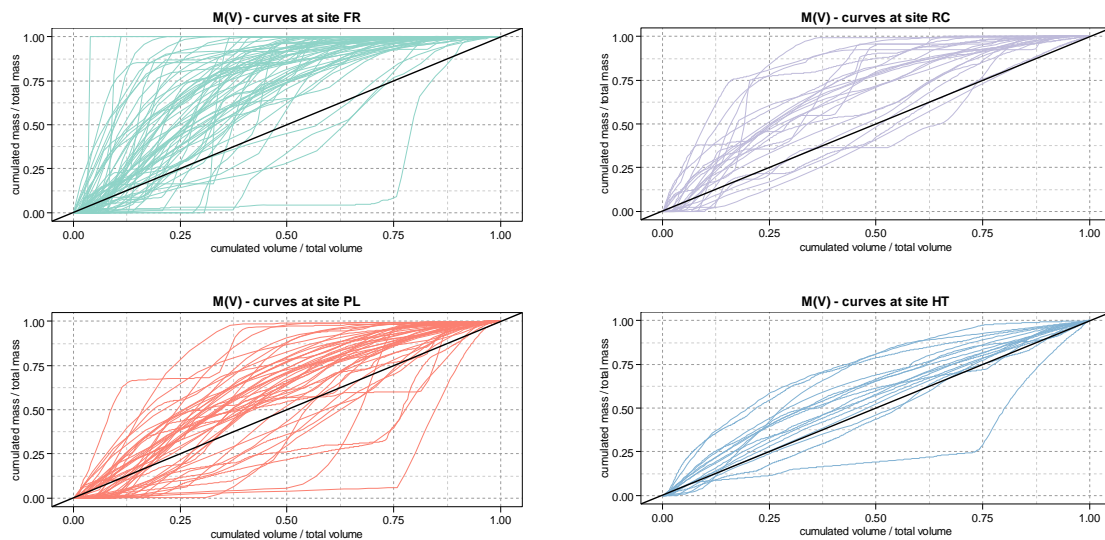


Figure 2. Site-specific $M(V)$ -curves (FR: flat roof, RC: residential catchment, PL: parking lot, HT: high-traffic street).

Figure 3 shows boxplots of $M(V)$ -curve distributions at given runoff volume quantiles for each of the study sites. At site FR, in most cases a large portion of pollution loads tend to be washed-off in the first period of an event. In addition, distances between the first and third quartile (interquartile range, IQR) increases until 20% of runoff volume and decreases afterwards. This generally indicates a

decreasing event variability. In this respect, after 60% of runoff volume, most pollutants are already washed off. With regard to site **PL** and **RC**, the IQR rises until 20% of runoff volume and almost constantly continues up to 60% of runoff volume. At site **HT**, the IQR is merely changing in the first 80% of runoff volume. Although, the number of events taken into account is likely to affect the interquartile ranges, $M(V)$ -curves from site **HT** are noticeably closer to the bisecting line than $M(V)$ -curves from site **FR**. Similarly, $M(V)$ -curves from **PL** are closer to the bisecting line compared to the $M(V)$ -curves from site **RC**.

3.6. Seasonal Intra-Event TSS Load Distribution

Figure 4 shows $M(V)$ -curve distributions for different seasons. At **FR**, the $M(V)$ -curves start steeper in spring, summer, and autumn periods, which indicates a more pronounced first flush. Contrarily, in winter, the $M(V)$ -curves show a less dominant wash-off behavior at the beginning of the events. At site **PL**, the variability is highest during spring and autumn periods. Events during summer months show similar wash-off behavior, which is indicated by relatively low IQR. The three events in the winter are characterized by a delayed wash-off, but cannot be statistically interpreted due to small number of events. $M(V)$ -curve distributions at site **RC** are comparable to **PL** with the highest variability during spring and autumn months. Pollutants tend to be washed-off in the first periods of an event. For site **HT**, monitored events are available in the autumn and winter months, only. Both seasons show comparable wash-off behavior, which is characterized by runoff almost proportional to washed-off loads, low IQR, and close distance to the bisecting line.

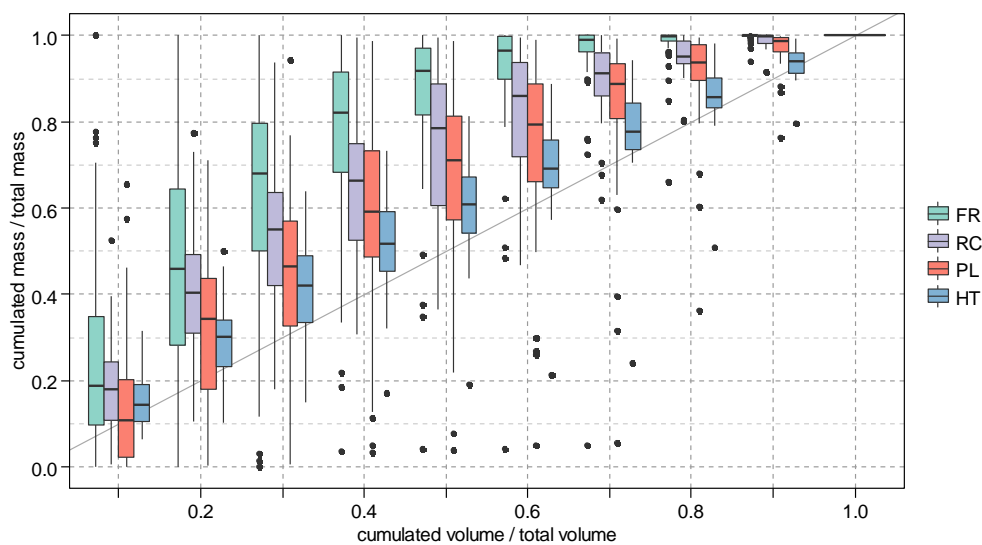


Figure 3. Site-specific boxplots of $M(V)$ -curve distributions at runoff volume quantiles (FR: flat roof, RC: residential catchment, PL: parking lot, HT: high-traffic street). Box ranges correspond to the first and third quartiles. Median is indicated by a solid black horizontal line. Whiskers comprise lowest/highest value within $1.5 \times$ inter-quartile range. Outliers exceed whiskers' ends and are indicated by solid black dots.

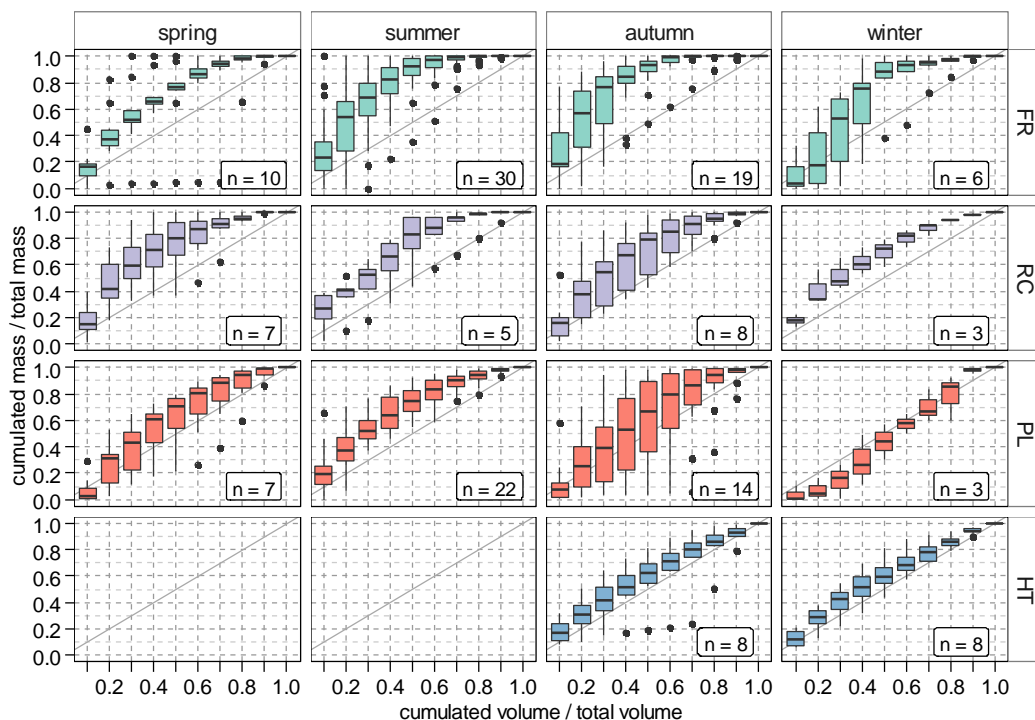


Figure 4. Seasonal- (horizontal) and site- (vertical) specific boxplots of $M(V)$ -curve distributions at runoff volume quantiles (FR: flat roof, RC: residential catchment, PL: parking lot, HT: high-traffic street). Box ranges correspond to the first and third quartiles. Median is indicated by a solid black horizontal line. Whiskers comprise lowest/highest value within $1.5 \times$ inter-quartile range (IQR). Outliers exceed whiskers' ends and are indicated by solid black dots.

4. Discussion

From the correlation analysis it is stated, that firstly rainfall intensity ($I_{\max 5}$, $I_{\max 60}$) has a strong influence on TSS loads at small catchments with a high proportion of impervious surfaces (FR, PL, HT). Secondly, this effect decreases with increasing catchment size. Thirdly, in residential catchments which consist of multiple subcatchments (e.g., roofs, streets, parking lots) the correlation between rainfall event characteristics and TSS loads are strongly attenuated. The low correlation of the antecedent dry weather period suggests that this parameter is inappropriate to describe the pollutant build-up. However, in this study, the average antecedent dry weather period is about three days. This means pollutants are mostly accumulated shortly after an event and therefore exposed to other influential processes such as wind-driven processes.

Analysis of $M(V)$ -curves suggests, that firstly, microscale sites show, in general, a more pronounced first-flush effect and only a few events with a delayed wash-off process. Secondly, the wash-off process at FR seems to be source limited because of the majority of particles are washed-off after 60% of runoff volume and the IQR is significantly low at the end of the events. Thirdly, in contrast, PL and HT show a more transport-limited wash-off because the IQR is closer to the bisecting line at the end of the events. Finally, it is assumed, that RC's wash-off processes are influenced by a composition of subcatchments, such as roofs, streets, and parking lots, which is explained by the intermediate position of RC in comparison to FR, HT, and PL. In fact, runoff from different surfaces is superposed and therefore pollution transport processes are mixed.

From seasonal $M(V)$ -curves it can be observed, firstly, that $M(V)$ -curve distributions at FR show the largest variability in the first 50% of runoff volume throughout the seasons except for spring. The delayed wash-off process during winter months can be caused by a low pollutant potential on surfaces, coarser particles with high densities, or by events with low rain intensities. Secondly, variability of $M(V)$ -curve distribution, in general, is largest during autumn, especially

for sites FR, RC, and PL. It can be assumed that this is mainly caused by high variability of rainfall intensities in conjunction with varying pollutant masses available at the surface. It must also be noted, that only few events were monitored during the winter months, which must be taken into account for further statistical analysis.

5. Conclusions

A long-term monitoring campaign was conducted to analyze stormwater pollutant processes at microscale sites with online sensors. Rainfall runoff events were statistically analyzed and intra-event TSS load distributions were site- and season-specifically examined by means of $M(V)$ -curves. The correlation analysis reveals a strong relationship between rainfall intensity and event loads for small catchments with a high proportion of impervious surfaces, but not for the larger residential catchment. Furthermore, grouping $M(V)$ -curves with boxplots at runoff volume quantiles enables the comparison of wash-off behaviors of different catchments. In general, the wash-off process at site FR (flat roof) tends to be source-limited. In contrast, sites PL (parking lot) and HT (high-traffic) show a transport-limited behavior. A seasonal analysis of $M(V)$ -curve distributions demonstrated the large variability, especially during autumn.

With these results, this paper clearly highlights the need for a spatially more detailed assessment of stormwater quality runoff. This can be drawn from the subcatchment-specific wash-off behavior. Consequently, it can be recommended to use different wash-off models for different catchment types to adequately address transport-limited and source-limited catchments.

Acknowledgments: The research work and software developments are part of the research project “Modelle für Stofftransport und -behandlung in der Siedlungshydrologie” (STBMOD) which has been supported by the German Federal Ministry of Education and Research (BMBF, FKZ 03FH033PX2).

Author Contributions: Dominik Leutnant and Mathias Uhl conceived, designed, performed and evaluated the experiments; Dominik Leutnant analyzed the data; Dirk Muschalla contributed to Sections 3 and 4; Dominik Leutnant wrote the paper.

Conflicts of Interest: The authors declare no conflict of interest.

References

- Dotto, C.B.S.; Kleidorfer, M.; Deletic, A.; Fletcher, T.D.; McCarthy, D.T.; Rauch, W. Stormwater quality models: Performance and sensitivity analysis. *Water Sci. Technol.* **2010**, *62*, 837–843. [[CrossRef](#)] [[PubMed](#)]
- Sage, J.; Bonhomme, C.; Al Ali, S.; Gromaire, M.-C. Performance assessment of a commonly used “accumulation and wash-off” model from long-term continuous road runoff turbidity measurements. *Water Res.* **2015**, *78*, 47–59. [[CrossRef](#)] [[PubMed](#)]
- Alias, N.; Liu, A.; Goonetilleke, A.; Egodawatta, P. Time as the critical factor in the investigation of the relationship between pollutant wash-off and rainfall characteristics. *Ecol. Eng.* **2014**, *64*, 301–305. [[CrossRef](#)]
- Egodawatta, P.; Miguntanna, N.S.; Goonetilleke, A. Impact of roof surface runoff on urban water quality. *Water Sci. Technol.* **2012**, *66*, 1527–1533. [[CrossRef](#)] [[PubMed](#)]
- Liu, A.; Egodawatta, P.; Guan, Y.; Goonetilleke, A. Influence of rainfall and catchment characteristics on urban stormwater quality. *Sci. Total Environ.* **2013**, *444*, 255–262. [[CrossRef](#)] [[PubMed](#)]
- Métadier, M.; Bertrand-Krajewski, J.-L. The use of long-term on-line turbidity measurements for the calculation of urban stormwater pollutant concentrations, loads, pollutographs and intra-event fluxes. *Water Res.* **2012**, *46*, 6836–6856. [[CrossRef](#)] [[PubMed](#)]
- Sun, S.; Barraud, S.; Castebrunet, H.; Aubin, J.-B.; Marmonier, P. Long-term stormwater quantity and quality analysis using continuous measurements in a French urban catchment. *Water Res.* **2015**, *85*, 432–442. [[CrossRef](#)] [[PubMed](#)]
- United States Environmental Protection Agency. *Methods for the Chemical Analysis of Water and Wastes*; Environmental Protection Agency: Cincinnati, OH, USA, 1979.
- Dierschke, M.; Welker, A. Bestimmung von Feststoffen in Niederschlagsabflüssen. *GWF Wasser Abwasser* **2015**, *156*, 440–446.

10. Leutnant, D.; Henrichs, M.; Muschalla, D.; Uhl, M. OSCAR—An online supervisory control and urban drainage data acquisition system with R. In Proceedings of the 10th International Conference on Urban Drainage Modelling, Mont-Sainte-Anne, QC, Canada, 20–23 September 2015; pp. 135–138.
11. Bertrand-Krajewski, J.-L. TSS concentration in sewers estimated from turbidity measurements by means of linear regression accounting for uncertainties in both variables. *Water Sci. Technol.* **2004**, *50*, 81–88. [[PubMed](#)]
12. Hannouche, A.; Chebbo, G.; Ruban, G.; Tassin, B.; Lemaire, B.J.; Joannis, C. Relationship between turbidity and total suspended solids concentration within a combined sewer system. *Water Sci. Technol.* **2011**, *64*, 2445–2452. [[CrossRef](#)] [[PubMed](#)]
13. Lepot, M.; Aubin, J.-B.; Bertrand-Krajewski, J.-L. Accuracy of different sensors for the estimation of pollutant concentrations (total suspended solids, total and dissolved chemical oxygen demand) in wastewater and stormwater. *Water Sci. Technol.* **2013**, *68*, 462–471. [[CrossRef](#)] [[PubMed](#)]
14. Geiger, W.F. Flushing effects in combined sewer systems. In Proceedings of the 4th International Conference in Urban Storm Drainage, Lausanne, Switzerland, 31 August–4 September 1987; pp. 40–46.
15. Bertrand-Krajewski, J.L.; Chebbo, G.; Saget, A. Distribution of pollutant mass vs. volume in stormwater discharges and the first flush phenomenon. *Water Res.* **1998**, *32*, 2341–2356. [[CrossRef](#)]
16. Lacour, C.; Joannis, C.; Gromaire, M.; Chebbo, G. Potential of turbidity monitoring for real time control of pollutant discharge in sewers during rainfall events. *Water Sci. Technol.* **2009**, *59*, 1471–1478. [[CrossRef](#)] [[PubMed](#)]
17. Bai, S.; Li, J. Sediment Wash-Off from an Impervious Urban Land Surface. *J. Hydrol. Eng.* **2013**, *18*, 488–498. [[CrossRef](#)]
18. Zhao, H.; Chen, X.; Hao, S.; Jiang, Y.; Zhao, J.; Zou, C.; Xie, W. Is the wash-off process of road-deposited sediment source limited or transport limited? *Sci. Total Environ.* **2016**, *563–564*, 62–70. [[CrossRef](#)] [[PubMed](#)]
19. Dierschke, M.; Welker, A. Feine Feststoffe (PM63) in Dachabflüssen. *GWF Wasser Abwasser* **2013**, *154*, 1242–1249.
20. Förster, J. Variability of roof runoff quality. *Water Sci. Technol.* **1999**, *39*, 137–144. [[CrossRef](#)]
21. Kobencic, R. *Verunreinigung des Regenwasserabflusses von Dachflächen*; Diplomarbeit, TU Graz: Graz, Austria, 2002.
22. Brombach, H.; Weiss, G.; Fuchs, S. A new database on urban runoff pollution: Comparison of separate and combined sewer systems. *Water Sci. Technol.* **2005**, *51*, 119–128. [[PubMed](#)]
23. Helmreich, B.; Hilliges, R.; Schriewer, A.; Horn, H. Runoff pollutants of a highly trafficked urban road—Correlation analysis and seasonal influences. *Chemosphere* **2010**, *80*, 991–997. [[CrossRef](#)] [[PubMed](#)]



© 2016 by the authors; licensee MDPI, Basel, Switzerland. This article is an open access article distributed under the terms and conditions of the Creative Commons Attribution (CC-BY) license (<http://creativecommons.org/licenses/by/4.0/>).

Paper II - Statistical Distribution of TSS Event Loads From Small Urban Environments

Article

Statistical Distribution of TSS Event Loads From Small Urban Environments

Dominik Leutnant ^{1,*} , Dirk Muschalla ² and Mathias Uhl ¹

¹ Muenster University of Applied Sciences - Institute for Infrastructure, Water, Resources, Environment
Correnstr. 25, 48149 Muenster, Germany; leutnant@fh-muenster.de; uhl@fh-muenster.de

² Graz University of Technology - Institute of Urban Water Management and Landscape Water Engineering,
Stremayrgasse 10/I, 8010 Graz, Austria; d.muschalla@tugraz.at

* Correspondence: leutnant@fh-muenster.de

Received: date; Accepted: date; Published: date

Abstract: Based on the results of a long-term stormwater quality monitoring program, empirical TSS event load distributions were derived at four small urban environments (flat roof, parking lot, residential catchment, high traffic street). Theoretical distribution functions were fitted and used to describe the measurement data. Parameters of the theoretical distribution functions were optimized with respect to a likelihood function to get both optimized parameters and standard errors. Kolmogorov-Smirnov and Anderson-Darling test statistics were applied to assess the goodness-of-fit between empirical and theoretical distribution. The lognormal distribution function was found to be most expressive to approximate empirical TSS event load distributions at all sites. However, the goodness-of-fit of the statistical model strongly depends on the number of events available. Results of a Monte-Carlo-based resampling strategy suggest to provide about 40 events.

Keywords: urban stormwater pollution; probabilistic TSS event loads model; empirical cumulative distribution function; lognormal distribution function; stormwater quality monitoring

1. Introduction

The development of advanced on-line monitoring techniques in the past two decades allows both researchers and practitioners to get more insights of stormwater pollutant processes. Continuous signals of UV-Vis spectrometers or turbidity sensors are frequently used to study intra-event pollutant processes and to estimate event loads or event mean concentrations [1–5]. Ideally, those measurements are used to support the implementation of urban stormwater management strategies. For this, an in depth understanding of pollutant processes is required to design appropriate and cost-effective measures. In this respect, intra-event dynamics have been studied and analysed by means of Mass-Volume-Curves [1,5–7] to explain environmental, temporal and spatial influences on flushing characteristics of e.g. the parameter total suspended solids (TSS). Although the studies revealed site-specific tendencies in the proportion of washed-off load during storm events, the heterogeneous data presented clearly demonstrate the complex nature of pollutant processes which is expressed by significant variability of pollutographs [5].

Pollutant processes on surfaces are generally characterised by wash-off and build-up [8]. While wash-off is mainly driven by rainfall [9–12], surface type and use [13–15] and pollutant [10,14] characteristics, the build-up is assumed to be highly affected by stochastic inputs [16]. Moreover, given the fact that rainfall also can be assumed to be a stochastic variable or at least to some extent, the entire pollutant process consequently aggregates to a stochastic process and thus can hardly be explained deterministically. However, as the pollutant process contains stochastic variables, statistical and probabilistic analyses are allowed to be applied.

Probabilistic analyses are generally based on records of random events [17] and commonly used in hydrology (e.g. hydrologic frequency estimates) and urban hydrology (e.g. storm drainage design). However, the concept itself has not been applied in the field of urban stormwater quality in particular. Since a deterministic process description is currently not possible though high resolution on-line data of stormwater quality is available, a novel opportunity to explore pollutant process characteristics is created.

Several stormwater management design guidelines take pollutant event loads or annual loads (e.g. TSS) into account instead of focusing on intra-event processes. This highlights the importance of this parameter from a practical point of view.

The presented work therefore aims to statistically model TSS event loads from small catchments. For this, empirical cumulative distribution functions are derived from a given stormwater quality event database and used to approximate theoretical distribution functions. Theoretical distribution functions with known or estimated parameters offer the possibility to be used as a proxy and provide seamless information while an empirical distribution may hold gaps due to limited sampling duration or erroneous data. In addition, describing TSS event loads by means of a theoretical distribution function allows to compare pollutant processes among different sites.

Because selecting an appropriate probability model is of particular importance, four commonly used theoretical distributions are applied and site-specifically evaluated. Finally, it is analysed how many events are required to describe the TSS event loads characteristic with statistical significance.

2. Materials and Methods

2.1 Monitoring sites and data

In this paper, the database of TSS event loads published in [1] is used. In their work, the authors installed compact monitoring stations at the outlet of four common types of urban catchments and estimated TSS event loads by means of continuous turbidity sensors as a surrogate. Data from a flat roof (FR, 50 m², 65 events), a high traffic street (HT, 2.5 ha, 16 events), a parking lot (PL, 2350 m², 46 events) and a residential catchment (RC, 9.4 ha², 23 events) are available. A summary of descriptive statistics is given in Table 1. Furthermore, Figure 1 depicts the distribution of site-specific TSS event loads as empirical cumulative distribution functions and box-plots, respectively.

Table 1. Descriptive statistics (min, 0.1-, 0.25-, 0.5-, 0.75-, 0.9-percentiles, max, mean, standard deviation) of site-specific TSS event loads (FR: Flat Roof, HT: High Traffic Street, PL: Parking Lot, RC: Residential Catchment)

| site | n | TSS event loads (g m ⁻²) | | | | | | | | |
|------|----|--------------------------------------|----------|-----------|----------|-----------|----------|-------|-------|-------|
| | | min | 0.1-Perc | 0.25-Perc | 0.5-Perc | 0.75-Perc | 0.9-Perc | max | mean | sd |
| FR | 65 | 0.001 | 0.002 | 0.008 | 0.024 | 0.169 | 0.492 | 1.942 | 0.174 | 0.358 |
| HT | 16 | 0.164 | 0.313 | 0.361 | 0.795 | 1.357 | 2.916 | 4.746 | 1.255 | 1.275 |
| PL | 46 | 0.011 | 0.046 | 0.086 | 0.126 | 0.257 | 0.633 | 1.109 | 0.230 | 0.255 |
| RC | 23 | 0.014 | 0.027 | 0.065 | 0.093 | 0.349 | 0.735 | 0.935 | 0.261 | 0.295 |

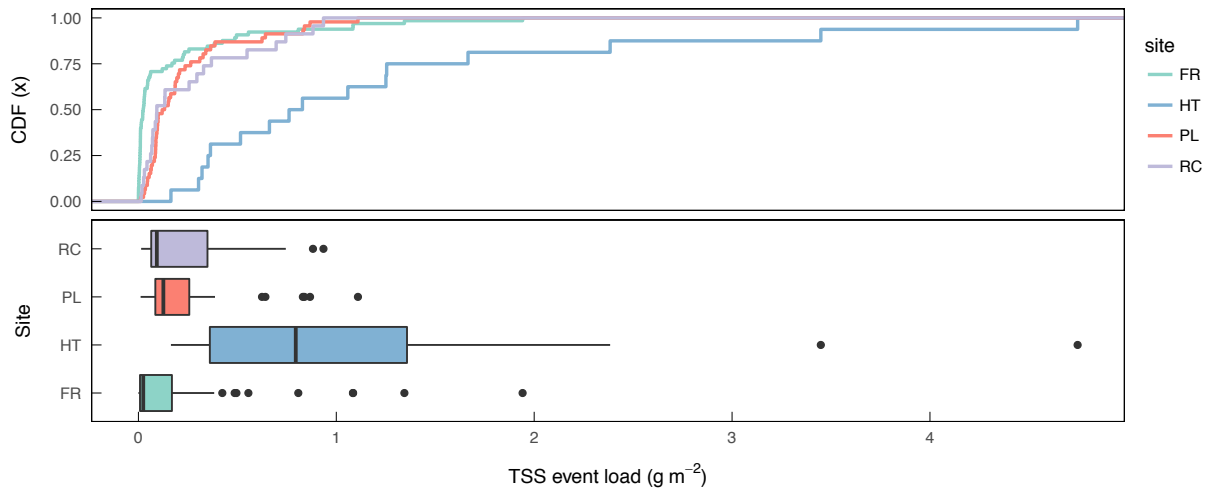


Figure 1. Empirical cumulative distribution functions and boxplots of site-specific monitored TSS event loads (FR: Flat Roof, HT: High Traffic Street, PL: Parking Lot, RC: Residential Catchment)

2.2 Theoretical distribution functions

The site-specific distributions of empirical TSS event loads are derived and used to approximate theoretical distribution functions given in Table 2. For this purpose, distribution functions of type i) Exponential, ii) Gamma, iii) Lognormal and iv) Weibull are selected, as they closely correspond to observed distributions. In particular, these functions are only defined for positive values ($x > 0$) so that they inherently reflect one of the main characteristics of the empirical data. Additionally, parameters of the theoretical distribution functions are listed in the table. While the Exponential distribution has only one parameter, the Gamma, Lognormal and Weibull distributions offer two parameters to be estimated.

Table 2. Theoretical distribution functions

| name (abbreviation) | formula | parameter |
|---------------------|--|-----------------------------------|
| Exponential (exp) | $F(x) = \begin{cases} 0, & x \leq 0 \\ 1 - e^{-\alpha x}, & x > 0 \end{cases}$ | α (rate) |
| Gamma (gamma) | $F(x) = \begin{cases} 0, & x \leq 0 \\ \frac{b^p}{\Gamma(p)} \times \int_0^x t^{p-1} e^{-bt} dt, & x > 0 \end{cases}$ | p (shape), b (rate) |
| Lognormal (lnorm) | $F(x) = \begin{cases} 0, & x \leq 0 \\ \frac{1}{\sigma\sqrt{2\pi}} \times \int_0^x \frac{1}{t} e^{-\frac{1}{2}(\frac{\ln t - \mu}{\sigma})^2} dt, & x > 0 \end{cases}$ | μ (meanlog), σ (sdlog) |
| Weibull (weibull) | $F(x) = \begin{cases} 0, & x \leq 0 \\ 1 - e^{-\alpha x^\beta}, & x > 0 \end{cases}$ | α (scale), β (shape) |

2.3 Distribution fitting and goodness-of-fit assessment

To fit theoretical distribution functions to an empirical distribution, distribution parameters need to be optimized. In this study, parameters are estimated by maximum likelihood strategy (exact standard error model: $\mu = 0, \sigma = 1$) because this also enables to analyse the standard error of estimated parameter. The likelihood function in general can be stated as follows (Equation 1):

$$\mathcal{L}(\theta) = f(x_1, x_2, \dots, x_n | \theta) = \prod_{i=1}^n f(x_i | \theta) \tag{1}$$

with x_i the n observation of variable X (i.e., TSS event loads) and $f(\cdot|\theta)$ the density function of the theoretical distribution function used. Parameters to be optimized are denoted by θ .

Since computation of likelihoods could result in very small numbers which may cause numerical precision problems, the logarithm of likelihoods (LL) is taken instead. Fitting of theoretical distribution functions and numerical goodness-of-fit computations were utilized with R [18] and the package *fitdistrplus* [19]. Once optimal parameters are estimated, the goodness-of-fit is evaluated by Kolmogorov-Smirnov (KS) and Anderson-Darling (AD) test statistics which are calculated according to Table 3.

Table 3. Goodness-of-fit statistics used to evaluate the fitting (F_n denotes the empirical distribution function, F represents the fitted theoretical distribution function, *sup* abbreviates supremum which indicates the least element of x that is greater than or equal to all elements of x (“least upper bound”).

| statistic (abbreviation) | Formula |
|--------------------------|--|
| Kolmogorov-Smirnov (KS) | $D_n = \sup_x F_n(x) - F(x) $ (2) |
| Anderson-Darling (AD) | $A^2 = n \int_{-\infty}^{\infty} \frac{(F_n(x) - F(x))^2}{F(x)(1 - F(x))} dF(x)$ (3) |

In general, both tests are used to test whether a sample follows a specific distribution by calculating the maximum distance between empirical and theoretical distribution function. This means smaller test statistics indicate a lower numerical distance to the distribution analyzed. The AD test refines the KS test and gives more weight to the distribution tails. The tests are applied to decide whether the null hypothesis H_0 “The sample follows a specified distribution” can be accepted or must be rejected at a specified significance level. Alternatively, hypothesis H_A is defined as “the sample does not follow a specified distribution”. Critical values for the acceptance decision of the KS test are calculated according to Equation 4 for sample sizes > 35 . For sample sizes below 35, critical values are obtained from [20].

$$d_\alpha = \sqrt{\frac{-0.5 \ln(\frac{\alpha}{2})}{\sqrt{n}}}, \text{ for } n > 35 \quad (4)$$

with sampling size n and significance level α .

2.4 Monte-Carlo resampling strategy

A Monte-Carlo simulation based resampling strategy without replacement has been conducted to analyse the effect of different sample sizes on the quality of distribution fitting. Motivated by the idea to determine a minimum sample size required, the computational steps are as follows:

1. Estimating parameters of lognormal distribution function by maximum likelihood taking all samples into account.
2. Sampling k ($k \in \mathbb{N}, 0 < k \leq n$) events from all events n with 1000 repetitions. If less than 1000 repetitions are possible, all possible combinations are taken into account (Equation 3).

$$\text{repetitions} = \text{MIN} \left(\binom{n}{k}, 1000 \right) \quad (3)$$

with population n and sample size k .

3. Computing of KS distance between empirical cumulative distribution function of sample and theoretical distribution function with estimated parameters for all repetitions.
4. Computing of mean, standard deviations of KS distances for all repetitions.

The results are then interpreted and visually compared to the critical values for the Kolmogorov-Smirnov test statistic at 90 % significance level.

3. Results

3.1. Distribution fitting

Results of fitting theoretical distribution functions to the empirical TSS event load distribution are presented in Table 4. It shows site- and distribution-specific goodness-of-fit values and estimated parameters. Figure 2 illustrates the approximation with Lognormal distribution function at site FR and PL.

Table 4. Results of fitting empirical TSS load distribution functions to theoretical distribution functions (FR: Flat Roof, HT: High Traffic Street, PL: Parking Lot, RC: Residential Catchment, LL: LogLikelihood, AD: Anderson-Darling statistic A^2 , KS: Kolmogorov-Smirnov statistic D_n)

| site | distr. | goodness-of-fit | | | parameter estimates (standard error) | | | | |
|------|---------|-----------------|--------------|--------------|--------------------------------------|------------------|------------------|------------------|------------------|
| | | LL | AD | KS | rate | shape | meanlog | sdlog | scale |
| FR | exp | 48.66 | 29.074 | 0.442* | 5.747 (0.713) | - | - | - | - |
| | gamma | 88.29 | 2.254 | 0.186* | 1.994 (0.504) | 0.347 (0.049) | - | - | - |
| | lnorm | 89.9 | 0.806 | 0.099 | - | - | -3.69 (0.301) | 2.429 (0.213) | - |
| | weibull | 92.05 | 1.123 | 0.131 | - | 0.484 (0.046) | - | - | 0.077 (0.021) |
| HT | exp | -19.64 | 0.379 | 0.153 | 0.797 (0.199) | - | - | - | - |
| | gamma | -19.25 | 0.394 | 0.136 | 1.068 (0.412) | 1.341 (0.428) | - | - | - |
| | lnorm | -18.18 | 0.192 | 0.128 | - | - | -0.19 (0.228) | 0.912 (0.161) | - |
| | weibull | -19.46 | 0.382 | 0.137 | - | 1.121 (0.208) | - | - | 1.316 (0.312) |
| PL | exp | 21.69 | 1.168 | 0.126 | 4.356 (0.642) | - | - | - | - |
| | gamma | 22.03 | 1.279 | 0.157 | 5.093 (1.175) | 1.169 (0.218) | - | - | - |
| | lnorm | 25.31 | 0.398 | 0.116 | - | - | -1.96 (0.146) | 0.987 (0.103) | - |
| | weibull | 21.72 | 1.203 | 0.137 | - | 1.030 (0.111) | - | - | 0.233 (0.035) |
| RC | exp | 7.91 | 1.011 | 0.222 | 3.833 (0.799) | - | - | - | - |
| | gamma | 8.1 | 0.681 | 0.189 | 3.283 (1.120) | 0.857 (0.219) | - | - | - |
| | lnorm | 9.07 | 0.38 | 0.131 | - | - | -2.03 (0.259) | 1.243 (0.183) | - |
| | weibull | 8.23 | 0.586 | 0.174 | - | 0.882 (0.142) | - | - | 0.244 (0.061) |

* rejecting H_0

Table 5 shows results of fitting the Lognormal distribution to TSS event load distributions grouped by year. Sites FR and PL are considered only as they provide sufficient samples per group. The goodness-of-fit is given for each individual group and compared to the original sample from all years. Additionally, the goodness-of-fit is visualised in Figure 2.

Table 5. Results of fitting empirical TSS load distribution functions grouped by year to lognormal distribution function (FR: Flat Roof, HT: High Traffic Street, PL: Parking Lot, LL: LogLikelihood, AD: Anderson-Darling statistic A^2 , KS: Kolmogorov-Smirnov statistic D_n)

| site | year | n | distr. | goodness-of-fit | | | parameter estimates (standard error) | |
|------|-----------|----|--------|-----------------|-------|-------|---|---------------|
| | | | | LL | AD | KS | meanlog | sdlog |
| FR | all years | 65 | lnorm | 89.9 | 0.806 | 0.099 | -3.69 (0.301) | 2.429 (0.213) |
| | 2015 | 25 | lnorm | 24.54 | 0.64 | 0.138 | -2.99 (0.359) | 1.80 (0.254) |
| | 2014 | 17 | lnorm | 41.63 | 0.288 | 0.142 | -5.04 (0.786) | 3.24 (0.556) |
| | 2013 | 23 | lnorm | 32.52 | 0.365 | 0.12 | -3.45 (0.388) | 1.86 (0.274) |
| PL | all years | 46 | lnorm | 25.31 | 0.398 | 0.116 | -1.96 (0.146) | 0.987 (0.103) |
| | 2014 | 30 | lnorm | 23.76 | 0.616 | 0.167 | -2.08 (0.161) | 0.88 (0.114) |
| | 2013 | 16 | lnorm | 2.93 | 0.243 | 0.105 | -1.72 (0.281) | 1.12 (0.199) |

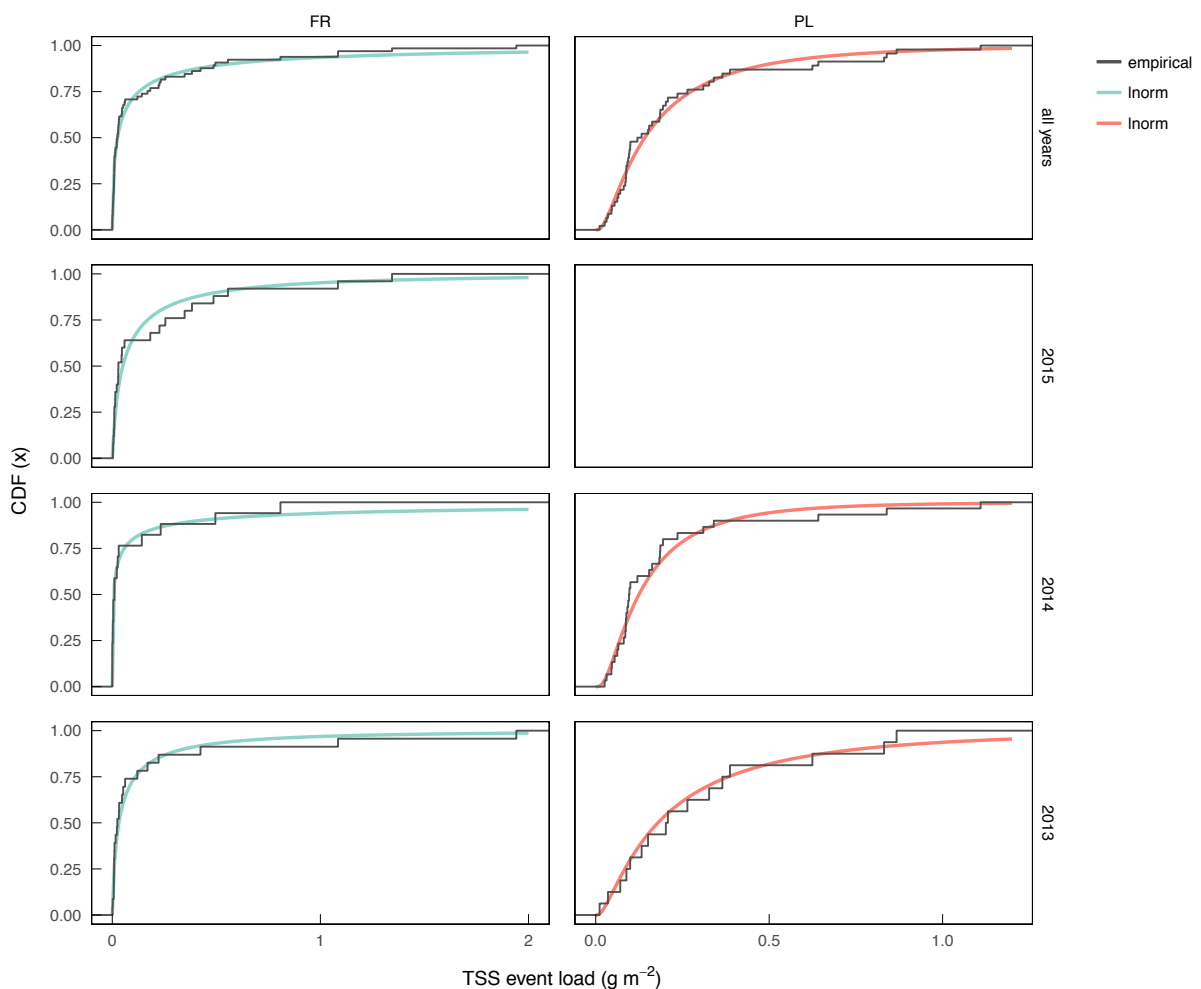


Figure 2. Approximation of empirical TSS event load distribution function grouped by year with lognormal distribution function at site FR and PL

3.2. Effect of sample size

The results obtained from the Monte-Carlo-based sampling are visualised in Figure 3. It shows the mean (colored solid line) and regions of one and two standard deviations (grey shaded areas) of Kolmogorov-Smirnov's statistic as function of sample size for site FR and PL. Furthermore, critical values for the 90 % significance level are illustrated (black solid line).

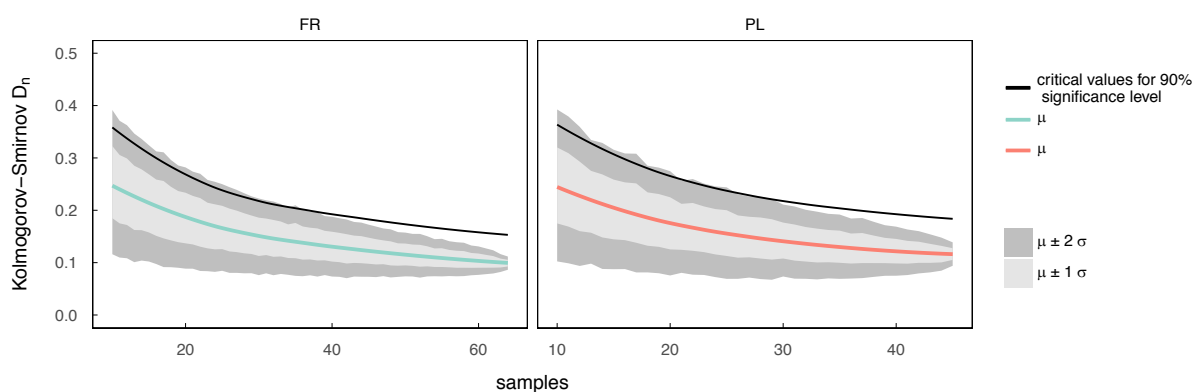


Figure 3. Mean and regions of one and two standard deviations of Kolmogorov-Smirnov's statistic as function of sample size from Monte-Carlo-based sampling for sites FR and PL. Critical values for 90% confidence are indicated as black solid line.

4. Discussion

4.1. Distribution fitting

All selected theoretical distribution functions were able to approximate the empirical distribution with statistical significance except for the Exponential and the Gamma distribution at site FR (H_0 gets rejected). These two functions are not able to reflect the initially steep gradient and subsequent moderate gradient of the empirical distribution. The Exponential function has the least flexibility among the analysed functions because it only provides one parameter to be fitted. This explains the poor approximation results. Thus, a statistical significant description of TSS event distributions requires at least a two-parameter distribution.

Using the Weibull distribution which basically extends the Exponential distribution function with an additional parameter, clearly improves the fitting. The application of Weibull and Gamma distribution lead to comparable results which is indicated by similar goodness-of-fit measures. Highest goodness-of-fit is obtained with the Lognormal distribution that accordingly approximates the underlying dataset best.

The goodness-of-fit of the Lognormal distribution however, varies between sites. On the one hand, this might be caused by insufficient samples, which lead to more pronounced steps in the empirical distribution function. On the other hand, this also could reflect a site-specific behavior, which is expressed by the shape of distribution function. While the monitored small roof catchment has significantly more events with low loads, this effect is attenuated for the other catchments. The differences in the results of the two-parameter functions are marginal which demonstrates the functions are general able to replicate the empirical distribution.

Comparing the fitted parameters also indicates that distributions of site PL and RC are comparable which is confirmed by their empirical distribution functions (Figure 1).

The results of distribution fitting grouped by year shows that also subsamples can be well approximated by Lognormal distribution. According to the KS statistic, for both sites the year 2013 has been fitted best. Only the AD statistic of the year 2014 for site FR indicates a slightly better fit which is caused by a relative low maximum load in this year (2013: 1.94 gm^{-2} , 2014: 0.8 gm^{-2} , 2015: 1.34 gm^{-2}). The optimized parameters of the Lognormal distribution for both sites highlight the

individuality of each year as they strongly vary. This is also expressed by the spread of goodness-of-fit values. Consequently, this indicates the sensitivity of the sampling characteristics which is induced by the utilized database. In the present study the database available does not cover all events of an entire year mainly due to measurement issues and predefined rainfall-runoff criteria for event selection [1]. However, rainfall-runoff events are affected by numerous environmental variables and generally occur randomly in time, space and intensity. Therefore, although the event database grouped by year undoubtedly is incomplete, the approach reflects natural variability in which the number of events per year and their characteristics change. Robust fitting of a theoretical distribution function should therefore prioritize sample size over sampling period (c.f. 4.2).

4.2. Effect of sample size

The results of the Monte-Carlo analysis show, that the mean of the calculated goodness-of-fit values improves with increasing sample size and approximates to the value obtained when all samples are taken into account (FR: 0.099, PL: 0.12). The standard deviation decreases with increasing sampling size by implication. With respect to critical values for 90% confidence level, accepting the null hypothesis H_0 ("The data follow the Lognormal distribution") generally requires Kolmogorov-Smirnov's D_n to be approximately below the $\mu + 2\sigma$ threshold which is satisfied for minimum sample sizes of roughly 40 at site FR and of roughly 30 at site PL. It can be legitimately assumed that simulated KS statistics follow a normal distribution which according to the *empirical rule*¹ consequently implies that more than approximately 95 % of samples lead to KS statistics lower than 0.188 at site FR and 0.211 at site PL. Narrowing the uncertainty range to the upper limit of $\mu + \sigma$ threshold results in KS statistics of 0.159 at site FR and 0.176 at site PL (approx. more than 68% of samples are within this range).

Generally, the simulated dataset confirms that the more samples are taken into account, the more precise the estimates get which as a matter of fact is the basic assumption for any statistical significance test. In order to determine the minimum sample size which leads to accepting the null hypothesis H_0 with high probability, it is suggested to choose at least the minimum of 40 samples because of i) the chance of having a sample which can be statistically represented by the Lognormal distribution is high (>95 %) and ii) the mean of KS statistic in this case only slightly differs from the optimal value taking all samples into account (0.131 > 0.099 at site FR and 0.122 > 0.12 at site PL). However, the choice of criteria remains subjective and might be adapted as further data becomes available. Of course, using more data to approximate the Lognormal distribution may probably lead to more appropriate fitting results, but this requires to provide more samples which in turn needs more measurement data. The criteria proposed therefore are presenting a compromise solution between measurement duration and quality of approximation.

5. Conclusions

Empirical TSS event load distributions of four small common types of urban catchments (Flat Roof (FR), Parking Lot (PL), Residential Catchment (RC), High Traffic Street (RC)) are successfully described by theoretical distribution functions. The goodness-of-fit was evaluated and effects of sampling sizes were investigated. From the analysis, it was found that:

- The Lognormal distribution function is most expressive to approximate empirical TSS event load distributions at all experimental sites.
- Successfully derived and fitted distribution functions provide a closed characterization of TSS event load distributions allowing to intra- and extrapolate of probabilistic event characteristics not observed.
- A robust fitting should prioritize sample size over sampling period.

¹ The empirical rule states that for a normal distribution 99.7% of the data fall within three standard deviations, 95% are within two standard deviations and 68 % fall within one standard deviation [20].

- Roughly 40 events are required to reasonably fit the Lognormal distribution. Using more samples potentially improves the goodness-of-fit but subsequently requires to extend the duration of cost-intensive monitoring campaigns.

When applying the concept of probabilistic description of TSS event loads based on theoretical distribution function, the results of this study may also support the evaluation of stormwater quality runoff monitoring campaigns with respect to their duration/information ratio. Also, the fitted distribution functions provide an excellent basis to calibrate urban stormwater quality models by focusing on probabilistic TSS event load characteristics.

Acknowledgments: The research is part of the project “Modelle für Stofftransport und -behandlung in der Siedlungshydrologie” (STBMOD) at the Institute for Infrastructure, Water, Resources and Environment, Muenster University of Applied Sciences. The project was funded by the German Federal Ministry of Education and Research (BMBF, FKZ 03FH033PX2).

Author Contributions: Dominik Leutnant, Dirk Muschalla and Mathias Uhl conceived and designed the numerical experiments; Dominik Leutnant performed the numerical computations and evaluated the results; Dominik Leutnant wrote the paper and thanks Dirk Muschalla and Mathias Uhl for professional discussions.

Conflicts of Interest: The authors declare no conflict of interest.

References

1. Leutnant, D.; Muschalla, D.; Uhl, M. Stormwater Pollutant Process Analysis with Long-Term Online Monitoring Data at Micro-Scale Sites. *Water* **2016**, *8*, 299, doi:10.3390/w8070299.
2. Gruber, G.; Winkler, S.; Pressl, A. Quantification of pollution loads from CSOs into surface water bodies by means of online techniques. *Water Science and Technology* **2004**, *50*, 73–80.
3. Bertrand-Krajewski, J.-L. TSS concentration in sewers estimated from turbidity measurements by means of linear regression accounting for uncertainties in both variables. *Water Science and Technology* **2004**, *50*, 81–88.
4. Caradot, N.; Sonnenberg, H.; Rouault, P.; Gruber, G.; Hofer, T.; Torres, A.; Pesci, M.; Bertrand-Krajewski, J.-L. Influence of local calibration on the quality of online wet weather discharge monitoring: feedback from five international case studies. *Water Science & Technology* **2015**, *71*, 45, doi:10.2166/wst.2014.465.
5. Métadier, M.; Bertrand-Krajewski, J.-L. The use of long-term on-line turbidity measurements for the calculation of urban stormwater pollutant concentrations, loads, pollutographs and intra-event fluxes. *Water Research* **2012**, *46*, 6836–6856, doi:10.1016/j.watres.2011.12.030.
6. Bertrand-Krajewski, J. L.; Chebbo, G.; Saget, A. Distribution of pollutant mass vs volume in stormwater discharges and the first flush phenomenon. *Water Research* **1998**, *32*, 2341–2356.
7. Di Modugno, M.; Gioia, A.; Gorgoglione, A.; Iacobellis, V.; la Forgia, G.; Piccinni, A.; Ranieri, E. Build-Up/Wash-Off Monitoring and Assessment for Sustainable Management of First Flush in an Urban Area. *Sustainability* **2015**, *7*, 5050–5070, doi:10.3390/su7055050.
8. Bertrand-Krajewski, J.-L. Stormwater pollutant loads modelling: epistemological aspects and case studies on the influence of field data sets on calibration and verification. *Water Science and Technology* **2007**, *55*, 1–17.
9. Egodawatta, P.; Thomas, E.; Goonetilleke, A. Understanding the physical processes of pollutant build-up and wash-off on roof surfaces. *Sci Total Environ* **2009**, *407*, 1834–41, doi:10.1016/j.scitotenv.2008.12.027.
10. Al Ali, S.; Bonhomme, C.; Dubois, P.; Chebbo, G. Investigation of the wash-off process using an innovative portable rainfall simulator allowing continuous monitoring of flow and turbidity at the urban surface outlet. *Science of The Total Environment* **2017**, *609*, 17–26, doi:10.1016/j.scitotenv.2017.07.106.
11. Alias, N.; Liu, A.; Goonetilleke, A.; Egodawatta, P. Time as the critical factor in the investigation of the relationship between pollutant wash-off and rainfall characteristics. *Ecological Engineering* **2014**, *64*, 301–305,

doi:10.1016/j.ecoleng.2014.01.008.

12. Egodawatta, P.; Thomas, E.; Goonetilleke, A. Mathematical interpretation of pollutant wash-off from urban road surfaces using simulated rainfall. *Water Research* **2007**, *41*, 3025–3031.
13. Muthusamy, M.; Tait, S.; Schellart, A.; Beg, M. N. A.; Carvalho, R. F.; de Lima, J. L. M. P. Improving understanding of the underlying physical process of sediment wash-off from urban road surfaces. *Journal of Hydrology* **2018**, *557*, 426–433, doi:10.1016/j.jhydrol.2017.11.047.
14. Zhao, H.; Jiang, Q.; Xie, W.; Li, X.; Yin, C. Role of urban surface roughness in road-deposited sediment build-up and wash-off. *Journal of Hydrology* **2018**, *560*, 75–85, doi:10.1016/j.jhydrol.2018.03.016.
15. Liu, A.; Egodawatta, P.; Guan, Y.; Goonetilleke, A. Influence of rainfall and catchment characteristics on urban stormwater quality. *Science of the total environment* **2013**, *444*, 255–262.
16. Shaw, S. B.; Stedinger, J. R.; Walter, M. T. Evaluating urban pollutant buildup/wash-off models using a Madison, Wisconsin catchment. *Journal of Environmental Engineering* **2009**.
17. Haan, C. T. *Statistical methods in hydrology*; 1st ed.; Iowa State University Press: Ames, 1977; ISBN 978-0-8138-1510-7.
18. R Core Team *R: A Language and Environment for Statistical Computing*; R Foundation for Statistical Computing: Vienna, Austria, 2017;
19. Delignette-Muller, M. L.; Dutang, C. fitdistrplus: An R package for fitting distributions. *Journal of Statistical Software* **2015**, *64*, 1–34.
20. Hedderich, J.; Sachs, L. *Angewandte Statistik: Methodensammlung mit R*; 14., überarb. und erg. Aufl.; Springer: Heidelberg, 2012; ISBN 978-3-642-24400-1.



© 2018 by the authors. Submitted to *Water* for possible open access publication under the terms and conditions of the Creative Commons Attribution (CC BY) license (<http://creativecommons.org/licenses/by/4.0/>).

Paper III - swmmr - An R package to interface SWMM

swmmr - An R package to interface SWMM

Dominik Leutnant^{a,*}, Anneke Döring^b, Mathias Uhl^a

^a*Muenster University of Applied Sciences - Institute for Infrastructure, Water, Resources, Environment, Corrensstr. 25, 48149 Muenster, Germany*

^b*Leibniz University Hannover - Institute for Fluid Dynamics and Environmental Physics, Appelstr. 9a, 30167 Hannover, Germany*

Abstract

The stormwater management model software SWMM of the US EPA is widely used to analyse, design or optimise urban drainage systems. To perform advanced analysis and visualisations of model data this short communication introduces the R package swmmr. It contains functions to read and write SWMM files, initiate simulations from the R console and to convert SWMM model files to and from GIS data. Additionally, model data can be transformed to produce high quality visualisations. In accordance with SWMM's open source policy the package can be obtained through github.com or the Comprehensive R Archive Network (CRAN).

Keywords: SWMM, R, urban drainage modelling, model data management

Highlights

- An R package to read and write SWMM files is introduced
- SWMM's .out files are read with high performance
- Functions to convert between GIS and SWMM files are provided
- Modern plotting systems are used to visualise model data

*Corresponding Author

Email addresses: leutnant@fh-muenster.de (Dominik Leutnant),
doering@hydromech.uni-hannover.de (Anneke Döring), uhl@fh-muenster.de (Mathias Uhl)

Software availability

swmmr is available on the Comprehensive R Archive Network (CRAN) at <https://cran.r-project.org/package=swmmr> and GitHub at <https://github.com/dleutnant/swmmr>
License: GPL-3
System requirements: R ($\geq 3.0.0$)
Installation: `install.packages("swmmr")` or
`remotes::install_github("dleutnant/swmmr")`

Introduction

Modelling urban drainage systems has become essential to develop and assess resilient urban stormwater management strategies. Analysing the impact of different climatic or demographic scenarios on urban water infrastructure or optimising urban drainage networks are only some of the applications. Various software products are available to model urban drainage systems. Amongst others, the stormwater management model SWMM (Rossman 2010) is widely used by researchers and practitioners to simulate dynamic hydrology-hydraulic water quality processes. Its source code is released under public domain specification and online available from the US EPA¹. Besides the availability of the open source engine of SWMM, a pre-compiled software for Microsoft Windows operating systems is available. The software also provides a graphical user interface (GUI) to design drainage networks and to assign attributes to elements of the system. While the open source software facilitates basic analysis and visualisations of model data, advanced features such as time series data management, parameter uncertainty analysis or extended statistics are reserved to commercialised versions of SWMM, only.

In this respect, the free software environment for statistical computing and graphics R (R Core Team 2017) is frequently used by both scientists and engineers. It provides a huge variety of add-on packages to address issues related to urban drainage modeling such as model parameter optimisation (e.g. *DEoptim* - Ardia et al. (2016)), visualisation (e.g. *dygraphs* - Vanderkam et al. (2017); *ggplot2* - Wickham (2016)), time series management (e.g. *xts* - Ryan and Ulrich (2017)) or statistical analysis. Moreover, R's spatial data processing capabilities have been significantly advanced with the recent development of the simple features (*sf*) package (Pebesma 2018).

Modelling in general involves both pre- and post-processing of different types of data such as spatial or time series data. Consequently, the availability of these packages enables an efficient data management and supports modelling with SWMM.

To bridge the gap between modelling and advanced model analytics, we herein introduce the freely available R package *swmmr* which provides functions to

¹<https://www.epa.gov/water-research/storm-water-management-model-swmm>

interface SWMM. Core functions of the package comprise fast reading and writing of SWMM files, conversion between GIS data and the SWMM input file format as well as model data transformation to produce expressive visualisation. This short communication describes design principles of the `swmmr` package and exemplifies its usage. This includes a demonstration of how to produce high quality figures of model results and model structure enabled by further R packages. Finally, a conclusion is given and further developments are outlined.

What is the package useful for?

The main purpose of the `swmmr` package is to assist the modeller during the modelling process. Typically, this includes processing and visualisation of measurement and spatial data, which the R ecosystem provides matured packages for. However, its capabilities of interactively creating and modifying spatial data are limited and should not yet be compared to a specialised GIS software, though remarkable progress can be observed (*mapview* - Appelhans et al. (2018); *mapedit* - Appelhans and Russell (2017)). Thus, the package is especially useful to modellers who use R for model data management and/or need to perform advanced analysis, visualisation or optimisation tasks of a given model or model results, respectively.

Package design and core functions

At its core, the package heavily relies on the tidy data concept (Wickham 2014) which is expressed through a set of harmonized packages sharing common data representation principles (“tidyverse” - Wickham (2017)). Although most tasks could have been addressed with *base R*², packages from the “tidyverse” tend to simplify both the programming and the data analysis. For example, `swmmr` uses `tibbles` (Müller and Wickham 2017) instead of R’s build-in `data.frame` to represent SWMM sections. This becomes apparent in functions which parse SWMM text files, i.e. `read_inp()`, `read_rpt()` and `read_lid_rpt()` (Table 1). Generally, these functions take the path to a corresponding SWMM file (*.inp or *.rpt) and parse its content to a named list of `tibbles` or a single `tibble`, respectively. `read_inp()` creates an object of class `inp`, whose list element names are identical to the names of SWMM input sections available in lower letters (e.g. `options`, `subcatchments`). `read_rpt()` creates a named list of class `rpt` containing summary sections from the report file of SWMM (e.g. `subcatchment_runoff_summary`). While both of the aforementioned functions maintain the original SWMM file structure, `read_lid_rpt()` interprets text files from specific LID elements. A single `tibble` or index-based time series data as `xts` object is returned accordingly.

²“base R” refers to a set of default packages which R is actually based upon without any additional packages loaded.

Reading simulation output data from the binary *.out* file is supported by `read_out()`. Because of the potentially huge size of *.out* data, the function design aims for fast data processing, thus C++ code is embedded through Rcpp (Eddelbuettel and François 2011). Output data per system element and model variable is always represented as *xts* object and conveniently stored in a list environment.

The function `write_inp()` writes an *inp* object to disk, which addresses cases where an *inp* object has been modified within R and changes need to be saved back to disk (e.g. model parameter calibration). Thus, it takes an existing *inp* object and creates a model file on disk which can be read and run by SWMM. A SWMM simulation run can be initiated from the R console with `run_swmm()` which takes the path to an *.inp* file and calls the SWMM executable with the required file paths as arguments.

Moreover, converting SWMM input sections with spatial reference to simple feature objects is supported with `*_to_sf()` functions. Based on the conversion of SWMM input sections to simple feature objects, an *inp* object can be converted to the popular *.shp* format with `inp_to_files()`. Additionally, *.txt* files containing simulation settings, storage and pumping curves are returned as well as files containing SWMM time series data. As a counterpart the function `shp_to_inp()` converts spatial data given in *.shp* files into an *inp* object. Information on simulation settings, rainfall time series etc. can be given in *.txt* files to complete the model data. While the conversion to *sf* objects already enables common spatial analysis of SWMM model data in R, this also allows using the plotting interface of *ggplot2* through `geom_sf()`.

Table 1: Functions for the R environment provided by `swmmr`.

| Name | Inputs | Description |
|---|---|---|
| model run <code>run_swmm()</code> | paths of <code>.inp</code> , <code>.rpt</code> and <code>.out</code> file | Initiate a SWMM run from the R console |
| reading files <code>read_inp()</code> | path of <code>.inp</code> file | Reads a SWMM model as list of tibbles (i.e. <code>inp</code> object) |
| <code>read_out()</code> | path of <code>.out</code> file | Reads SWMM simulation results (time series) as list of <code>xts</code> objects |
| <code>read_rpt()</code> | path of <code>.out</code> file | Reads SWMM simulation results (summary) as list of tibbles |
| <code>read_lid_rpt()</code> | path of LID report file | Reads a SWMM LID Report File as tibble or <code>xts</code> object |
| writing files <code>write_inp()</code> | <code>inp</code> object (optionally modified) and filename | Writes an <code>inp</code> file to disk which can be read and run by SWMM |
| simple feature conversion <code>*_to_sf()</code> | <code>inp</code> object | Converts SWMM objects as tibble with simple feature geometries (supported objects are junctions, links, orifices, outfalls, pumps, raingages, storages, subcatchments, weirs) |
| <code>inp_to_sf()</code> | <code>inp</code> object | Converts an entire <code>inp</code> object as list of tibbles with simple feature geometries |
| .shp file conversion <code>inp_to_files()</code> | <code>inp</code> object, model name and directory path | Converts <code>.inp</code> to <code>.shp</code> and <code>.txt</code> files |
| <code>shp_to_inp()</code> | s. package manual | Converts <code>.shp</code> files as list of tibbles (i.e. <code>inp</code> object) |

Example Usage

In this short communication, the basic usage of the package is demonstrated using the model “Example1” which is included in the SWMM software for Microsoft Windows. The model file usually locates at “C:/Users/.../Documents/EPA SWMM Projects/Examples/Example1.inp”. Alternatively, it is also attached to the package (cf. Listing 1). In addition, the reader is referred to three package vignettes which cover topics beyond the scope of this short communication. For example, instructions how to auto-calibrate a SWMM model with `swmmr` or how to convert GIS and SWMM model data with `swmmr` are given.

Setup and model execution

To install `swmmr` from CRAN and to add its namespace to R’s search list, the following commands need to be executed from the R command line (Listing 1). In this example, the model file attached to the package is used and its path is assigned to the variable `inp_path`. Subsequently, `run_swmm()` initiates a model run.

```
if (!require("swmmr")) install.packages("swmmr")
library(swmmr)
library(tidyverse)
inp_path <- system.file("extdata", "Example1.inp", package = "swmmr")
swmm_files <- run_swmm(inp = inp_path,
                      rpt = tempfile(),
                      out = tempfile())
```

Listing 1: Installation and model execution.

Analysis of model data

SWMM’s model files (`.inp`, `.rpt` and `.out`) can be accessed from the named list variable `swmm_files`. Since the results of both the `read_rpt()` and `read_inp()` function comprises a list of named `tibbles` (Listings 2 and 3), elements can be accessed via R’s common extracting mechanism.

```
inp_object <- read_inp(swmm_files$inp)
summary(inp_object)
```

```
#>           Length Class Mode
#> title           1 tbl_df list
#> options         2 tbl_df list
#> evaporation     2 tbl_df list
#> raingages       5 tbl_df list
#> subcatchments   9 tbl_df list
#> subareas        8 tbl_df list
#> infiltration    6 tbl_df list
#> junctions       6 tbl_df list
#> outfalls        6 tbl_df list
#> conduits        9 tbl_df list
#> xsections       8 tbl_df list
#> pollutants     11 tbl_df list
#> landuses        4 tbl_df list
#> coverages       3 tbl_df list
```

```

#> buildup          7      tbl_df list
#> washoff          7      tbl_df list
#> timeseries       4      tbl_df list
#> report           2      tbl_df list
#> map              2      tbl_df list
#> coordinates      3      tbl_df list
#> vertices         3      tbl_df list
#> polygons         3      tbl_df list
#> symbols          3      tbl_df list

glimpse(inp_object$subcatchments)

#> Observations: 8
#> Variables: 9
#> $ Name          <chr> "1", "2", "3", "4", "5", "6", "7", "8"
#> $ `Rain Gage`   <chr> "RG1", "RG1", "RG1", "RG1", "RG1", "RG1", "RG1", "...
#> $ Outlet        <chr> "9", "10", "13", "22", "15", "23", "19", "18"
#> $ Area          <int> 10, 10, 5, 5, 15, 12, 4, 10
#> $ Perc_Imperv   <int> 50, 50, 50, 50, 50, 10, 10, 10
#> $ Width         <int> 500, 500, 500, 500, 500, 500, 500, 500
#> $ Perc_Slope    <dbl> 0.01, 0.01, 0.01, 0.01, 0.01, 0.01, 0.01, 0.01
#> $ CurbLen       <int> 0, 0, 0, 0, 0, 0, 0, 0
#> $ Snowpack      <lgl> NA, NA, NA, NA, NA, NA, NA, NA

```

Listing 2: Reading and analysing model data.

```

rpt_object <- read_rpt(swmm_files$rpt)
summary(rpt_object)

#>
#> analysis_options          Length Class Mode
#> runoff_quantity_continuity 3      tbl_df list
#> runoff_quality_continuity  3      tbl_df list
#> flow_routing_continuity    3      tbl_df list
#> quality_routing_continuity 3      tbl_df list
#> highest_flow_instability_indexes 2      tbl_df list
#> routing_time_step_summary  2      tbl_df list
#> subcatchment_runoff_summary 9      tbl_df list
#> subcatchment_washoff_summary 3      tbl_df list
#> node_depth_summary         8      tbl_df list
#> node_inflow_summary        9      tbl_df list
#> node_flooding_summary      7      tbl_df list
#> outfall_loading_summary    7      tbl_df list
#> link_flow_summary          8      tbl_df list
#> conduit_surchARGE_summary  6      tbl_df list
#> link_pollutant_load_summary 3      tbl_df list

```

Listing 3: Reading report of model results.

Time index-based model results from an *.out* file are imported as given in Listing 4. The model variables total runoff (in flow units, *vIndex* = 4) and total rainfall (in/hr or mm/hr) from the system (*iType* = 3) are read. A general dictionary covering the mapping between variable and number is included in the package documentation.

```

sim <- read_out(swmm_files$out, iType = 3, vIndex = c(1,4))
sim$system_variable %>%

```

```

invoke(merge, .) %>%
summary

#>      Index                total_rainfall    total_runoff
#> Min.   :1998-01-01 01:00:00  Min.   :0.00000  Min.   : 0.0000
#> 1st Qu.:1998-01-01 09:45:00  1st Qu.:0.00000  1st Qu.: 0.0000
#> Median :1998-01-01 18:30:00  Median :0.00000  Median : 0.0000
#> Mean   :1998-01-01 18:30:00  Mean   :0.07361  Mean   : 2.1592
#> 3rd Qu.:1998-01-02 03:15:00  3rd Qu.:0.00000  3rd Qu.: 0.1033
#> Max.   :1998-01-02 12:00:00  Max.   :0.80000  Max.   :24.2530

```

Listing 4: Reading and statistical analysis of model results.

Convert between GIS and SWMM model data

`inp_to_files()` utilizes the conversion functions `*_to_sf()` for all SWMM sections containing spatial data (Table 1). Sections without spatial information are returned and saved separately. Thus, sub-folders containing `.shp`, `.txt` and `.dat` files are created in a specified directory (Listing 5). Information on supported SWMM sections for both `inp_to_files()` and `shp_to_inp()` is given in the package manual.

```

out_dir <- tempdir()
inp_to_files(x = inp_object, name = "Example1", path_out = out_dir)

c("dat", "shp", "txt") %>%
  map(~ list.files(file.path(out_dir, .), pattern = .))

#> [[1]]
#> [1] "Example1_timeseries_TS1.dat"
#>
#> [[2]]
#> [1] "Example1_link.shp"      "Example1_outfall.shp" "Example1_point.shp"
#> [4] "Example1_polygon.shp"
#>
#> [[3]]
#> [1] "Example1_options.txt"

```

Listing 5: Converting SWMM model data into shape files.

Column names of the `.shp` file attribute table correlate with the original SWMM encoding or the abbreviation to 7 characters. `shp_to_inp()` reads `.shp` and `.txt` files and converts them to an `inp` object (Listing 6). Missing values are completed with default values or can be specified separately. The vignette provides more information of the conversion details.

```

converted_inp <- shp_to_inp(
  path_options = file.path(out_dir, "txt/Example1_options.txt"),
  path_line = file.path(out_dir, "shp/Example1_link.shp"),
  path_outfall = file.path(out_dir, "shp/Example1_outfall.shp"),
  path_point = file.path(out_dir, "shp/Example1_point.shp"),
  path_polygon = file.path(out_dir, "shp/Example1_polygon.shp"),
  path_timeseries = file.path(out_dir, "dat/Example1_timeseries_TS1.dat")
)
summary(converted_inp)

```

```

#>
#> options          2      tbl_df list
#> evaporation      2      tbl_df list
#> raingages        5      tbl_df list
#> subcatchments    9      tbl_df list
#> subareas         8      tbl_df list
#> infiltration     6      tbl_df list
#> junction         6      tbl_df list
#> outfalls         6      tbl_df list
#> conduits         7      tbl_df list
#> xsections        7      tbl_df list
#> pollutants       11     tbl_df list
#> landuses         4      tbl_df list
#> coverages        3      tbl_df list
#> buildup          7      tbl_df list
#> washoff          7      tbl_df list
#> timeseries       1      tbl_df list
#> report           2      tbl_df list
#> coordinates      3      tbl_df list
#> polygons         3      tbl_df list

```

Listing 6: Converting shape files into SWMM model data.

Usage with other R packages

Visualisation

Modelling involves visualisation of spatial and temporal data. With *base* (R Core Team 2017), *lattice* (Sarkar 2008) and *ggplot2* (Wickham 2016), R currently offers three different plotting systems. Because of *ggplot2*'s flexibility and declarative way of constructing graphics, a demonstration of how to create expressive and customisable figures of model data is given in Listings 7 and 8. Listing 7 aims to visualise rainfall and simulated runoff data. Temporal data is read from an *.out* file and converted to `data.frame`. Both variables are plotted as different geometric objects (`geom_col()`, `geom_line()`) and separated into facets. The result is shown in Figure 1.

```

library(ggplot2)      # ggplot2 >= 2.2.1.9000 required
library(broom)       # to convert an sts object to data.frame

sim$system_variable %>%
  invoke(merge, .) %>%
  tidy(.) %>%
  {
    ggplot(mapping = aes(x = index, y = value)) +
      geom_col(data = filter(., series == "total_rainfall")) +
      geom_line(data = filter(., series == "total_runoff")) +
      scale_x_datetime(date_breaks = "3_hour", date_labels = "%H:%M") +
      facet_wrap(
        ~series, ncol = 1, scales = "free_y", strip.position = "left",
        labeller = as_labeller(c(
          total_rainfall = "total_rainfall_(in/hr)",
          total_runoff = "total_runoff_(CFS)"
        ))
      ) +

```

```

theme_light() +
theme(
  strip.placement = "outside",
  strip.text = element_text(colour = "black"),
  strip.background = element_rect(fill = "white"),
  panel.grid.major = element_blank(),
  panel.grid.minor = element_blank()
) +
labs(
  y = NULL, x = NULL,
  subtitle = paste(range(.$index), collapse = "_-")
)
}

```

Listing 7: Creation of ggplot2-based visualisation of simulation results.

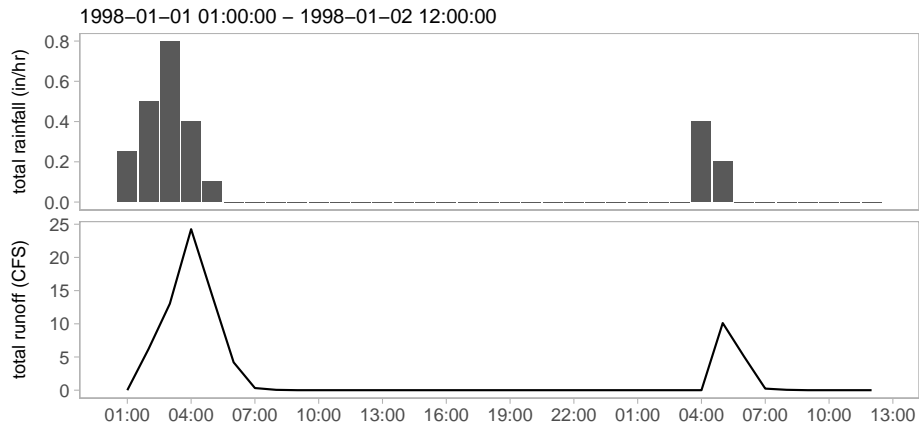


Figure 1: Example of ggplot2-based visualisation of simulation results.

Listing 8 is used to visualise the model structure with subcatchments, links, junctions and raingages. Initially, SWMM objects to be plotted are converted as *sf* objects. Coordinates for labelling subcatchments and raingages are calculated afterwards. Since *ggplot2* provides the geometric object `geom_sf()`³, *sf* objects are directly passed to *ggplot2* and interpreted accordingly. Figure 2 illustrates the result.

```

# initially, SWMM objects to be plotted are converted as sf objects
# here: subcatchments, links, junctions, raingages
sub_sf <- subcatchments_to_sf(inp_object)
lin_sf <- links_to_sf(inp_object)
jun_sf <- junctions_to_sf(inp_object)
rg_sf <- raingages_to_sf(inp_object)

# calculate coordinates for label position of subcatchments
# here: centroid of subcatchment
coord_subc <- sub_sf %>%

```

³Note that *ggplot2* \geq 2.2.1.9000 is required

```

sf::st_centroid() %>%
sf::st_coordinates() %>%
tibble::as_tibble()

# update coordinates to label raingage label
coord_rg <- rg_sf %>%
{sf::st_coordinates(.) + 500} %>% # add offset
tibble::as_tibble()

# add coordinates to tibble containing sf geometries
sub_sf <- dplyr::bind_cols(sub_sf, coord_subc)
rg_sf <- dplyr::bind_cols(rg_sf, coord_rg)

# create the plot
ggplot() +
  # subcatchments and label
  geom_sf(aes(fill = Area), data = sub_sf) +
  geom_label(aes(X, Y, label = Name), sub_sf,
             alpha = 0.5, size = 3) +
  # links
  geom_sf(aes(colour = Geom1), lin_sf,
          size = 2) +
  # junctions
  geom_sf(aes(size = Elevation), jun_sf,
          colour = "darkgrey") +
  # raingage and label
  geom_sf(data = rg_sf, shape = 10) +
  geom_label(aes(X, Y, label = Name), rg_sf,
             alpha = 0.5, size = 3) +
  # change scales and theme
  scale_fill_viridis_c() +
  scale_colour_viridis_c(direction = -1) +
  theme_linedraw() +
  theme(panel.grid.major = element_line(colour = "white"))

```

Listing 8: Creation of ggplot2-based visualisation of model structure.

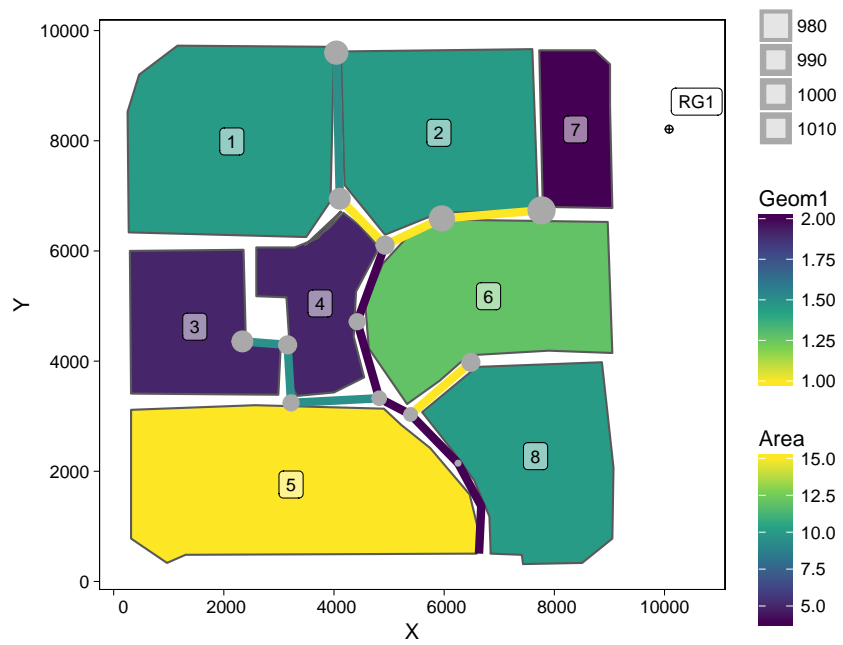


Figure 2: Example of ggplot2-based visualisation of SWMM Example1 model structure.

Since simple features are supported by the *mapview* package, a model structure converted to simple feature geometries can also be interactively visualised. Figure 3 shows a screenshot of a browser-based visualisation of the “Example1” model, obtained by executing Listing 9.

```
library(mapview)
inp_to_sf(inp_object) %>%
  mapview()
```

Listing 9: Creation of mapview-based visualisation.

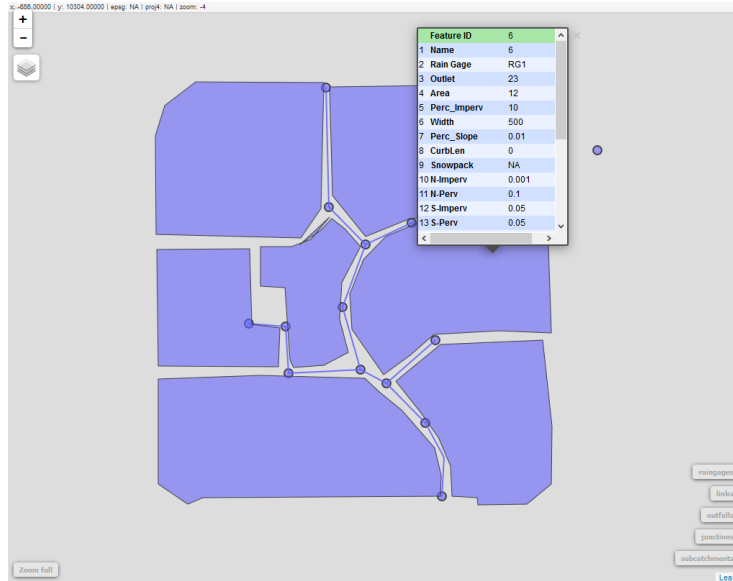


Figure 3: Browser-based interactive visualisation of SWMM Example 1 model structure.

Calibration

Calibration of model parameters is an essential part within the modelling chain to improve the model quality. During calibration, model parameter values are systematically modified to optimise an objective function, which numerically expresses the difference between observed and simulated data.

Because *swmmr* provides the functions `write_inp()` to save an *inp* object to disk and `run_swmm()` to potentially run the written model file afterwards, it especially facilitates autocalibration of model parameters. *swmmr*, however, does not depend on particular optimisation packages. The package vignette “How to autocalibrate a SWMM model with *swmmr*” exemplifies the application of the DEoptim package (Ardia et al. 2016) for single objective optimisation.

Conclusions

A brief introduction of the R package `swmmr` is given. `swmmr` interfaces the stormwater management model SWMM with R and bridges the gap between modelling and advanced model analytics. It offers functions to represent SWMM models in R which subsequently can be modified or visualised with modern technologies. Simulation results are efficiently read with help of `Rcpp` to streamline further time series analysis. This facilitates efficient model calibration and parameter uncertainty analysis. Future developments will integrate generic functions for plotting and model statistics. The package is freely available and is especially open to both the SWMM and R community. The authors would like to promote the open source project and welcome any contribution to the package through the project page on GitHub.

Acknowledgements

This package has been mainly developed in the course of the project STBMOD funded by the German Federal Ministry of Education and Research (BMBF, FKZ 03FH033PX2). The development significantly benefits from the Interface Guide of SWMM and was inspired by the work of Peter Steinberg. The authors would like to thank Bradley J. Eck whose short communication on the `epanetReader` (Eck 2016) motivated us to work on this contribution.

References

- Appelhans, Tim, and Kenton Russell. 2017. *Mapedit: Interactive Editing of Spatial Data in R*. <https://CRAN.R-project.org/package=mapedit>.
- Appelhans, Tim, Florian Detsch, Christoph Reudenbach, and Stefan Woel-lauer. 2018. *Mapview: Interactive Viewing of Spatial Data in R*. <https://CRAN.R-project.org/package=mapview>.
- Ardia, David, Katharine M. Mullen, Brian G. Peterson, and Joshua Ulrich. 2016. *DEoptim: Differential Evolution in R*. <https://CRAN.R-project.org/package=DEoptim>.
- Eck, Bradley J. 2016. “An R Package for Reading EPANET Files.” *Environmental Modelling & Software* 84 (October): 149–54. doi:10.1016/j.envsoft.2016.06.027.
- Eddelbuettel, Dirk, and Romain François. 2011. “Rcpp: Seamless R and C++ Integration.” *Journal of Statistical Software* 40 (8): 1–18. doi:10.18637/jss.v040.i08.
- Müller, Kirill, and Hadley Wickham. 2017. *Tibble: Simple Data Frames*. <https://CRAN.R-project.org/package=tibble>.
- Pebesma, Edzer. 2018. *Sf: Simple Features for R*. <https://CRAN.R-project.org/package=sf>.
- R Core Team. 2017. *R: A Language and Environment for Statistical Computing*. Vienna, Austria: R Foundation for Statistical Computing. <https://www.R-project.org/>.

Rossman, Lewis A. 2010. “Storm Water Management Model - User’s Manual Version 5.0.” Cincinnati, OH, USA: United States Environmental Protection Agency (US EPA).

Ryan, Jeffrey A., and Joshua M. Ulrich. 2017. *Xts: EXTensible Time Series*. <https://CRAN.R-project.org/package=xts>.

Sarkar, Deepayan. 2008. *Lattice: Multivariate Data Visualization with R*. New York: Springer. <http://lmdvr.r-forge.r-project.org>.

Vanderkam, Dan, J. J. Allaire, Jonathan Owen, Daniel Gromer, Petr Shevtsov, and Benoit Thieurmel. 2017. *Dygraphs: Interface to 'Dygraphs' Interactive Time Series Charting Library*. <https://CRAN.R-project.org/package=dygraphs>.

Wickham, Hadley. 2014. “Tidy Data.” *Journal of Statistical Software* 59 (10). doi:10.18637/jss.v059.i10.

———. 2016. *Ggplot2: Elegant Graphics for Data Analysis*. Springer-Verlag New York. <http://ggplot2.org>.

———. 2017. *Tidyverse: Easily Install and Load the 'Tidyverse'*. <https://CRAN.R-project.org/package=tidyverse>.

Paper IV - Distribution-based Calibration of a Storm-water Quality Model

Article

Distribution-based Calibration of a Stormwater Quality Model

Dominik Leutnant ^{1,*} , Dirk Muschalla ² and Mathias Uhl ¹

¹ Muenster University of Applied Sciences - Institute for Infrastructure, Water, Resources, Environment
Correnstr. 25, 48149 Muenster, Germany; leutnant@fh-muenster.de; uhl@fh-muenster.de

² Graz University of Technology - Institute of Urban Water Management and Landscape Water Engineering,
Stremayrgasse 10/I, 8010 Graz, Austria; d.muschalla@tugraz.at

* Correspondence: leutnant@fh-muenster.de

Received: date; Accepted: date; Published: date

Abstract: An innovative calibration approach based on TSS event load distribution is developed and applied on stormwater quality models for a flat roof and a parking lot. Exponential functions are employed for both TSS buildup and washoff. Model parameters are calibrated by means of an evolutionary algorithm to minimize the distance between a parameterized lognormal distribution function and the cumulated distribution of simulated TSS event loads. Since TSS event load characteristics are probabilistically considered, the approach especially respects the stochasticity of TSS buildup and washoff and therefore improves conventional stormwater quality calibration concepts which usually focus on event pollutographs. The results show that both experimental models were calibrated with high goodness-of-fit (KS: 0.05). However, it is shown that events with high TSS event loads (> 0.8 percentile) are generally underestimated. While this leads to a relative deviation of -28 % of total TSS loads for the parking lot, the error gets compensated for the flat roof (+5 %). Calibrated model parameters generally tend to generate washoff proportional to runoff, which is indicated by Mass-Volume-Curves. The approach itself is general applicable and creates new opportunity to calibrate stormwater quality models especially when calibration data is limited.

Keywords: stormwater quality modelling; model calibration; probabilistic TSS event loads; SWMM; lognormal distribution; annual TSS loads

1. Introduction

Stormwater quality models are essential tools to support planning of urban water infrastructure. Having reliable model outputs is of high relevance since infrastructural stormwater measures are cost-intensive and have a long service life. Available stormwater quality models still replicate natural pollutant processes in a simplified manner, which in turn lead to uncertain model results [1,2].

Pollutant processes are commonly differentiated into two conceptual phases i) *buildup* and ii) *washoff* which both are deterministically described by empirical formula [3]. These model concepts assume that the amount of pollutant masses at surface generally increases to a maximum as a function of antecedent dry weather periods and decreases in consequence of rainfall/runoff.

Previous studies however demonstrated the inadequacy of this simplified concept to continuously model pollutant concentrations. [4] calibrated a buildup/washoff approach of a stormwater quality model to simulate chemical oxygen demand (COD) concentrations in stormwater discharges by means of a multi-objective auto-calibration scheme. Results obtained did not outperform a model employing a constant stormwater concentration approach. [5] applied a bayesian calibration scheme based on Markov chain Monte-Carlo (MCMC) method to assess the

build/washoff model performance to replicate continuous total suspended solid (TSS) concentrations and event loads. The authors confirmed the poor predictive power of the model applied and generally questioned the buildup/washoff approach.

[6] indicate that pollutant models and its parameters lack of a physical meaning and thus represent rather black-box models. In fact, numerous authors propose a modified washoff equation to appropriately account for rainfall characteristics. [7] and [8] for example introduce a capacity factor to reflect the impact of rainfall intensity and that only a fraction of pollutants are mobilized during storm events. Both rainfall intensity and a ratio of sediment mass per unit catchment area to rainfall intensity are also considered in a modification suggested by [9]. Besides the sensitivity of rainfall intensity on the washoff process, [10] highlights the intra-event variability of rainfall as another influential factor. Obviously, washoff is also influenced by particle characteristics and environmental variables such as surface type and land use as pointed out by [7] and [11].

While a more physical-based description of rainfall induced washoff which also appropriately respects environmental conditions would clearly improve representativity of model outputs, both pollutant buildup and washoff are significantly affected by stochastic inputs [12] which in turn can hardly be predicted. As a consequence, [5] stress the need for an alternative modelling approach, which also incorporates effects of stochasticity on pollutant buildup and washoff. This aligns with [13] who already claimed to respect stochasticity when using stormwater quality data.

Calibration of stormwater quality models conventionally aims to minimize the difference between observed and simulated pollutographs. While this allows to incorporate intra-event variability, pollutant stochasticity is rarely taken into account as goodness-of-fit is calculated event-specific.

Several studies in the past decades respected probabilistic pollutant characteristics. [14] applied an autoregressive moving-average modelling approach for both continuously buildup and washoff of pollutant concentrations to account for unpredictable environmental impacts. However, the approach could not be appropriately calibrated because of lack of data. Motivated by unavailable urban storm runoff quality data, [15] analytically derived a frequency distribution to predict annual solids washoff from impervious urban areas. His concept takes rainfall characteristics and catchment parameters for buildup and washoff into account and is exemplified for an artificial industrial catchment. Due to lack of data, the approach could not be validated. A probabilistic approach to model TSS loads and dynamics of urban areas has also been proposed by [16]. Their concept uses i) a parameterized power function to approximate intra-event TSS dynamics with normal distributed exponent ii) log-normal distributed event mean concentrations (EMC) to estimate total TSS masses per event and iii) a uniform distributed daily wastewater discharge combined with a constant TSS concentration. While the practical benefit of the model is clearly highlighted, the authors point out the simplified process description and its limited predictive power. [17] introduce a general probability distribution approach in which cumulated distribution functions for pollutant loads and event mean concentrations are obtained from probabilistic rainfall-runoff transformation. [18] performed Monte-Carlo simulations and used corresponding results to assess the effects of stormwater best management practices on water quality for six toxic metals. As [16] they also assumed a power law relationship between runoff and pollutant concentrations during an event. However, they stochastically considered the exponent of the used power equation for the intra-event relationship, which in turn led to a large amount of pollutographs to be analyzed.

A refinement of the exponential washoff equation by incorporating stochastic fluctuations is analyzed by [19]. Here, the coefficient dominating the washoff process is assumed to be random and consequently addressed by adding gaussian noise. A good agreement to empirical distributions for TSS and TN (Total Nitrogen) is reported, which required large amount of data, though. [20] obtained frequency distributions of i) event pollutant load, ii) event mean concentration and iii) peak concentration of COD from a continuous simulation of an urbanized catchment. Exponential equations for buildup and washoff were employed and calibrated with regard to continuous COD concentration measurement data using a genetic algorithm. It is

however mentioned, that the predictive power is limited because the study site undergoes further developments. Annual loads for micropollutants have been estimated based on theoretical distribution functions of event mean concentration for three residential catchments by [21].

The literature shows various approaches to take stochasticity of pollutant processes into account. While early studies primarily used probabilistic methods to overcome scarcity of stormwater quality data, recent studies using continuous quality data tend to admit the variability of natural pollutant processes by employing stochastic concepts. With regard to continuous long-term stormwater quality simulations, alternative modelling approaches presented incorporate stochasticity through i) probabilistic description and transformation of model input data (rainfall-runoff), ii) modification of empirical pollutant buildup/washoff equations, iii) distribution-based parameterization of intra-event dynamics and iv) probabilistic analysis of model results after calibration (post-processing).

It has however not been investigated, whether available stormwater quality models can be calibrated towards probabilistic pollutant characteristics. Using a distribution-based calibration proposes an additional alternative to incorporate pollutant stochasticity. In contrast to approaches already introduced, this method maintains existing model concepts and avoids expensive post-processing.

The present paper reports on the development of an innovative stormwater quality model calibration approach using TSS event load distribution. The approach is demonstrated on two real-world models. Calibrated models are finally used to estimate annual TSS loads which is a key parameter for emission control in several stormwater management guidelines.

2. Materials and Methods

2.1 Concept of model calibration

In this study, stormwater quality models are calibrated using a distribution-based approach. Instead of replicating single-event characteristics or pollutographs, the approach aims to minimize the difference between observed and simulated TSS event load distribution. Since observed TSS event load distributions can be well approximated with theoretical distribution functions [22], the calibration uses a parameterized lognormal distribution as reference (cf. 2.3).

The approach focuses probabilistic event load distribution and puts less emphasize on intra-event dynamics. Model results are therefore required to be analyzed by means of Mass-Volume-Curves (MV-Curves) [23].

2.2 Experimental Sites and Measurement Data

Stormwater runoff and quality processes of a flat roof (FR, 50 m²) and a parking lot (PL, 2350 m²,) are considered. At both sites, a long-term online monitoring campaign has been conducted and continuous runoff and quality data at the outlet of the catchment was collected [24]. Stormwater quality data are available from 2013/03 – 2015/11. Rainfall measurement is still operated. Based on site-specific correlation functions for the relationship of TSS and turbidity, continuous TSS time series were estimated from online turbidity measurements. Data was subjected to statistical analyses which are presented and discussed in [24]. The authors successfully measured 65 rainfall-runoff events at site FR and 46 events at site PL. The average of all event mean concentrations (μ EMC) is 33 mgL⁻¹ at site FR and 60 mgL⁻¹ at site PL. Summing up the estimated TSS loads of all observed events yields 11.3 gm⁻² at site FR and 10.6 gm⁻² at site PL. Table 1 shows a summary of site and measurement data.

Table 1. Characteristics of experimental sites and summary of measurement data obtained

| Parameter | flat roof | parking lot |
|--|--|--|
| area (m ²) | 50 | 2.350 |
| surface type (-) | bitumen sheeting (100%) | asphalt (55%), porous pavement (40%), vegetated areas (5%) |
| slope (%) | 2 | 2.5 |
| stormwater quality observation period (-) | 2013/03 – 2015/11 | 2013/04 – 2014/10 |
| valid events observed (-) | 65 | 46 |
| total TSS loads of valid events (g m ⁻²) | 11.3 | 10.6 |
| average TSS event mean concentration of valid events observed (mg L ⁻¹) | 33 | 60 |
| | within stormwater quality observation period: 2013/03 – 2013/12: 475 2014: 897 2015/01 – 2015/11: 726 | |
| rainfall (yyyy/mm, mm per period) | after stormwater quality observation period: 2015/12: 42 2016: 700 2017: 734; 2018/01-2018/04: 203 | |

2.3 Theoretical Distribution Function for Site-specific TSS Event Loads

[22] use TSS event load data from [24] and describe site-specific empirical TSS event load distributions by means of theoretical distribution functions. It is demonstrated that the two-parameter lognormal distribution approximates the empirical TSS event load distribution well and can therefore be used to probabilistically describe TSS event loads. The authors optimized the parameters of the lognormal distribution with respect to a likelihood function and evaluated the goodness-of-fit by means of Kolmogorov-Smirnov and Anderson-Darling test statistics. Table 2 shows the general lognormal distribution formula and optimized parameter for μ (meanlog) and σ (sdlog) for sites FR and PL taken from [22].

Table 2. Lognormal distribution function and optimized parameters to describe TSS event load distribution for site FR and PL from [22]

| formula | optimized parameter | | | |
|---|---------------------|----------|-------------|----------|
| | flat roof | | parking lot | |
| | μ | σ | μ | σ |
| $F(x) = \begin{cases} 0, & x \leq 0 \\ \frac{1}{\sigma\sqrt{2\pi}} \times \int_0^x \frac{1}{t} e^{-\frac{1}{2}\left(\frac{\ln t - \mu}{\sigma}\right)^2} dt, & x > 0 \end{cases}$ | -3.69 | 2.429 | -1.96 | 0.987 |

2.4 Stormwater Quality Modelling

In this study pollutant processes for buildup and washoff are modelled with the widely used exponential equations implemented in the stormwater management model SWMM5 [25]. Buildup $B(t)$ is mathematically described as function of antecedent dry weather days t (Equation 1). Pollutant washoff $W(t)$ is expressed as function of current runoff rate $q(t)$ and available masses on surface $B(t)$ (Equation 2). Both functions offer two individual parameters to be calibrated. Additionally, the initial buildup B_0 at the beginning of simulation ($t=0$) needs to be estimated.

Table 3 shows the parameter used for calibration. Corresponding parameter ranges were extracted from literature [5,26] and harmonized with authors experience.

$$B(t) = k * (1 - e^{-\alpha t}) \quad (1)$$

with buildup coefficient k (g m^{-2}), buildup exponent α (d^{-1}), t denotes number of preceding dry weather days.

$$W(t) = C_1 * q(t)^{C_2} * B(t) \quad (2)$$

with washoff coefficient C_1 (-), washoff exponent C_2 (-), runoff rate q (mm h^{-1}), available pollutant masses on surface B (g m^{-2}) and time index t .

Table 3. Quality model parameters and corresponding ranges used for calibration

| parameter | description | unit | range |
|-----------|---|-------------------|---------------|
| B_0 | masses available at the beginning of simulation ($t = 0$) | g m^{-2} | [1; 5] |
| k | maximum possible buildup | g m^{-2} | [0.0001; 2] |
| α | rate constant of buildup per day | d^{-1} | [0.0001; 0.2] |
| C_1 | washoff coefficient | - | [0.0001; 1] |
| C_2 | washoff exponent | - | [0.0001; 3] |

2.5 Parameter estimation and goodness-of-fit assessment

For both sites, model parameters affecting runoff generation and hydrograph characteristics are initially calibrated by means of the multi-objective algorithm NSGA-2 [27]. The algorithm allows to optimize multiple objectives simultaneously and identifies pareto-optimal solutions from which a compromise can be drawn. Here, a single objective is defined as an event-specific Nash-Sutcliffe-Efficiency (NSE) [28]. 8 rainfall-runoff events were taken into account which consequently yields 8 objectives to be optimized. The compromise solution follows the L2-metric [29] which calculates the euclidean distance of all pareto-optimal solutions to an ideal solution. The solution with smallest euclidean distance is considered as compromise. Model parameters i) surface roughness, ii) depression storage and iii) characteristic width of the overland flow are considered for calibration. The calibration yielded an average event-specific NSE of 0.73 for site FR and 0.72 for site PL (results of water quantity calibration are not further discussed in this paper).

Once optimized parameters of runoff calibration are estimated, model parameters for pollutant buildup and washoff (cf. Table 3) are optimized. The calibration aim is to fit the simulated TSS event loads distribution to the parameterized lognormal distribution. For this purpose, the Kolmogorov-Smirnov (KS) statistic D_n which numerically describes the equality of two distributions and tests whether a sample follows a specific distribution [30] is used as objective function. This means the smaller the KS statistic D_n gets, the higher the goodness-of-fit of the calibration. The KS statistic ranges from $0 \leq D_n \leq 1$. As this calibration only considers a single objective, a single objective optimization algorithm is used. A differential evolution algorithm [31] implemented by [32] is applied. The following computation steps are performed:

1. Simulation with a new set of parameters generated by the optimization algorithm.
2. Determine and split events from simulation time series which satisfy selection criteria (Table 4). An event starts when runoff starts and ends if the maximum runoff within a predefined window is 0.
3. Computation of runoff volume and TSS load per event.
4. Selection of events which exceeds a minimum runoff volume (Table 4). This step is introduced because the small size of the catchments leads to a significant number of events with numerically low runoff volume which would result in disproportionately weights to these events.

5. Computation of cumulative TSS event load distribution function for the events remaining.
6. Computation of Kolmogorov-Smirnov Distance D_n according to Equation 3.

$$D_n = \sup_x |F_{SWMM}(x) - F_{lognormal(\mu,\sigma)}(x)| \quad (3)$$

with F_{SWMM} being the simulated cumulative TSS event load distribution function and $F_{lognormal}$ the site-specific parameterized lognormal distribution function.

7. Repeat steps 1 – 7 to minimize D_n until convergence.

Table 4. Summary of simulation period and rainfall-runoff event selection criteria

| | flat roof | parking lot |
|--|----------------------|-----------------------|
| simulation duration (observation period) | 2013/03 – 2015/11 | 2013/04 – 2014/10 |
| simulation duration (a) | 2.7 | 1.6 |
| days with rainfall ≥ 2 mm d ⁻¹ | 250 | 137 |
| <i>event selection criteria</i> | | |
| event window (min) | | 480 |
| min. runoff volume (L) | 19 (~0.4 percentile) | 465 (~0.2 percentile) |
| events selected (-) | 224 | 107 |

The goodness-of-fit of the calibrated stormwater quality model is numerically assessed and visually evaluated through a direct comparison of the simulated distribution function and the parameterized lognormal distribution function for TSS event loads. Residuals of the simulated event loads and observed event loads are computed. Simulated intra-event dynamics are analyzed by means of Mass-Volume-Curves (MV-Curves).

2.6 Concept of model validation

The calibration uses measurement data from site-specific stormwater quality observation period. Estimated parameters are expected to be valid beyond this period. The model validation therefore uses all available rainfall data from the 5 years period (2013/03 – 2018/04) (Table 1). Equality of simulated TSS event load distributions from the 5 years period and the observation period are evaluated using Kolmogorov-Smirnov's distance $KS D_n$.

2.7 Model parameter uncertainty analysis

The differential evolution algorithm applied belongs to the class of genetic algorithms which minimize an objective function by evolving a population of candidate solutions through successive generations [32]. In this study, the configuration of evolution strategy and mutating operators (crossover probability and differential weighting factor) follows the developers recommendation. However, the maximum number of iterations is set to 400 and the number of population members (i.e. parameter sets per iteration) is set to 100, which result in 40.000 simulation runs per model in total. For estimating model parameter uncertainties, simulation results are divided into behavioral and non-behavioral groups. Parameter sets which yield to the best 20 % solutions are attributed behavioral and subjected to descriptive statistical analysis (mean, standard deviation and coefficient of variation).

2.8 Estimation of annual TSS event loads

The calibrated stormwater quality models are further used to estimate annual TSS event loads and event mean concentrations originated from the study sites. Annual TSS event loads are estimated by considering all event loads from a moving window of 12 consecutive months to

account for natural rainfall variability. Using the extended rainfall series, the simulation period comprises ~5 years with 62 months which yields 50 (62 – 12) moving years.

3. Results

Calibration results for both sites are shown in Table 5. Statistics for both model parameters and the Kolmogorov-Smirnov-based objective function are given. The best fit parameter sets yielded to an objective function of roughly 0.05 for both models.

Table 5. Calibrated model parameters and corresponding uncertainty statistics (FR: Flat Roof, PL: Parking lot, sd: standard deviation, CoV: Coefficient of Variation, KS D_n: Kolmogorov-Smirnov distance)

| site | statistic | objective function | | parameter | | | |
|------|-----------|--------------------|-------------------|-------------------|-----------------|----------------|----------------|
| | | KS D _n | B ₀ | k | α | C ₁ | C ₂ |
| | | - | g m ⁻² | g m ⁻² | d ⁻¹ | - | - |
| FR | best fit | 0.053 | 2.713 | 1.899 | 0.022 | 0.017 | 2.040 |
| | mean | 0.056 | 3.437 | 1.706 | 0.024 | 0.021 | 2.070 |
| | sd | 0.003 | 0.608 | 0.201 | 0.005 | 0.006 | 0.054 |
| | CoV | 0.053 | 0.177 | 0.118 | 0.212 | 0.277 | 0.026 |
| PL | best fit | 0.049 | 4.545 | 0.891 | 0.194 | 0.472 | 1.120 |
| | mean | 0.050 | 4.726 | 0.882 | 0.204 | 0.470 | 1.103 |
| | sd | 0.002 | 0.257 | 0.053 | 0.021 | 0.043 | 0.070 |
| | CoV | 0.032 | 0.054 | 0.061 | 0.105 | 0.091 | 0.063 |

Table 6 compares the total TSS event loads of simulated and observed TSS event loads. At site FR, the calibrated model yields to 11.9 g m⁻² (+5%), site PL gives 7.57 g m⁻² (-28%). TSS event mean concentrations of observed and simulated events are given in Table 7.

Table 6. Observed and simulated total TSS event loads (observed values are taken from [24])

| site | events | total TSS event loads (g m ⁻²) | | |
|------|--------|--|-----------|--------------------|
| | | observed | simulated | relative deviation |
| FR | 65 | 11.3 | 11.9 | + 5 % |
| PL | 46 | 10.6 | 7.57 | - 28 % |

Table 7. Observed (obs) and simulated (sim) TSS event mean concentrations (observed values are taken from [24])

| site | source | n | TSS event mean concentration (mg L ⁻¹) | | | | | | | | |
|------|--------|----|--|-----------|------------|--------|------------|-----------|-------|-------------|------|
| | | | Min | 0.1-Perc. | 0.25-Perc. | Median | 0.75-Perc. | 0.9-Perc. | Max | Mean | Sd |
| FR | obs | 65 | <0.1 | 1.2 | 2.8 | 9.0 | 35.1 | 94.0 | 249.9 | 33.2 | 54.6 |
| | sim | 65 | 1.2 | 5.8 | 9.6 | 20.6 | 35.5 | 82.6 | 178.2 | 33.4 | 36.5 |
| PL | obs | 46 | 4.7 | 13.2 | 24.4 | 49.4 | 80.1 | 112.4 | 253.7 | 60.3 | 49.3 |
| | sim | 46 | 0.2 | 4.6 | 13.9 | 45.4 | 98.8 | 156.6 | 161.6 | 62.9 | 54.7 |

Cumulative distribution functions of simulated TSS event loads are depicted for both models in Figure 1 (FR) and Figure 2 (PL). Simulation results are opposed to the parameterized lognormal distribution function used for calibration and the original empirical distribution function from

observation. Additionally, absolute residuals between observed and simulated TSS event loads are presented on the right-hand side of the figures. For site FR, the mean of TSS event loads residuals is -0.0087 g m^{-2} (sd: 0.19; min: -0.41; max: 0.94), at site PL, the mean of TSS event loads residuals is 0.065 g m^{-2} (sd: 0.19; min: -0.27; max: 0.74).

Observed and simulated MV-Curves are shown in Figure 3. Simulated MV-Curves are calculated for both the stormwater quality observation period and the 5 years period using all available rainfall data. Simulated distribution functions from the observation period (calibration) are compared to the results using the 5 years period (validation) in Figure 4. Corresponding goodness-of-fit is given in Table 8.

Furthermore, based on the calibrated models, annual TSS event loads for moving years of the 5 years period are site-specifically estimated and presented in Table 9. The mean of all 50 moving years is $9.9 \text{ g m}^{-2} \text{ a}^{-1}$ (sd: 0.75) for site FR and $13.7 \text{ g m}^{-2} \text{ a}^{-1}$ (sd: 1.17) at site PL.

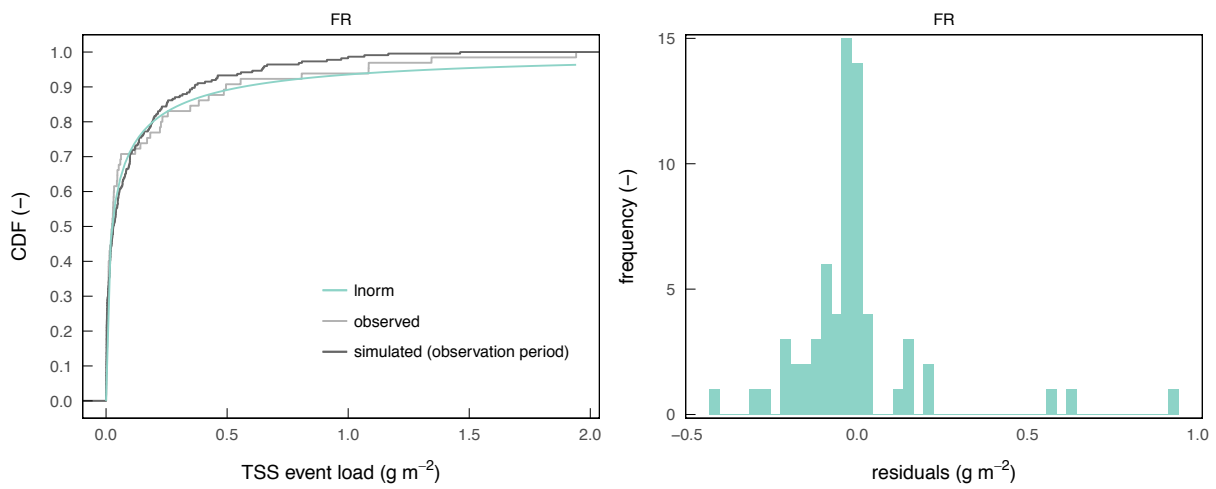


Figure 1. Cumulative distribution functions of lognormal, observed and simulated TSS event loads (left) and distribution of residuals between observed and simulated event loads (right) at site Flat roof

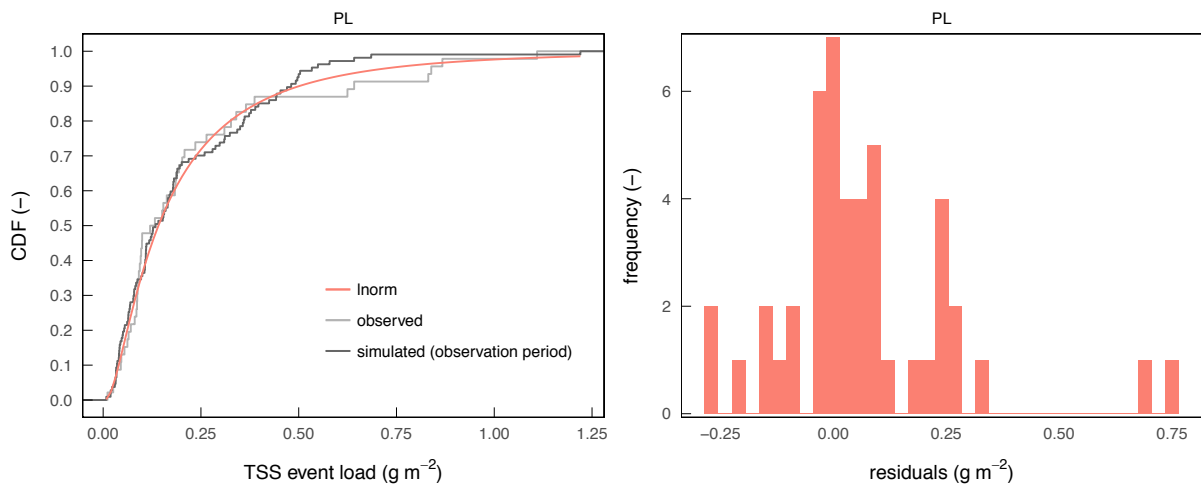


Figure 2. Cumulative distribution functions of lognormal, observed and simulated TSS event loads (left) and distribution of residuals between observed and simulated event loads (right) at site Parking Lot.

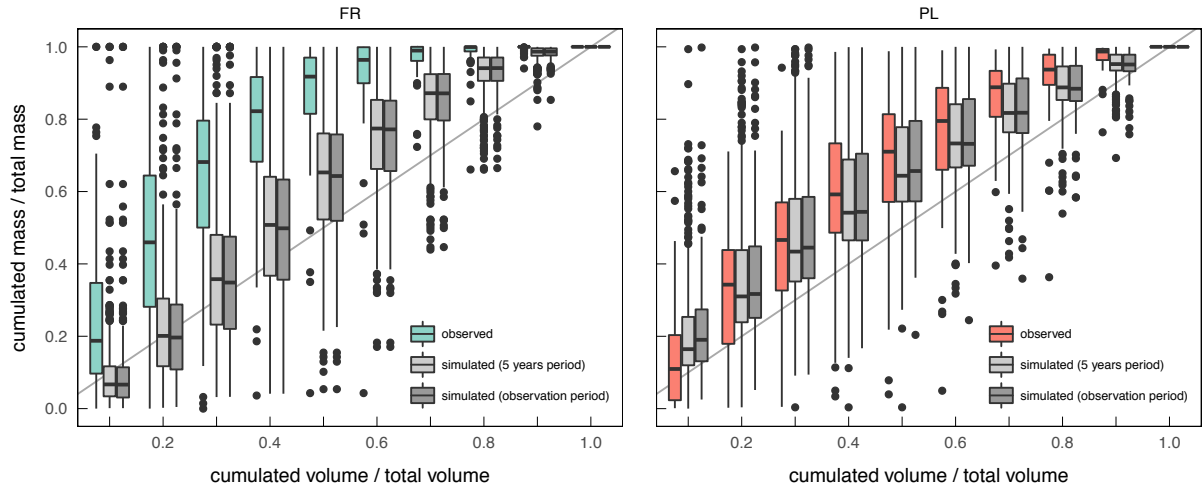


Figure 3. Comparison of observed and simulated Mass-Volume-Curves for sites Flat Roof (left) and Parking Lot (right)

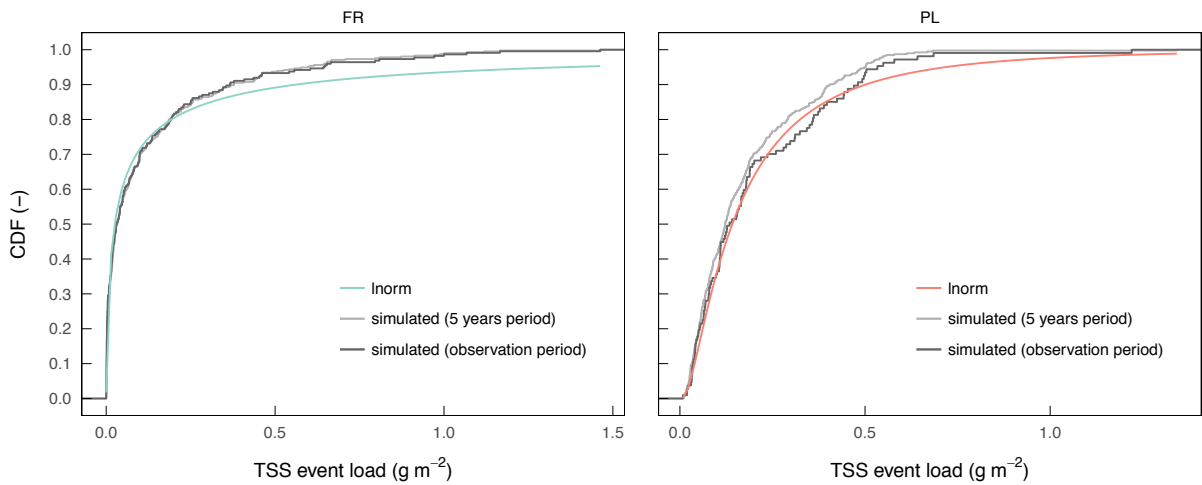


Figure 4. Cumulative distribution functions of lognormal and simulated TSS event loads for the observation period (calibration) and the 5 years period (validation) for sites Flat Roof (left) and Parking Lot (right).

Table 8. Goodness-of-fit matrix for observation period (calibration) and 5 years period (validation) (FR: Flat Roof, PL: Parking lot, KS D_N: Kolmogorov-Smirnov distance).

| site | | KS D _N | | |
|------|--------------------|-------------------|--------------------|----------------|
| | | Inorm | observation period | 5 years period |
| FR | Inorm | - | | |
| | observation period | 0.053 | - | |
| | 5 years period | 0.062 | 0.035 | - |
| PL | Inorm | - | | |
| | observation period | 0.049 | - | |
| | 5 years period | 0.073 | 0.083 | - |

Table 9. Simulated annual TSS loads (FR: Flat Roof, PL: Parking lot).

| site | n (moving years within 5 years period) | annual TSS loads ($\text{g m}^{-2} \text{a}^{-1}$) | |
|------|--|--|------|
| | | mean | sd |
| FR | 50 | 9.9 | 0.75 |
| PL | 50 | 13.7 | 1.17 |

4. Discussion

According to the low Kolmogorov-Smirnov statistic D_n of approx. 0.05 for both sites (Table 5), the best-fit parameter sets obtained by the distribution-based calibration approach lead to well-approximated parameterized lognormal distributions. From a statistical perspective which also takes the number of samples into account, it can be legitimately assumed that both distributions (lognormal and simulated TSS event loads) follow the same distribution. Both KS statistics are below the critical values at 90% significance level (0.082 for site FR and 0.118 at site PL).

At site FR, the calibrated model replicates the distribution function until the 0.8-percentile with a high goodness-of-fit (Figure 1). Events exceeding this value are generally underestimated by the model and lead to lower simulated event loads than suggested by the lognormal distribution. Since the KS statistic represents the maximum distance between two cumulative distribution functions, maximum 5% of the events with more than the 0.8-percentile of event loads are underestimated.

The results for site PL show a similar effect (Figure 2). Here, the model shows a good fitting of the distribution function until the 0.9-percentile which accordingly implies that maximum 5 % of the events with more than the 0.9-percentile of event loads are underestimated.

Both calibrated models tend to underestimate events with high TSS loads which indicates that the calibration approach and the objective function applied is heavily influenced by events with low TSS event load which as a matter of fact is the case for the majority of events for both sites. Applying an alternative goodness-of-fit measure as objective function which also emphasize the upper tailing of a distribution function could lead to superior model performance. This however remains unclear as the applied pollutant model itself also induces limitations to replicate natural pollutant processes [5,12,33].

The fact, that events with high TSS event loads are underestimated affects the goodness-of-fit concerning the total TSS event load of the events observed (Table 6). This is especially evident at site PL, where the total TSS event load is underestimated by roughly 28 %. Events with more than 0.5 g m^{-2} are poorly represented (cf. Figure 2). At site FR, the relative deviation is only about 5 %. This signals that the error is compensated by events whose simulated TSS event load is higher than the observed (intersection at approx. 0.1 g m^{-2} , cf. Figure 1).

Mass-Volume-Curves (Figure 3) for site FR reveal, that intra-event processes simulated do not reflect the observed dynamics in general. Especially, the prevailing first-flush characteristic is not appropriately replicated. Instead simulated washoff tends to occur proportionally to runoff.

In contrast, statistics of simulated intra-event processes at site PL correspond well to the data observed. It can be seen that the calibrated model also tends to generate wash proportional to runoff. The high agreement of observed and simulated MV-Curves at site PL is obtained since observed MV-Curves already show a more runoff proportional washoff behavior. Although the general characteristic at site PL is satisfactorily represented, the results from both sites indicate that the observed intra-event dynamic can hardly be deterministically described by the model for a continuous simulation period. As pointed out in previous studies by [5,12] pollutant buildup and washoff is highly affected by stochastic inputs which consequently limits the goodness-of-fit of replicating intra-event dynamics.

Distributions of simulated and observed event mean concentrations (EMC) are compared in Table 7. A notably high agreement of mean EMC is obtained for both sites (FR: 33 mg L^{-1} , PL: 62 mg

L⁻¹). It can also be observed that EMC percentiles of simulation for site FR are slightly higher than observed percentiles until the 0.75-Percentile. Site PL shows the opposite behavior: EMC percentiles of simulation are slightly lower than observed percentiles until the 0.5-Percentile. However, in both cases, the maximum observed EMC are strongly underestimated which again suggests an inappropriate accumulation process model to account for random influences (e.g. traffic induced pollutant emissions [34]).

Figure 4 and Table 8 compares results from the calibration and validation period. At site FR, the difference between both distributions is marginal implying the observation period being highly representative. The KS statistic of 0.062 from validation only slightly differs from calibration (KS: 0.053) which indicates a successful model validation. In contrast, the distribution function from validation at site PL underestimates the assumed lognormal distribution constantly. This is also expressed by a higher KS statistic of 0.073. The distance between calibration and validation period is slightly higher (KS: 0.083) indicating a less successful model validation. However, it is noticeable that the simulated TSS event distribution of observation period falls below the lognormal distribution between 0.25 g m⁻² and 0.4 g m⁻² and exceeds the lognormal distribution for event loads higher 0.5 g m⁻². This indicates the observation period being less representative as the number of events is significantly lower.

The validated models were finally used to estimate annual TSS loads (Table 9) which is of special interests for practical purposes. In the present study, the estimated mean annual TSS loads for site FR is 9.9 g m⁻² a⁻¹ which according to [35] represents a roof with “low to normal” load contribution. Annual TSS loads for site PL was estimated at 13.7 g m⁻² a⁻¹ which is significant lower than reported from measurements by [36] (~ 40 g m⁻² a⁻¹). As already stated, the model disregards traffic related stochastic inputs, which could explain the low annual TSS loads estimated. Consequently, the result must be carefully interpreted. This highlights the need to especially account for load intensive events either through an alternative objective function or modification of the model concept.

Generally, the distribution-based calibration approach allows to calibrate stormwater quality models even if data is incomplete but tends to underestimate events with high TSS loads. However, compared to the conventional calibration the approach has clearly two advantages. First, the occurrence of events and its corresponding pollutant contribution is probabilistically considered which implies stochasticity is taken into account. Second, measurement data of stormwater quality processes are rarely completely available for continuous periods which consequently complicates the application of a conventional calibration approach and could result in misleading model outputs. Theoretical distribution functions are continuously defined.

5. Conclusions

An innovative calibration approach for stormwater quality models with respect to TSS event load distribution is introduced. The approach was applied on the two experimental sites i) flat roof and ii) parking lot for which parameterized lognormal distribution functions were available. From this study it can be concluded:

- Both models have been successfully calibrated, indicated by the low Kolmogorov-Smirnov distance measure. Distribution functions from simulation were validated with 5 years rainfall data.
- Maximum deviation between lognormal and simulated TSS event load distribution is 5%.
- A high agreement of observed and simulated mean of event mean concentrations (μEMC) was achieved for both sites (FR: 33.2 vs. 33.4 mg L⁻¹, PL: 60.3 vs. 62.9 mg L⁻¹).
- Using a theoretical distribution for calibration provides continuous probabilities and allows to calibrate stormwater quality models even if data is incomplete.

- The approach is general applicable and especially powerful if distribution functions get generalizable on a catchment-scale.
- The objective function used for calibration employs the Kolmogorov-Smirnov statistic. Despite its simplicity it has been shown, that events with high TSS event loads tend to be underestimated. A more behavioral distance measure which also accounts for events with high loads remains open for future research.
- Based on the calibrated models, annual TSS event loads were estimated. $9.9 \text{ g m}^{-2} \text{ a}^{-1}$ were obtained for site flat roof, $13.7 \text{ g m}^{-2} \text{ a}^{-1}$ for site parking lot.

The calibration approach still needs to be tested on larger catchments which consists of multiple subcatchments with different land use. Additionally, it could be of interest whether model parameters are correlated to parameters of the theoretical distribution function or catchment characteristics.

Acknowledgments: The research is part of the project “Modelle für Stofftransport und -behandlung in der Siedlungshydrologie” (STBMOD) at the Institute for Infrastructure, Water, Resources and Environment, Muenster University of Applied Sciences. The project was funded by the German Federal Ministry of Education and Research (BMBF, FKZ 03FH033PX2).

Author Contributions: Dominik Leutnant, Dirk Muschalla and Mathias Uhl conceived and designed the numerical experiments; Dominik Leutnant performed the numerical computations and evaluated the results; Dominik Leutnant wrote the paper and thanks Dirk Muschalla and Mathias Uhl for professional discussions.

Conflicts of Interest: The authors declare no conflict of interest.

References

1. Dotto, C. B. S.; Kleidorfer, M.; Deletic, A.; Rauch, W.; McCarthy, D. T.; Fletcher, T. D. Performance and sensitivity analysis of stormwater models using a Bayesian approach and long-term high resolution data. *Environmental Modelling & Software* **2011**, *26*, 1225–1239, doi:10.1016/j.envsoft.2011.03.013.
2. Dotto, C. B. S.; Deletic, A.; Fletcher, T. D. Analysis of parameter uncertainty of a flow and quality stormwater model. *Water Science & Technology* **2009**, *60*, 717, doi:10.2166/wst.2009.434.
3. Sartor, J. D.; Boyd, G. B. *Water pollution aspects of street surface contaminants*; US Environmental Protection Agency, Washington, DC, USA, 1972;
4. Muschalla, D.; Schneider, S.; Gamerith, V.; Gruber, G.; Schroter, K. Sewer modelling based on highly distributed calibration data sets and multi-objective auto-calibration schemes. *Water Sci Technol* **2008**, *57*, 1547–1554, doi:10.2166/Wst.2008.305.
5. Sage, J.; Bonhomme, C.; Al Ali, S.; Gromaire, M.-C. Performance assessment of a commonly used “accumulation and wash-off” model from long-term continuous road runoff turbidity measurements. *Water Research* **2015**, *78*, 47–59, doi:10.1016/j.watres.2015.03.030.
6. Bonhomme, C.; Petrucci, G. Should we trust build-up/wash-off water quality models at the scale of urban catchments? *Water Research* **2017**, *108*, 422–431, doi:10.1016/j.watres.2016.11.027.
7. Egodawatta, P.; Thomas, E.; Goonetilleke, A. Mathematical interpretation of pollutant wash-off from urban road surfaces using simulated rainfall. *Water Research* **2007**, *41*, 3025–3031.
8. Muthusamy, M.; Tait, S.; Schellart, A.; Beg, M. N. A.; Carvalho, R. F.; de Lima, J. L. M. P. Improving understanding of the underlying physical process of sediment wash-off from urban road surfaces. *Journal of Hydrology* **2018**, *557*, 426–433, doi:10.1016/j.jhydrol.2017.11.047.
9. Zhao, J.; Chen, Y.; Hu, B.; Yang, W. Mathematical Model for Sediment Wash-Off from Urban Impervious Surfaces. *J. Environ. Eng.* **2015**, *142*, 04015091, doi:10.1061/(ASCE)EE.1943-7870.0001058.
10. Alias, N.; Liu, A.; Goonetilleke, A.; Egodawatta, P. Time as the critical factor in the investigation of the relationship

- between pollutant wash-off and rainfall characteristics. *Ecological Engineering* **2014**, *64*, 301–305, doi:10.1016/j.ecoleng.2014.01.008.
11. Zhao, H.; Jiang, Q.; Xie, W.; Li, X.; Yin, C. Role of urban surface roughness in road-deposited sediment build-up and wash-off. *Journal of Hydrology* **2018**, *560*, 75–85, doi:10.1016/j.jhydrol.2018.03.016.
 12. Shaw, S. B.; Stedinger, J. R.; Walter, M. T. Evaluating Urban Pollutant Buildup/Wash-Off Models Using a Madison, Wisconsin Catchment. *Journal of Environmental Engineering* **2010**, *136*, 194–203, doi:10.1061/(ASCE)EE.1943-7870.0000142.
 13. Harremoës, P. Stochastic models for estimation of extreme pollution from urban runoff. *Water research* **1988**, *22*, 1017–1026.
 14. Scholz, K. Stochastische Simulation urbanhydrologischer Prozesse (“Stochastic simulation of urban hydrological processes”). Dissertation (in German), University of Hannover, 1995.
 15. Osman Akan, A. Derived Frequency Distribution for Storm Runoff Pollution. *Journal of Environmental Engineering* **1988**, *114*, 1344–1351, doi:10.1061/(ASCE)0733-9372(1988)114:6(1344).
 16. Rossi, L.; Krejci, V.; Rauch, W.; Kreikenbaum, S.; Fankhauser, R.; Gujer, W. Stochastic modeling of total suspended solids (TSS) in urban areas during rain events. *Water Research* **2005**, *39*, 4188–4196, doi:10.1016/j.watres.2005.07.041.
 17. Chen, J.; Adams, B. J. A derived probability distribution approach to stormwater quality modeling. *Advances in Water Resources* **2007**, *30*, 80–100, doi:10.1016/j.advwatres.2006.02.006.
 18. Sharifi, S.; Massoudieh, A.; Kayhanian, M. A Stochastic Stormwater Quality Volume-Sizing Method with First Flush Emphasis. *Water Environment Research* **2011**, *83*, 2025–2035, doi:10.2175/106143011X12989211.
 19. Daly, E.; Bach, P. M.; Deletic, A. Stormwater pollutant runoff: A stochastic approach. *Advances in Water Resources* **2014**, *74*, 148–155, doi:10.1016/j.advwatres.2014.09.003.
 20. Qin, H.; Tan, X.; Fu, G.; Zhang, Y.; Huang, Y. Frequency analysis of urban runoff quality in an urbanizing catchment of Shenzhen, China. *Journal of Hydrology* **2013**, *496*, 79–88, doi:10.1016/j.jhydrol.2013.04.053.
 21. Hannouche, A.; Chebbo, G.; Joannis, C.; Gasperi, J.; Gromaire, M.-C.; Moilleron, R.; Barraud, S.; Ruban, V. Stochastic evaluation of annual micropollutant loads and their uncertainties in separate storm sewers. *Environmental Science and Pollution Research* **2017**, *24*, 28205–28219, doi:10.1007/s11356-017-0384-5.
 22. Leutnant, D.; Muschalla, D.; Uhl, M. Statistical Distribution of TSS Event Loads From Small Urban Environments. *Water* **2018**, submitted on April 12th.
 23. Bertrand-Krajewski, J. L.; Chebbo, G.; Saget, A. Distribution of pollutant mass vs volume in stormwater discharges and the first flush phenomenon. *Water Research* **1998**, *32*, 2341–2356.
 24. Leutnant, D.; Muschalla, D.; Uhl, M. Stormwater Pollutant Process Analysis with Long-Term Online Monitoring Data at Micro-Scale Sites. *Water* **2016**, *8*, 299, doi:10.3390/w8070299.
 25. Rossman, L. A. *Storm Water Management Model - User's Manual Version 5.0*; United States Environmental Protection Agency (US EPA): Cincinnati, OH, USA, 2010; p. 285;.
 26. Gamerith, V.; Neumann, M. B.; Muschalla, D. Applying global sensitivity analysis to the modelling of flow and water quality in sewers. *Water Research* **2013**, *47*, 4600–4611, doi:10.1016/j.watres.2013.04.054.
 27. *A Fast Elitist Non-dominated Sorting Genetic Algorithm for Multi-objective Optimization: NSGA-II*; Deb, K., Agrawal, S., Pratap, A., Eds.; Proceedings of the Parallel Problem Solving Form Nature VI Conference, Lect. Notes in Comput. Sci.; Springer: New York, 2000; Vol. 1917;.
 28. Nash, J. E.; Sutcliffe, J. V. River flow forecasting through conceptual models part I - A discussion of principles. *Journal of Hydrology* **1970**, *10*, 282–290.
 29. Deb, K. *Multi-Objective Optimization using Evolutionary Algorithms*; John Wiley & Sons, LTD: Chichester, 2008; ISBN 978-0-470-74361-4.

30. Hedderich, J.; Sachs, L. *Angewandte Statistik: Methodensammlung mit R*; 14., überarb. und erg. Aufl.; Springer: Heidelberg, 2012; ISBN 978-3-642-24400-1.
31. Price, K. V.; Storn, R. M.; Lampinen, J. A. *Differential evolution: a practical approach to global optimization*; Natural computing series; Springer: Berlin ; New York, 2005; ISBN 978-3-540-20950-8.
32. Ardia, D.; Mullen, K. M.; Peterson, B. G.; Ulrich, J. *DEoptim: Differential Evolution in R*; 2016;
33. Bertrand-Krajewski, J.-L. Stormwater pollutant loads modelling: epistemological aspects and case studies on the influence of field data sets on calibration and verification. *Water Science and Technology* **2007**, *55*, 1–17.
34. Gunawardena, J. M. A.; Liu, A.; Egodawatta, P.; Ayoko, G. A.; Goonetilleke, A. *Influence of Traffic and Land Use on Urban Stormwater Quality - implications for urban stormwater treatment design*; SpringerBriefs in Water Science and Technology; Springer Singapore: Singapore, 2018; ISBN 978-981-10-5301-6.
35. Dierschke, M. Methodischer Ansatz zur Quantifizierung von Feinpartikeln (PM63) in Niederschlagsabflüssen in Abhängigkeit von der Herkunftsfläche (“Methodical approach for quantifying of fine particles (PM63) in rainfall runoffs depending on the surface of origin”). Dissertation (in German), University of Kaiserslautern, 2014.
36. Allen Burton, G.; Pitt, R. *Stormwater Effects Handbook: A Toolbox for Watershed Managers, Scientists, and Engineers*; CRC Press, 2001; ISBN 978-0-87371-924-7.



© 2018 by the authors. Submitted to *Water* for possible open access publication under the terms and conditions of the Creative Commons Attribution (CC BY) license (<http://creativecommons.org/licenses/by/4.0/>).